

Effects of Surface Chemistry
on Deposition Kinetics of Colloidal Hematite ($\alpha\text{-Fe}_2\text{O}_3$)
in Packed Beds of Silica Sand

Thesis by

Jeff Noelte

In Partial Fulfillment of the Requirements

for the Degree of

Doctor of Philosophy

California Institute of Technology

Pasadena, California

2002

(Submitted May 2002)

© 2002

Jeff Noelte

All Rights Reserved

to what's most important... family

Acknowledgements

I would like to thank my advisors Professor Michael Hoffmann and Professor Jim Morgan. I am very grateful for their support, guidance, and patience. I would also like to thank the other members of my examining committee, Professor Mark Davis and Professor Geoff Blake. The generosity of Mark Davis and Jeremy Heidel in the making of electrophoretic mobility measurements, as well as the advice and encouragement of Professor Norman Brooks are greatly appreciated.

The daily rigors of graduate life were made much easier by Linda Scott and Fran Matzen. Their ever-present smiles and kind words could be counted on as much as their invaluable help. The final push to finish my experimental program was enhanced by many helpful and enjoyable conversations with Tim Lesko.

I am extremely fortunate to have parents, step-parents, and a brother like I do. Dad, thanks for being an amazing parent and role model. To my wife, Melissa, thank you for your love and support, and for the greatest gift of all, our son Jordan.

Abstract

The removal of colloidal (sub-micrometer) particles from flowing suspensions by deposition on surfaces is important in many natural and industrial processes (e.g., the fate of colloids and associated pollutants in groundwater systems and water treatment involving separation processes). In deposition, colloidal particles are transported to the vicinity of the collector surface by advection and diffusion. Colloidal interactions at short distances determine whether a particle will attach to a collector. Deposition rates are reduced by the presence of repulsive colloidal interactions. Van der Waals attraction and electric double layer repulsion are combined in DLVO theory to describe the total interaction energy between two surfaces. The total interaction energy depends on the solution chemistry and the electric charge and potential of the interacting surfaces. To understand the attachment step of particle deposition, an understanding of the role of simple chemical changes in the water altering the electrostatic interaction is critical.

Deposition experiments using hematite particles and a silica sand were conducted to investigate the influence of specific adsorption to hematite on deposition kinetics. A variety of electrolytes, both inorganic and organic, were studied (e.g., phosphate, small organic acids, and polymeric organic compounds including fulvic and humic acid). Electrokinetic measurements were carried out, under chemical conditions similar to those in the deposition experiments, to provide information about the sign and magnitude of the surface charge on hematite particles.

Experimental results show that the deposition rate is influenced primarily by electrostatic interactions, which are determined by the adsorption of potential-

determining ions. In the absence of specifically adsorbed species, hematite deposition is transport limited (favorable deposition) at pH 6.5 and 1 millimolar NaCl. The addition of 100 micromolar total phosphate results in unfavorable deposition in which the deposition rate is reduced by approximately two orders of magnitude. Polymeric organic compounds produce unfavorable deposition at total concentrations around 10^{-5} g/L. It was observed that electrokinetic measurements in the presence of polymeric organic compounds are influenced by the particle concentration when hematite mobility is measured as a function of the total solute concentration. Experimental results indicated that adjusting the total polyelectrolyte concentration by the same factor relating the particle concentrations in the mobility measurements and deposition experiments resulted in matching the hematite surface properties in the mobility measurements to the deposition experiments.

The experimental collision efficiency for hematite deposition was consistent with deposition under conditions of surface heterogeneity (i.e., the collision efficiency decreased gradually as electrostatic repulsion increased). The natural silica sand used (Ottawa 30) has a high degree of surface roughness and is expected to be chemically heterogeneous.

Table of Contents

Acknowledgements	iv
Abstract	v
List of Plates	xi
List of Tables.....	xii
List of Figures	xiii
1. Introduction	1-1
1.0 Introduction	1-1
1.1 Motivation to Use Hematite as Model Colloid	1-3
1.2 Scope and Objectives Research.....	1-3
2. Background and Models.....	2-1
2.0 Introduction	2-1
2.1 Clean-Bed Particle Deposition.....	2-2
2.2 Modeling the Deposition of Brownian Particles	2-4
2.2.1 The Advection-Dispersion Equation.....	2-4
2.2.2 The Single Collector Efficiency.....	2-5
2.2.3 Experimental Collision Efficiency	2-6
2.3 Colloidal Interactions in Aquatic Systems	2-8
2.3.1 London-Van der Waals Attraction Energy.....	2-8
2.3.2 Electrostatic Interaction.....	2-9
2.3.3 Total Interaction Energy (DLVO Theory)	2-10
2.4 Oxide/Water Interface	2-11
2.4.1 The Origin of the Surface Hydroxyl Group	2-11
2.4.2 Surface Chemical Speciation Model.....	2-14
2.4.3 Models of the Oxide/Water Interface.....	2-15
2.4.4 Adsorption of Anions on Hematite	2-16
3. Materials and Methods	3-1
3.0 General Remarks	3-1

3.1	Particle Preparation and Characterization	3-1
3.1.1	Preparation of Hematite Particles.....	3-1
3.1.2	Particle Characterization	3-2
3.2	Particle Surface Properties	3-5
3.2.1	Specific Surface Area.....	3-5
3.2.2	Surface Site Density	3-5
3.3	Granular Porous Medium.....	3-6
3.3.1	Porous Medium Physical and Chemical Composition.....	3-6
3.3.2	Cleaning of Porous Medium	3-9
3.4	Electrophoretic Mobility Measurements.....	3-10
3.4.1	Electrophoretic Mobility of Hematite Particles	3-10
3.4.2	Electrophoretic Mobility of Sand Particles	3-11
3.5	Particle Deposition Experiments.....	3-11
3.5.1	Experimental Apparatus for Particle Deposition	3-11
3.5.2	Particle Deposition Procedure.....	3-14
3.5.3	Determination of Particle Concentration.....	3-17
3.5.4	Tracer Experiments	3-18
4.	Experimental Results	4-1
4.0	Introduction	4-1
4.1	Tracer Experiments	4-1
4.2	Particle Deposition Rates	4-3
4.2.1	Effect of NaCl on Hematite Deposition	4-3
4.2.2	Effect of Inorganic Compounds on Hematite Deposition.....	4-5
4.2.2.1	Effect of Phosphate and Arsenate on Hematite Deposition	4-5
4.2.2.2	Effect of Fluoride on Hematite Deposition.....	4-7
4.2.3	Effect of Low Molecular Weight Organic Compounds on Hematite Deposition.....	4-10
4.2.3.1	Effect of Oxalate and Related Compounds on Hematite Deposition	4-10
4.2.3.2	Effect of Phthalate and Related Compounds on Hematite Deposition	4-10

4.2.3.3	Effect of Aspartic Acid on Hematite Deposition	4-14
4.2.3.4	Effect of Butyric Acid on Hematite Deposition.....	4-14
4.2.3.5	Effect of Lauryl Sulfate on Hematite Deposition.....	4-19
4.2.4	Effect of Polymeric Organic Compounds on Hematite Deposition.....	4-19
4.3	Electrokinetic Measurements	4-23
4.3.1	Effect of pH on Silica Sand Mobility.....	4-26
4.3.2	Effect of pH on Hematite Mobility	4-26
4.3.3	Hematite Mobility in the Presence of Inorganic Compounds.....	4-26
4.3.4	Hematite Mobility in the Presence of Oxalate and Related Compounds.....	4-30
4.3.5	Hematite Mobility in the Presence of Phthalate and Related Compounds.....	4-30
4.3.6	Hematite Mobility in the Presence of Aspartic Acid	4-32
4.3.7	Hematite Mobility in the Presence of Butyric Acid.....	4-32
4.3.8	Hematite Mobility in the Presence of Lauryl Sulfate.....	4-32
4.3.9	Hematite Mobility in the Presence of Polymeric Organic Compounds.....	4-32
5.	Discussion of Results	5-1
5.0	Introduction	5-1
5.1	Particle Mobility, ζ -Potential and Surface Potential	5-1
5.2	Hematite Deposition in the Presence of Inorganic Solutes.....	5-2
5.2.1	Hematite Deposition in the Presence of Phosphate and Arsenate.....	5-2
5.2.2	Hematite Deposition in the Presence of Fluoride.....	5-5
5.2.3	Effect of Particle Concentration on Hematite Mobility	5-5
5.3	Hematite Deposition in the Presence of Small Organic Molecules	5-7
5.3.1	Hematite Deposition in the Presence of Oxalate and Related Compounds.....	5-7
5.3.2	Hematite Deposition in the Presence of Phthalate and Related Compounds.....	5-10
5.3.3	Hematite Deposition in the Presence of Aspartic Acid.....	5-12
5.3.4	Hematite Deposition in the Presence of Butyric Acid	5-12

5.3.5 Effect of Particle Concentration on Hematite Mobility 5-14

5.4 Hematite Deposition in the Presence of Polymeric Organic Compounds 5-15

5.4.1 Comparison of Deposition Results and Mobility Measurements..... 5-15

5.4.2 The Langmuir Equation and Total Adsorbate Concentration 5-20

6. Summary and Conclusions..... 6-1

6.0 Introduction 6-1

6.1 The Collision Efficiency and Electrostatic Repulsion 6-1

6.1.1 Theory and Observations 6-1

6.1.2 Cases Contrary to Electrostatic Considerations 6-8

6.2 Implications for Environmental Systems 6-10

6.3 Summary of Main Conclusions..... 6-11

References R-1

Appendix A-1

List of Plates

Plate		Page
I	Transmission electron micrograph of synthesized hematite particles used in this research	3-4
II	Darkfield photograph of Ottawa 30 sand grains (5x magnification)	3-8

List of Tables

Table		Page
3.1	Comparison of hematite properties used in various studies.....	3-5
3.2	Chemical composition of Ottawa 30 sand.....	3-7
3.3	Summary of the conditions for particle deposition experiments.....	3-18

List of Figures

Figure	Page
<hr/>	
1.1	Typical size ranges for aqueous particles..... 1-2
1.2	Schematic representation of particle deposition and aggregation 1-2
2.1	Generalized clean-bed particle breakthrough curve..... 2-3
2.2	Generalized particle breakthrough curve showing blocking and ripening..... 2-3
2.3	Typical total interaction energy profile when electrostatic repulsion is significant 2-12
2.4	Schematic representation of the metal oxide surface 2-13
2.5	Schematic representation of possible surface complexation reactions of a diprotic acid..... 2-18
3.1	X-ray diffraction pattern of hematite prepared for this research compared to a hematite standard..... 3-3
3.2	Sieve analyses of Ottawa 30 sand 3-7
3.3	Schematic diagram of the particle deposition apparatus 3-12
3.4	Total light extinction as a function of particle concentration..... 3-19
4.1	Tracer breakthrough curve 4-2
4.2	Hematite breakthrough curves in the presence of NaCl..... 4-4
4.3	Hematite breakthrough curves in the presence of phosphate..... 4-6
4.4	Experimental collision efficiency as a function of total phosphate concentration 4-6
4.5	Hematite breakthrough curves in the presence of arsenate 4-8
4.6	Experimental collision efficiency as a function of total arsenate concentration 4-8
4.7	Hematite breakthrough curves in the presence of fluoride 4-9
4.8	Experimental collision efficiency as a function of total fluoride concentration 4-9

Figure	Page
4.9 Hematite breakthrough curves in the presence of oxalic acid (C ₂)	4-11
4.10 Hematite breakthrough curves in the presence of succinic acid (C ₄).....	4-11
4.11 Hematite breakthrough curves in the presence of adipic acid (C ₆)	4-12
4.12 Hematite breakthrough curves in the presence of suberic acid (C ₈)	4-12
4.13 Experimental collision efficiency as a function of total dicarboxylic acid concentration	4-13
4.14 Hematite breakthrough curves in the presence of phthalate	4-15
4.15 Hematite breakthrough curves in the presence of benzene-tri	4-15
4.16 Hematite breakthrough curves in the presence of benzene-tetra.....	4-16
4.17 Experimental collision efficiency as a function of total carboxylic acid concentration.....	4-16
4.18 Hematite breakthrough curves in the presence of aspartic acid.....	4-17
4.19 Experimental collision efficiency as a function of total aspartic acid concentration.....	4-17
4.20 Hematite breakthrough curves in the presence of butyric acid	4-18
4.21 Experimental collision efficiency as a function of total butyric acid concentration	4-20
4.22 Hematite breakthrough curves in the presence of lauryl sulfate	4-20
4.23 Experimental collision efficiency as a function of total lauryl sulfate concentration	4-21
4.24 Hematite breakthrough curves in the presence of polyaspartic acid.....	4-21
4.25 Hematite breakthrough curves in the presence of Leonardite humic acid	4-22
4.26 Hematite breakthrough curves in the presence of S.R. fulvic acid	4-24
4.27 Hematite breakthrough curves in the presence of S.R. humic acid.....	4-24
4.28 Experimental collision efficiency as a function of total polyelectrolyte concentration	4-25
4.29 Electrophoretic mobility of Ottawa 30 sand as a function of pH.....	4-27
4.30 Electrophoretic mobility of hematite particles as a function of pH	4-27

Figure	Page
4.31 Electrophoretic mobility of hematite particles as a function of total phosphate concentration.....	4-28
4.32 Electrophoretic mobility of hematite particles as a function of total arsenate concentration.....	4-28
4.33 Electrophoretic mobility of hematite particles as a function of total fluoride concentration	4-29
4.34 Electrophoretic mobility of hematite particles as a function of total concentration of oxalate and related compounds.....	4-31
4.35 Electrophoretic mobility of hematite particles as a function of total concentration of phthalate and related compounds.....	4-31
4.36 Electrophoretic mobility of hematite particles as a function of total aspartic acid concentration.....	4-33
4.37 Electrophoretic mobility of hematite particles as a function of total butyric acid concentration.....	4-33
4.38 Electrophoretic mobility of hematite particles as a function of total lauryl sulfate concentration.....	4-34
4.39 Electrophoretic mobility of hematite particles as a function of total concentration of polyelectrolyte.....	4-34
4.40 Electrophoretic mobility of hematite particles as a function of total polyaspartic acid (PAA) concentration	4-36
4.41 Electrophoretic mobility of hematite particles as a function of total Suwannee River humic acid concentration.....	4-36
5.1 Comparison of collision efficiency and hematite mobility as a function of total phosphate concentration	5-3
5.2 Comparison of collision efficiency and hematite mobility as a function of total arsenate concentration.....	5-3
5.3 Comparison of collision efficiency and hematite mobility as a function of total fluoride concentration.....	5-6

Figure	Page
5.4	Calculated hematite surface potential as a function of total phosphate concentration for different hematite particle concentrations.....5-8
5.5	Comparison of collision efficiency and hematite mobility as a function of total succinic acid concentration5-9
5.6	Comparison of collision efficiency and hematite mobility as a function of total phthalate concentration5-11
5.7	Comparison of collision efficiency and hematite mobility as a function of total benzene-tri concentration.....5-11
5.8	Comparison of collision efficiency and hematite mobility as a function of total benzene-tetra concentration5-13
5.9	Comparison of collision efficiency and hematite mobility as a function of total aspartic acid concentration.....5-13
5.10	Comparison of collision efficiency and hematite mobility as a function of total butyric acid concentration.....5-14
5.11	Comparison of collision efficiency and hematite mobility as a function of total polyaspartic acid concentration5-16
5.12	Comparison of collision efficiency and hematite mobility as a function of total Leonardite humic acid concentration.....5-16
5.13	Comparison of collision efficiency and hematite mobility as a function of total Suwannee R4er fulvic acid concentration5-17
5.14	Comparison of collision efficiency and hematite mobility as a function of total Suwannee R4er humic acid concentration.....5-17
5.15	Hematite mobility as a function of total polyaspartic acid concentration.....5-19
5.16	Hematite mobility as a function of total Suwannee R4er humic acid concentration5-19
5.17	Comparison of collision efficiency and “adjusted” hematite mobility as a function of total polyaspartic acid concentration5-21

Figure	Page
5.18 Comparison of collision efficiency and “adjusted” hematite mobility as a function of total Leonardite humic acid concentration	5-21
5.19 Comparison of collision efficiency and “adjusted” hematite mobility as a function of total Suwannee R4er fulvic acid concentration	5-22
5.20 Comparison of collision efficiency and “adjusted” hematite mobility as a function of total Suwannee R4er humic acid concentration	5-22
6.1 Collision efficiency as a function of the hematite mobility measured at the same chemical conditions of the deposition experiment	6-2
6.2 Comparison of theoretical and experimental collision efficiencies as a function of [KCl] (from Elimelech and O’Melia, 1990)	6-4
6.3 Theoretical collision efficiencies as a function of 1-1 electrolyte assuming a normal distribution of surface potentials for particles and collectors (from Elimelech et al., 1995)	6-6
6.4 Comparison of theoretical and experimental collision efficiencies as a function of pH for carboxylated latex particles for different porous medium cleaning techniques (from Litton and Olson, 1993).....	6-7
6.5 Experimental collision efficiencies as a function of the heterogeneity parameter (from Elimelech et al., 2000)	6-9

1. INTRODUCTION

1.0 Introduction

Particles dispersed in aqueous solution are common in natural systems and industry. Figure 1.1 shows some typical size ranges of particles. Colloidal particles, roughly 1 nm to 10 μm , are of particular interest because they have appreciable specific surface area and they don't settle out of solution under normal gravity. Therefore, colloids play an important role when surface processes are involved. Henceforth, the term "particle" will refer to a particle in the colloidal size range.

The deposition of colloidal particles from suspension onto solid surfaces is important in many natural and industrial processes. A schematic representation of the particle deposition process is given in Figure 1.2. Granular (deep bed) filtration is one process where particle deposition has great significance. In deep bed filtration, a liquid suspension is passed through a porous filter medium (usually sand grains) where fine particles are removed by deposition onto the surfaces of the filter medium (Tien, 1989). Another area where particle deposition is important is groundwater quality. Particles (e.g., metal oxides, clays, bacteria, and viruses) can undergo transport and deposition in subsurface environments (Ryan and Elimelech, 1996). Contaminants (e.g., metals, radionuclides, and hydrophobic organic compounds) are often associated with colloidal particles in groundwater. The deposition behavior will influence the extent of migration of these particles.

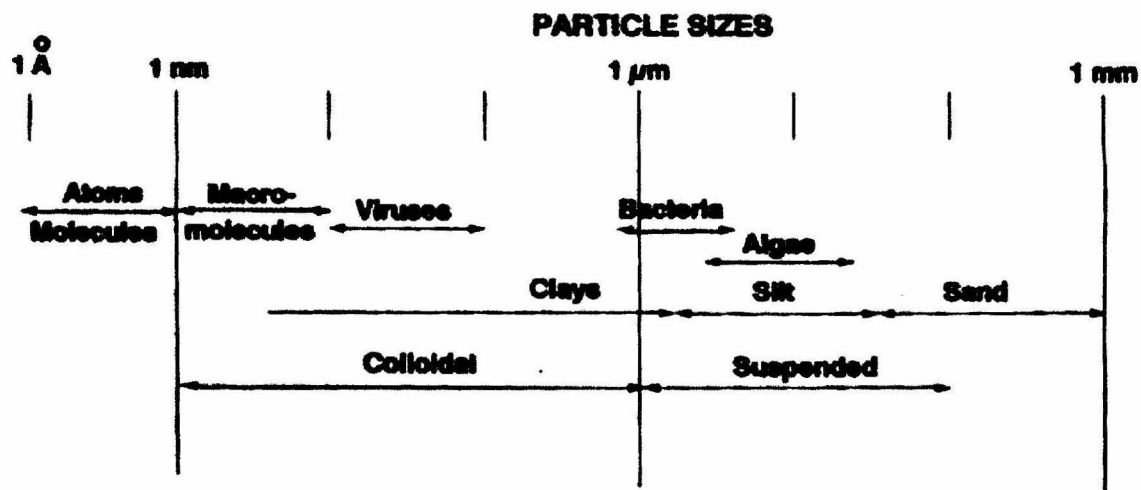


Figure 1.1: Typical size ranges for aqueous particulate matter. Adapted from Stumm and Morgan (1981).

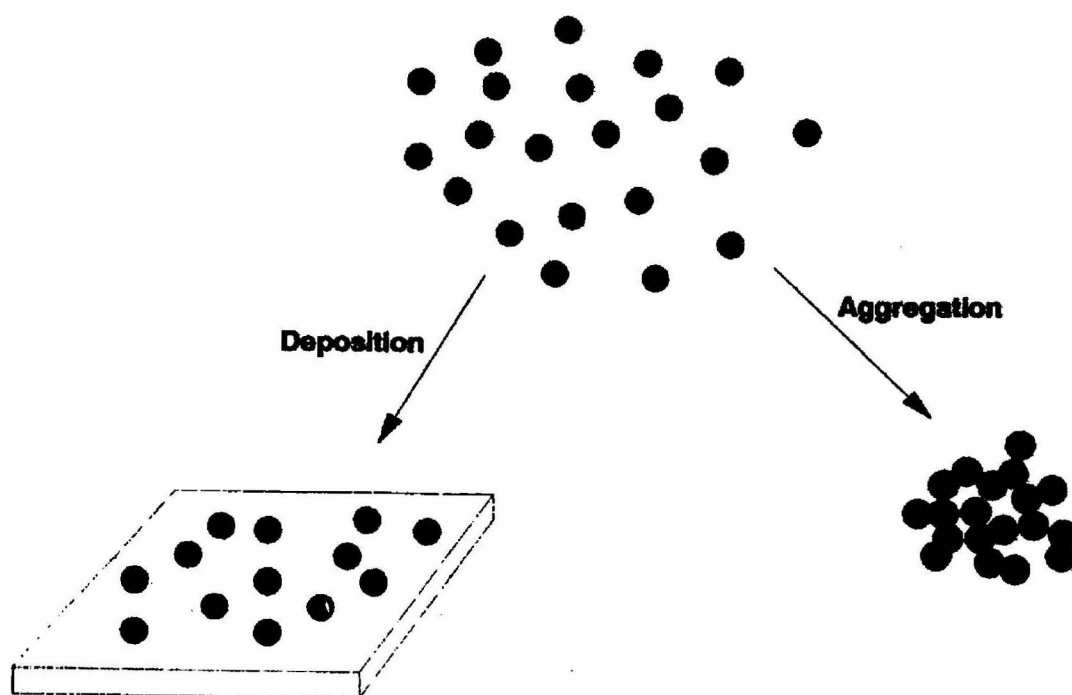


Figure 1.2: Schematic representation of particle deposition and aggregation. From Elimelech et al. (1995).

The main goal of this research is to gain a better understanding of the influence of surface chemistry on particle deposition kinetics in flow through porous media. A hematite particle suspension flowing through a silica sand bed served as a model system.

1.1 Motivation to Use Hematite as Model Colloid

Iron oxides and hydroxides are common in nature because iron is the fourth most abundant element in the earth's crust (4.7%). One of the iron minerals found in the environment is hematite ($\alpha\text{-Fe}_2\text{O}_3$). The formation of iron oxides and hydroxides is thought to result from the dissolution of minerals containing Fe(II), which is subsequently oxidized to form Fe(III). The solubility of Fe(III) oxides and hydroxides is extremely low, consequently precipitates form.

Hematite particles can be synthesized in the laboratory by hydrolysis of Fe(III) salts (Matijevic and Scheiner, 1978). Iron (III) has a strong tendency to form aqueous complexes with many ions. Studies have shown the adsorption of inorganic ions, organic ions, and polymeric organic compounds on iron oxide surfaces (Sigg and Stumm, 1981; Schlautman and Morgan, 1994). Another important reason to use hematite as a model colloid was that Liang (1988) studied the effects of surface chemistry on the coagulation kinetics of colloidal hematite. The results of Liang's (1988) research were valuable in the design of the experimental program for this research. Also, it was desirable to extend the body of knowledge concerning the behavior of hematite particles in aquatic systems.

1.2 Scope and Objectives of Research

A large amount of particle deposition data can be explained, at least in a semiquantitative manner, by the well-known DLVO theory (Derjaguin-Landau-Verwey-Overbeek theory). The basis of DLVO theory is Van der Waals' attraction and

electrostatic repulsion between surfaces. Particle coagulation studies have shown that specifically adsorbed species influence coagulation rates by affecting the surface charge on particles (Liang, 1988; Tiller, 1993). It is expected that specifically adsorbed species will influence particle deposition in a similar fashion.

In general, the goal of this research is to document and explain the impact of small changes in the aqueous chemistry (i.e., addition of specifically adsorbed species) on the deposition kinetics of hematite particles in a silica sand bed. The specific objectives of this research are

- 1) Determine the effect of various inorganic ions on the deposition rates of hematite particles. The species to be investigated are sodium salts of chloride, phosphate, arsenate, and fluoride.
- 2) Determine the effect of various organic species on hematite deposition rates. The species to be studied include (i) butyric acid and lauryl sulfate; (ii) phthalic acid, 1,2,4-benzenetricarboxylic acid, and 1,2,4,5-benzenetetracarboxylic acid; (iii) oxalic acid, succinic acid, adipic acid, and suberic acid; (iv) aspartic acid and polyaspartic acid.
- 3) Determine the effect of naturally occurring organic molecules on hematite deposition rates. The species to be studied are leonardite humic acid, Suwannee River humic acid, and Suwannee River fulvic acid.
- 4) Determine the effect of specifically adsorbed species used in particle deposition experiments on the electrokinetic properties of hematite, and relate the observations to hematite deposition.

- 5) Interpret the particle deposition and electrokinetic results in terms of surface chemical and particle deposition models.

2. Background and Models

2.0 Introduction

The purpose of this chapter is to present the theoretical background necessary for the interpretation of the results of this research.

The removal (deposition) of particles from aqueous suspension by a porous medium is considered to involve two distinct steps: the transport of suspended particles to the surface of a collector (grain), followed by the attachment of particles to the collector surface (Yao et al., 1971). The transport step is controlled by the physics of the system, while the attachment step is controlled by the chemistry of the system (O'Melia and Stumm, 1967). Mass transfer theories are able to successfully describe the particle transport step, as evidenced by the adequate description of particle deposition when conditions for deposition are favorable (i.e., particle deposition is transport limited due to the absence of repulsive forces) (Elimelech, 1991). However, the particle attachment step has not been described successfully. Particle deposition studies under unfavorable conditions (repulsive electrostatic interactions) have shown discrepancies between theoretical predictions and observations of particle deposition rates (Litton and Olson, 1993; Elimelech and O'Melia, 1990). These discrepancies have motivated a great deal of research focused on gaining a better understanding of the particle attachment step. This research, concerned with the effects of surface chemistry on particle deposition, also attempts to add to the understanding of the particle attachment step.

2.1 Clean-Bed Particle Deposition

Like most particle deposition studies to date, this research is concerned with the initial stage of deposition where previously retained particles do not influence the subsequent deposition of particles. This early stage of the particle deposition process is referred to as “clean-bed” deposition. Hence, the particle deposition parameters reported in this thesis can be viewed as “clean-bed” values.

Particle deposition rates in flow through porous media are determined from the response of a packed bed to a step input of suspended particles which is expressed in the form of a particle breakthrough curve. In a breakthrough curve, the effluent particle concentration is plotted as a function of time. A typical particle breakthrough curve for clean-bed deposition is shown in Figure 2.1. The key characteristic of a clean-bed particle breakthrough curve is that the effluent particle concentration remains constant once the breakthrough front passes.

For completeness, what happens when clean-bed conditions no longer exist will be described briefly. When particles retained on the collector surface result in the conditions for deposition becoming less favorable (increase in repulsive interactions), an increasing trend is observed in the particle breakthrough curve. This is referred to as “blocking.” Conversely, when retained particles lead to more favorable deposition conditions, a decreasing trend in the particle breakthrough curve is observed. The term used to describe this event is “ripening” (Tien, 1989). Figure 2.2 shows a graphical depiction of the blocking and ripening phenomena.

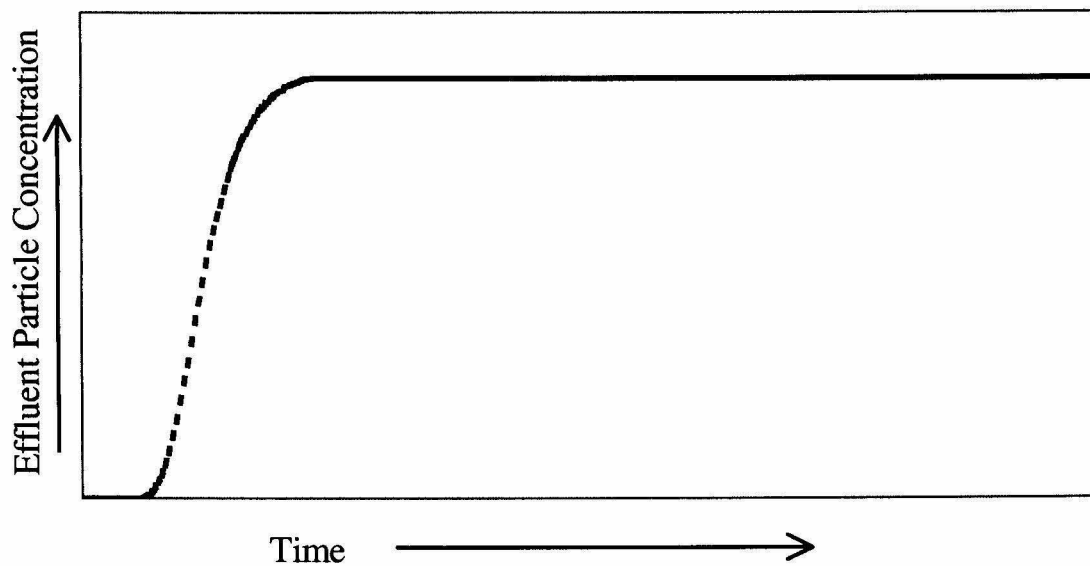


Figure 2.1: Generalized particle breakthrough curve under clean-bed conditions.

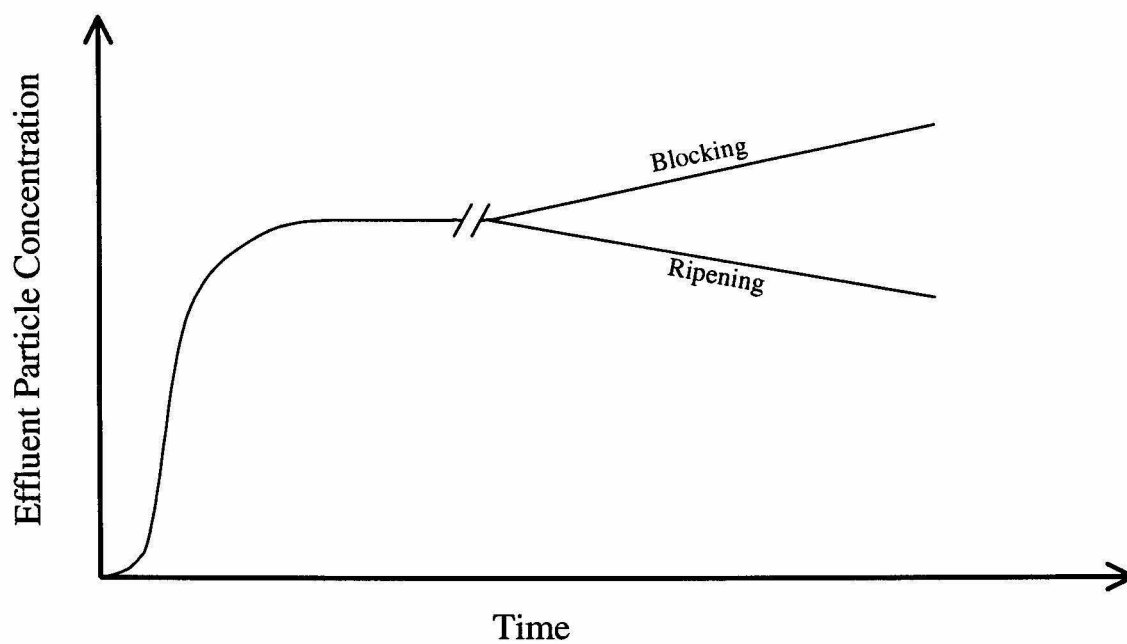


Figure 2.2: Generalized particle breakthrough curve showing blocking and ripening.

2.2 Modeling the Deposition of Brownian Particles

2.2.1 The Advection-Dispersion Equation

In flow through porous media, the spatial and temporal variations in suspended particle concentration can be described in mathematical terms by performing a mass balance on an elemental control volume within a packed bed. Three processes are significant for the construction of a balance equation for particle deposition, and they are

- (i) Hydrodynamic dispersion of particles resulting from uneven velocity profiles within pores and the finite size of colloidal particles.
- (ii) Advection of particles due to their entrainment in the traveling fluid.
- (iii) Removal of particles by deposition onto collector (sand grain) surfaces.

Combining these processes for an aqueous suspension of monodisperse particles flowing vertically through a packed bed of spherical collectors gives the one-dimensional form of the advection-dispersion equation (Bear, 1972; Rajagopalan and Chu, 1982; Grolimund et al., 1998):

$$\frac{\partial C}{\partial t} = D_h \frac{\partial^2 C}{\partial z^2} - v_p \frac{\partial C}{\partial z} - kC \quad , \quad (2.1)$$

where C is the particle concentration in aqueous suspension, t is time, and z is the spatial coordinate (vertical). Since a monodisperse particle suspension is being considered, C can be expressed as a number concentration or a mass concentration.

The first term on the right-hand side of Equation (2.1) accounts for the hydrodynamic dispersion of suspended particles, where D_h is the hydrodynamic dispersion coefficient. In advection-dominated systems, such as vertical flow through packed beds of large, sand-sized grains (collectors), hydrodynamic dispersion is generally of minor significance (Tien, 1989). The second term on the right-hand side of Equation

(2.1) is the advection term. Particles usually travel slightly faster than the average fluid velocity in a porous medium (Mau, 1992). Therefore, determining the particle velocity (v_p) requires an independent equation (Johnson and Elimelech, 1995). The sink term accounting for particle deposition is the last term in Equation (2.1), where k is the particle deposition rate coefficient. The goal of many particle deposition studies, including this research, is to determine the effect of changes in system chemistry on the particle deposition rate (i.e., k).

2.2.2 The Single Collector Efficiency

The particle deposition rate can be calculated from the removal of particles by the porous medium in a packed bed. The accumulation of captured particles in the packed bed is equal to the removal of particles by one collector (grain) multiplied by the number of collectors comprising the bed. At this point, it is useful to consider a dimensionless particle removal rate, η , called the single collector efficiency which is defined as (Yao et al., 1971; Elimelech et al., 1995):

$$\eta = \frac{\text{rate of particle removal by the collector}}{\text{rate of particle transport towards the projected area of the collector}} \quad (2.2)$$

Therefore, the particle removal rate by one spherical collector of radius a_c is $\eta\pi a_c^2 UC$, where U is the fluid approach (superficial) velocity and C is the particle concentration. In order to develop an expression for η , consider a differential slice of packed bed, with height dz and cross-sectional area A_c . The number of collectors in the differential volume, N_c , is given by

$$N_c = \frac{3(1-f)A_c dz}{4\pi a_c^3} \quad (2.3)$$

Consequently, the accumulation of captured particles in the volume element can be stated as

$$\frac{3}{4}\eta(1-f)\frac{U}{a_c}CA_c dz = -QdC \quad , \quad (2.4)$$

where Q is the volumetric flow rate ($Q=UA_c$). Integrating over the entire bed depth with the boundary conditions of $C=C_0$ at $z=0$ and $C=C_e$ at $z=L$ (L is the bed depth) gives

$$\int_{C_0}^{C_e} \frac{dC}{C} = -\frac{3}{4a_c}\eta(1-f)\int_0^L dz \quad (2.5)$$

Performing the integration results in

$$\eta_{\text{exp}} = -\frac{4}{3}\frac{a_c}{(1-f)L}\ln\left(\frac{C_e}{C_0}\right) \quad , \quad (2.6)$$

where C_e/C_0 is the normalized effluent particle concentration taken from the particle breakthrough curve of a deposition experiment and the subscript “exp” is used to indicate that the value is based on experimental results.

2.2.3 Experimental Collision Efficiency

When the particle deposition rate is slower than the transport limited rate (i.e., unfavorable deposition) due to repulsive interactions between the particle and collector surfaces, it is convenient to express the results in terms of the collision efficiency α (also termed attachment efficiency or sticking probability) (Ryan and Elimelech, 1996). Since the collision efficiencies considered in this research are determined from experiment, the experimental collision efficiency, α_{exp} , will be used. The experimental collision efficiency is defined as the ratio of the measured particle deposition rate to the particle deposition rate under favorable chemical conditions (i.e., in the absence of repulsive

interactions). For particle deposition in granular porous media, the experimental collision efficiency is given by

$$\alpha_{exp} = \frac{\eta_{exp}}{\eta_0} \quad , \quad (2.7)$$

where η_0 is the single collector efficiency under transport limited (favorable) conditions. The value of α_{exp} is between 0 (no deposition of particles) and 1 (particle deposition is transport limited).

Two approaches can be used to determine experimental collision efficiencies. In one approach, the collision efficiency is calculated as the ratio of the measured particle deposition rate (presented as η_{exp}) to the theoretical particle deposition rate under favorable conditions (η_0). The favorable single collector efficiency (η_0) is calculated from the advection-dispersion equation without including a term for electrostatic interactions. In the second approach, the collision efficiency is calculated from the ratio of the measured particle deposition rate (η_{exp}) to the measured particle deposition rate under favorable chemical conditions ($\eta_{0,exp}$).

The second approach for determining the experimental collision efficiency was used in this research. Favorable particle deposition was achieved by having the particles and collectors oppositely charged. At pH 6.5 and in the absence of specifically adsorbed species, the hematite particles are positively charged ($\text{pH}_{zpc} \sim 7.5$) and the silica sand grains are negatively charged ($\text{pH}_{zpc} \sim 2$). However, under these conditions there can be a significant enhancement in the particle deposition rate beyond the transport limited case because of the long range of the attractive electrostatic interactions. Therefore, the

particle deposition rate had to be measured at a high enough ionic strength so as to eliminate any possible enhancement of the transport limited deposition rate.

One must be aware of potential problems with using the measured single collector efficiency under favorable deposition conditions. At high ionic strength, particle coagulation may become significant. The formation of doublets, triplets, and higher-order aggregates prior to and during deposition would probably result in measured deposition rates different from the value for a monodisperse suspension. Also, at high ionic strength, hydration forces can result in additional repulsive interactions as particles approach collectors (Israelachvili, 1992). Preliminary experiments showed that these potential problems were not significant.

2.3 Colloidal Interactions in Aquatic Systems

The types of interaction that exist between particles or a particle and a surface as they approach each other will be presented. DLVO theory is based on two primary interactions, electrostatic and London-Van der Waals forces. The theory, which was developed to quantify the stability of colloidal suspensions, was introduced independently by Derjaguin and Landau, and Verwey and Overbeek (Derjaguin and Landau, 1941; Verwey and Overbeek, 1948).

2.3.1 London-Van der Waals Attraction Energy

London-Van der Waals forces result in a short-range attraction energy between atoms, molecules, and macroscopic bodies. These forces are a consequence of the fluctuation of charge in one atom polarizing another atom, and the other way around. For a colloidal particle and a collector grain, it is assumed that the pairwise attraction energies between atoms of the particle and the atoms of the collector are purely additive.

Following this assumption of pairwise additivity, Hamaker (1937) developed expressions to evaluate the attraction energy. For the sphere-plate case (corresponding to a particle and collector), the London-Van der Waals attraction energy is given by

$$V_A = -\frac{A}{6} \left[\frac{a_p}{h} + \frac{a_p}{h + 2a_p} + \ln \left(\frac{h}{h + 2a_p} \right) \right] , \quad (2.8)$$

where a_p is the particle radius, h is the distance of separation, and A is the Hamaker constant. The Hamaker constant depends on the composition of the two interacting solids and the medium that separates the two bodies (aqueous solution for this research). Typically, A lies between 10^{-21} Joules and 10^{-19} Joules (Elimelech, 1995).

2.3.2 Electrostatic Interaction

Metal oxides, like hematite ($\alpha\text{-Fe}_2\text{O}_3$) and silica (SiO_2), acquire charge when in contact with water. In order to maintain overall electroneutrality in the system, the aqueous medium near the oxide surface must develop equal charge of opposite sign. The result is a fixed layer of charge on the solid surface and a “diffuse layer” of charge adjacent to the fixed layer, which together are called the electrical double layer. The diffuse layer contains an excess of counter ions, opposite in sign to the fixed charge. The Gouy-Chapman theory describes the charge distribution and electric potential function in the diffuse layer (Stumm and Morgan, 1981).

When a particle approaches a collector at a short distance, the diffuse layers overlap causing electrostatic attraction or repulsion. Electrostatic attraction will not be considered further because it results in conditions favorable for particle deposition, which can be successfully described using transport theory (see Section 2.0). The repulsive interaction energy involved when a particle and collector have equal signs can be

calculated in two ways. One is to solve the Poisson-Boltzmann equation directly for a given set of conditions, but a simple analytical solution usually cannot be achieved. The other way is to build the formula from known expressions for each of the geometries involved (sphere-plate for particle deposition). A presentation of several expressions of this type is given by Elimelech et al. (1995). One such expression for the double layer interaction energy V_R , under constant surface charge conditions, is by Wiese and Healy (1970):

$$V_R = \pi\epsilon_0\epsilon a_p \left\{ 2\psi_1\psi_2 \ln\left(\frac{1 + \exp(-Kh)}{1 - \exp(-Kh)}\right) - (\psi_1^2 + \psi_2^2) \ln[1 - \exp(-2Kh)] \right\}, \quad (2.9)$$

where ϵ_0 is the permittivity in vacuum, ϵ is the relative permittivity, a_p is the particle radius, ψ_1 and ψ_2 are the surface potentials of the particles and collectors respectively, h is the distance of separation, and K^{-1} is the Debye-Hückel length. The equation is valid for (i) low surface potentials (less than 60 mV), (ii) $Ka_p > 5$, and (iii) 1:1 electrolyte. The Debye-Hückel length defines the diffuse layer thickness, and is given by

$$K^{-1} = \left(\frac{2 \times 10^3 e^2 N_A I}{\epsilon_0 \epsilon k T} \right)^{-1/2}, \quad (2.10)$$

where e is the elementary charge of an electron, N_A is Avogadro's number, I is the ionic strength, and k is Boltzmann's constant. For typical aqueous solutions, the diffuse layer thickness, $1/K$, ranges from 1-100 nm. The deposition experiments of this research had 10^{-3} moles/L NaCl which results in a diffuse layer thickness of approximately 10 nm.

2.3.3 Total Interaction Energy (DLVO Theory)

The combination of electrostatic and Van der Waals forces is the basis of DLVO theory. The total interaction energy V_T between a particle and collector is obtained by summing the electrostatic interaction (V_R) and Van der Waals interaction (V_A) (i.e.,

$V_T=V_R+V_A$). A total interaction energy profile results when V_T is shown as a function of separation distance. Figure 2.3 shows a typical total interaction energy profile when electrostatic repulsion is significant. Some general properties of the total interaction energy, with respect to particle deposition, are

- 1) When electrostatic repulsion exceeds Van der Waals attraction over a certain range, the resulting energy barrier hinders the approach of particles and prevents contact with the collector.
- 2) If the energy barrier is not present (i.e., no electrostatic repulsion), particles will deposit at a transport limited rate due to Van der Waals attraction.
- 3) Particle deposition rates can be decreased by raising the energy barrier (i.e., increasing the electrostatic repulsion). Increased electrostatic repulsion can be achieved by the addition of specifically adsorbed species that reverse the charge on the particles to the same sign as the charge on the collectors.

2.4 Oxide/Water Interface

2.4.1 The Origin of the Surface Hydroxyl Group

Dry metal oxide surfaces (e.g., hematite and silica) have metal ions that are not fully coordinated. When contacted by water, the surface metal ions coordinate with water molecules. Surface hydroxyl groups are produced by proton transfer from the adsorbed water molecules to nearby surface oxygen atoms (Schindler, 1981). This chemisorption process is shown schematically in Figure 2.4.

Various adsorption studies have reported values from 4.5 to 9 OH groups per nm^2 (Jurinak, 1966; Micale et al., 1985). Infrared spectroscopy studies suggest that multiple

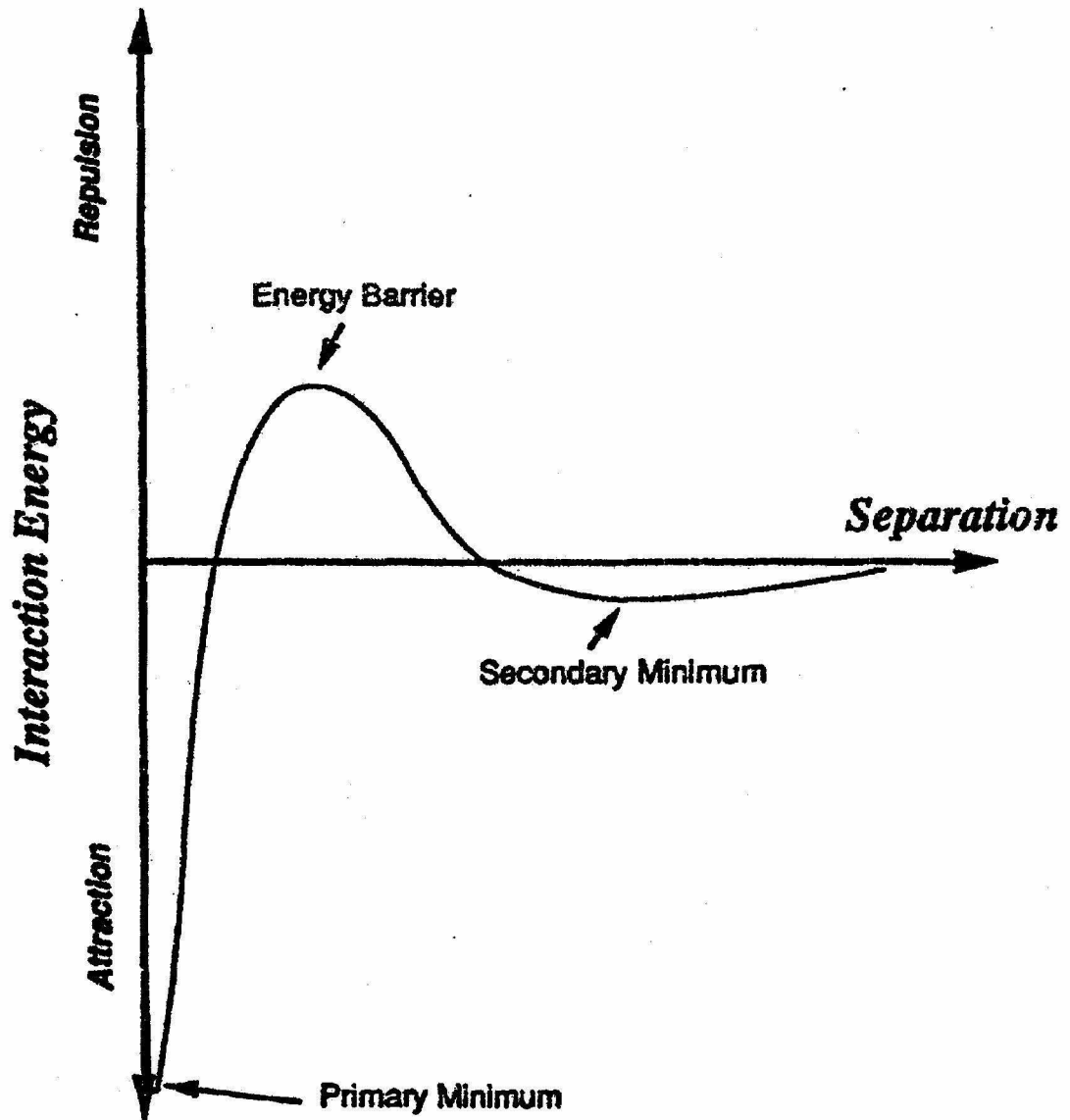
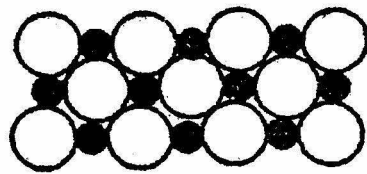
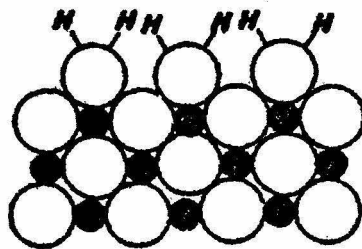


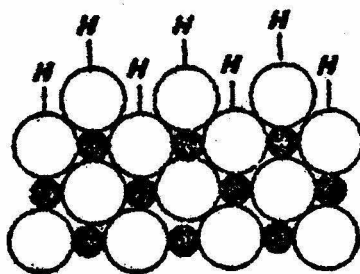
Figure 2.3: Typical total interaction energy profile when electrostatic repulsion is significant. (Units are arbitrary).



(a)



(b)



(c)

Figure 2.4: Schematic representation of the metal oxide surface layer (cross section).

● Metal atoms: ○ oxygen atoms. a) Dry metal oxide. b) Water molecules fill vacant coordination sites. c) Proton transfer produces surface hydroxyl groups. From Schindler (1981).

types of surface hydroxyl groups exist (Parfitt, 1978). However, for modeling purposes they are usually described by a single surface hydroxyl group (depicted as $\equiv\text{MeOH}$).

2.4.2 Surface Chemical Speciation Model

The surface charge on metal oxides exhibits a pH dependence because surface hydroxyl groups can gain or lose protons. Besides protons, other cations and anions can react with surface hydroxyl groups to determine surface speciation and charge (Stumm et al., 1980). Acid-base reactions at metal oxide surfaces result in three types of surface species. The reactions are expressed as follows:



The equilibrium constants are defined by

$$K_{a1}^{\text{int}} = \frac{(\equiv\text{MeOH})(\text{H}^+)}{(\equiv\text{MeOH}_2^+)} = \frac{[\equiv\text{MeOH}](\text{H}^+)}{[\equiv\text{MeOH}_2^+]} \frac{\gamma_{\equiv\text{MeOH}}}{\gamma_{\equiv\text{MeOH}_2^+}} \quad (2.13)$$

$$K_{a2}^{\text{int}} = \frac{(\equiv\text{MeO}^-)(\text{H}^+)}{(\equiv\text{MeOH})} = \frac{[\equiv\text{MeO}^-](\text{H}^+)}{[\equiv\text{MeOH}]} \frac{\gamma_{\equiv\text{MeO}^-}}{\gamma_{\equiv\text{MeOH}}}, \quad (2.14)$$

where the “int” superscript indicates an intrinsic constant, () represents activity, [] represents concentration, and γ_i is the activity coefficient for species i .

The charged surface species, $\equiv\text{MeOH}_2^+$ and $\equiv\text{MeO}^-$, produce surface charge and potential. An expression for the surface charge density (σ) is given by

$$\sigma = ([\equiv\text{MeOH}_2^+] - [\equiv\text{MeO}^-]) \frac{F}{S_a \cdot S_c}, \quad (2.15)$$

where F is the Faraday constant, S_a is the specific surface area of the solid, and S_c is the solid concentration in g/L. Applying a proton material balance to titration data allows the surface charge density to be evaluated by

$$\sigma = (C_A - C_B + [\text{OH}^-] - [\text{H}^+]) \quad , \quad (2.16)$$

where C_A and C_B are the resulting concentrations of acid and base, respectively, added to the system during titration. The relation of surface charge to pH is described by Equation (2.16). The pH value where proton-derived surface charge is zero (i.e., $[\equiv\text{MeOH}_2^+] = [\equiv\text{MeO}^-]$) is defined as pH_{zpc} . For the hematite used in this research, the pH_{zpc} determined from mobility measurements was 7.5. This is in the range of 6.5 to 9 reported by other investigators (Amirbahman and Olson, 1995; Tiller, 1993; Liang, 1988). The pH_{zpc} for the silica sand used in this research is approximately 2.2, which is similar to values reported in the literature (Litton and Olson, 1993; Elimelech et al., 2000).

2.4.3 Models of the Oxide/Water Interface

To effectively model adsorption on metal oxide surfaces, an electrostatic model is needed in addition to a description of surface chemical reactions. Inclusion of an electrostatic model facilitates surface species activity corrections in the presence of charged surfaces. There have been a number of surface complexation models developed, but they are based on the same fundamental principles (Dzombak and Morel, 1990):

- 1) Adsorption takes place at specific coordination sites.
- 2) Mass law equations can be used to describe adsorption reactions.
- 3) Adsorption results in surface charge on metal oxides.
- 4) A correction factor derived from electrical double layer theory can be used to account for the effect of surface charge on adsorption.

The diffuse layer model (Stumm et al., 1970) is used in this research to make model calculations to aid in the interpretation of experimental results. The model assumes a layer of fixed charge on the surface of the oxide with a diffuse layer of opposite charges in solution. The charges in the diffuse layer are distributed according to the Boltzmann distribution. The model is incorporated into the computer code MINEQL+ (Environmental Research Software). The reasons for choosing the diffuse layer model are: (i) it has the least number of fitting parameters as a result of the simple physical representation of the interface, and (ii) since the diffuse layers of a particle and collector overlap upon close approach, it is necessary to have a diffuse layer included in a model relating to particle deposition.

Restating the equilibrium constant expressions given in Equations (2.13) and (2.14) in terms of an electrostatic correction factor gives

$$K_{a1}^{int} = \frac{[\equiv \text{MeOH}](\text{H}^+)}{[\equiv \text{MeOH}_2^+]} \exp\left(-\frac{F\psi_0}{RT}\right) = K_{a1}^{app} \exp\left(-\frac{F\psi_0}{RT}\right) \quad (2.17)$$

$$K_{a2}^{int} = \frac{[\equiv \text{MeO}^-](\text{H}^+)}{[\equiv \text{MeOH}]} \exp\left(-\frac{F\psi_0}{RT}\right) = K_{a2}^{app} \exp\left(-\frac{F\psi_0}{RT}\right) , \quad (2.18)$$

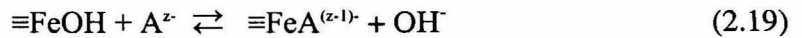
where ψ_0 is the surface potential and the superscript “app” indicates apparent constants which vary with surface charge and pH. Apparent constants can be determined experimentally, while intrinsic constants are determined by extrapolating apparent constants to zero surface charge.

2.4.4 Adsorption of Anions on Hematite

The deposition rate of hematite particles in packed beds of silica sand is expected to depend on the adsorption of inorganic and organic anions since the adsorption process

affects the hematite surface charge and potential. It should be noted that anion adsorption on silica (sand grains) is not expected to be important. There is no evidence that anions (either inorganic or organic) adsorb appreciably to silica surfaces at near neutral pH (experiments for this work were conducted at pH 6.5). Davis (1982) observed measurable amounts of natural organic matter on colloidal silica only at pH values less than 3. Therefore, the adsorption of anions on hematite will only be considered.

Specific adsorption can often be modeled as a ligand exchange process (Stumm et al., 1980), in which anion surface complexation releases hydroxyl ions:



The formation of bidentate complexes is possible, depending on ligand size and spacing of surface coordination sites. Examples of possible surface complexation reactions between hematite and a diprotic acid (e.g., oxalic acid or phthalic acid) are depicted in Figure 2.5. The effect of anion adsorption on the surface charge of hematite can be illustrated by the general equation for surface charge (σ):

$$\sigma = \frac{F}{S_a \cdot S_c} ([\equiv\text{FeOH}_2^+] - [\equiv\text{FeO}^-] - \sum_i (z_i - 1)[\equiv\text{FeA}_i^{(z_i-1)-}]) \quad , \quad (2.20)$$

where F , S_a , and S_c are as described in Equation (2.15) and z_i is the valence on anion A_i . If the affinity of an anion for the hematite surface is strong enough, specific adsorption may not only reduce the magnitude of the surface charge, but also reverse its sign. This has been observed by Liang (1988) for the adsorption of phosphate, humic acid, and other anions on hematite below pH_{zpc} (i.e., hematite has a positive surface charge in the absence of specifically adsorbed anions). Kallay and Matijevic (1985) also observed the charge reversal of hematite below pH_{zpc} due to the adsorption of oxalic and citric acids.

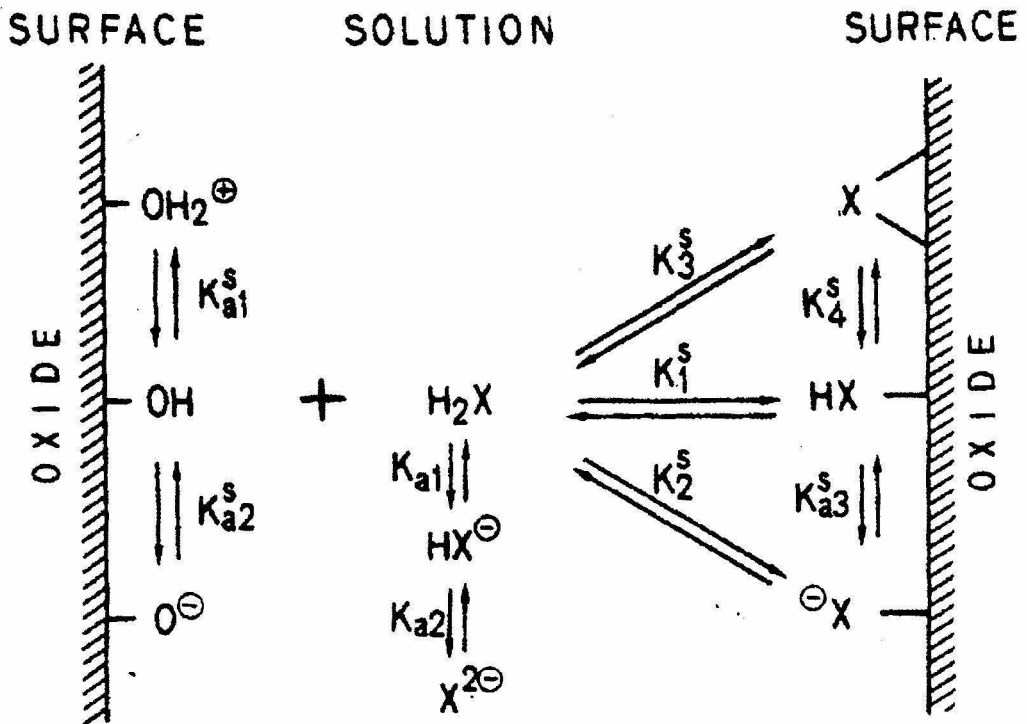


Figure 2.5: Schematic representation of possible surface complexation reactions of the diprotic acid H_2X (e.g., oxalic acid or phthalic acid) with the surface hydroxyl groups of hematite. From Kummert and Stumm (1980).

The tendency of an anion to form surface complexes follows the same trend as the anion's tendency to form anion-metal complexes in solution (Stumm and Morgan, 1981). Therefore, strong complexes in solution correspond to strong complexes at the metal oxide surface. This allows the equilibrium constants for an anion surface complex to be estimated from equilibrium constants for solution complexes, when equilibrium constants for surface complexes are not available.

3. Materials and Methods

3.0 General Remarks

All solutions were prepared with deionized water purified by a Millipore Milli-Q UV Plus system ($R=18.2 \text{ M}\Omega \text{ cm}$). Reagents were analytical grade and were used without further treatment. One fulvic and two humic acids were obtained from the International Humic Substances Society. The humic acids were leonardite humic acid which was isolated from a leonardite (also referred to as lignite) deposit (oxidized coal) in southeastern North Dakota, U.S.A.; and Suwannee River humic acid which was isolated from the Suwannee River near Fargo, Georgia, U.S.A. The fulvic acid was Suwannee River fulvic acid.

In general, pyrex glassware was used. The glassware was first cleaned in an ultrasonic bath (Bransonic model 1210) with a detergent solution (Micro® cleaning solution), soaked in 2.5 molar nitric acid at 45° C, rinsed with Milli-Q water, and finally oven dried.

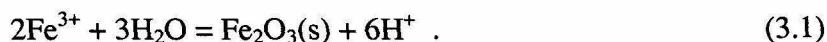
The pH of solution was monitored using a Beckman glass combination electrode (BK 511063) and a pH meter (Beckman model Φ 11 pH meter). NIST buffers were used to calibrate the pH electrode.

3.1 Particle Preparation and Characterization

3.1.1 Preparation of Hematite Particles

Hematite particles ($\alpha\text{-Fe}_2\text{O}_3$) were synthesized following the method of Liang (1988). A concentrated aqueous solution of $\text{Fe}(\text{ClO}_4)_3/\text{HClO}_4$ was quickly added to

Milli-Q water preheated to 100° C and mixed. The dilution ratio was 1 to 20, and the final solution concentrations of H⁺ and Fe(III) were 0.05 M and 0.035 M, respectively. The mixture was covered and placed in an oven at 100° C for 24 hours. The forced hydrolysis process that results in hematite formation can be described by



After the 24-hour heating period, the suspension was cooled to room temperature. The supernatant was drawn off and the remaining particles were soaked in 0.01 M HClO₄ for 24 hours. The procedure was repeated three times in order to remove amorphous iron oxide coatings that might be present (Faust, 1985). The final suspension was stored as stock at pH~3. The maximum yield of hematite particles possible from this synthesis procedure is approximately 4 g, when starting from a 1 liter mixture of Fe(ClO₄)₃/HClO₄ solution and heated Milli-Q water. However, due to incomplete conversion of Fe(III) to hematite (α -Fe₂O₃) and loss of particles in the repeated removal of supernatant solutions, the actual yield of hematite particles was approximately 1 g.

3.1.2 Particle Characterization

The mineral phase of the synthesized particles was determined by X-ray diffraction analysis using a Scintag PAD-5 X-Ray Diffractometer with an automated $\theta/2\theta$ goniometer. The observed diffraction pattern for the synthesized particles (Figure 3.1, top) is very similar to the diffraction pattern of standard hematite (Figure 3.1, bottom). This confirms that the synthesis procedure was successful in producing hematite as the bulk material.

The size and shape of the hematite particles were determined by TEM (Phillips 430 (300 kV) Analytical Electron Microscope). The chemical and heating conditions of

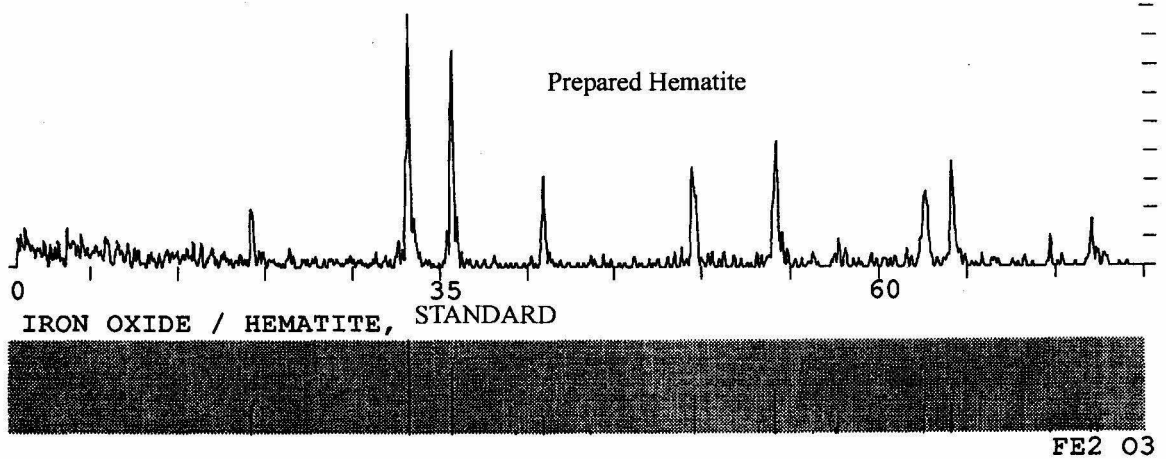


Figure 3.1: X-ray diffraction pattern of hematite prepared for this research (top) compared to the diffraction pattern for a hematite standard (bottom). The patterns match, suggesting that the synthesis procedure was successful in producing hematite.

each synthesis influence the particle size and shape (Matijevic and Scheiner, 1978). Plate I shows the particles to be approximately spherical with an average diameter of 67 nm (taken as average of 20 particles). Additional information on particle size was obtained using the technique of dynamic light scattering to measure the hydrodynamic size (ZetaPALS with a particle sizing BI-MAS accessory, Brookhaven Instruments, N.Y.). The hydrodynamic diameter was observed to be 82 ± 2 nm. One would expect the hydrodynamic diameter to be larger than the actual diameter because it is the diameter of a hypothetical hard sphere that diffuses with the same speed as the particle under consideration. However, the synthesized hematite particles are not perfect spheres, they tumble, and have water molecules associated with them which would result in the measured hydrodynamic diameter being greater than the actual diameter. In subsequent discussions and calculations, the diameter determined from transmission electron

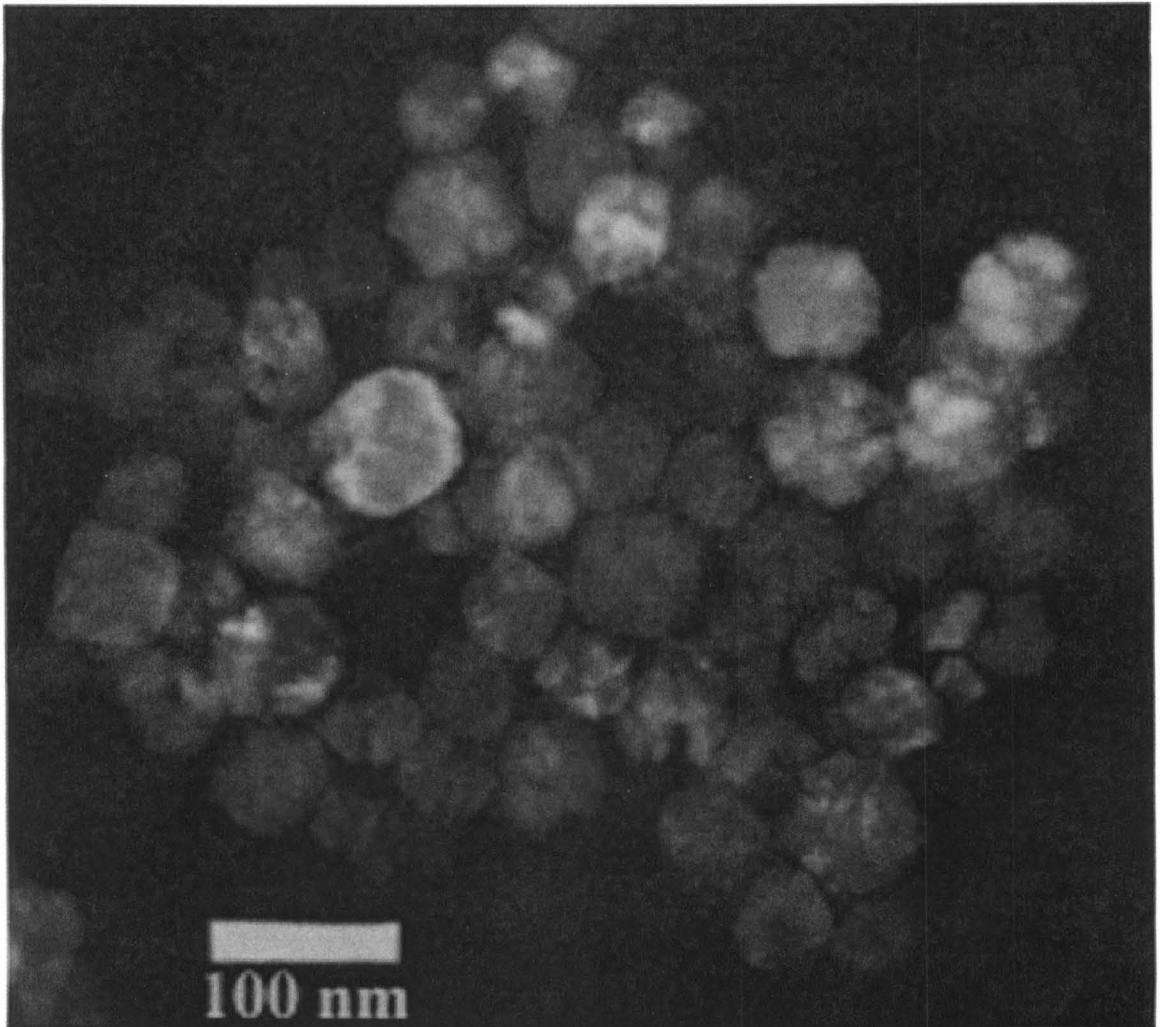


Plate I: Transmission electron micrograph of synthesized hematite particles used in this research.

micrographs (i.e., 67 nm) will be used. The properties of the hematite particles used in this study and others (both coagulation and deposition studies) are summarized in Table 3.1.

Reference	Sample Preparation	Particle diameter (nm)	pH _{zpc}
Liang (1988) (Coagulation)	Hydrolysis of Fe(ClO ₄) at 100°C	70	8.5
Tiller (1993) (Coagulation)	Hydrolysis of FeCl ₃ at 100°C	60	9.5
Kuo and Matijevic (1980) (Deposition)	Hydrolysis of FeCl ₃ at 100°C	170	7.5
Amirbahman and Olson (1993) (Deposition)	Hydrolysis of Fe(ClO ₄) at 100°C	170	6.5
This work (Deposition)	Hydrolysis of Fe(ClO ₄) at 100°C	67	7.5

Table 3.1: Comparison of hematite properties.

3.2 Particle Surface Properties

3.2.1 Specific Surface Area

The specific surface area was calculated by assuming that the particles were perfect spheres. Under this assumption, the specific surface area, S_a , was estimated to be 17.1 m²/g using the following equation:

$$S_a = \frac{1}{\rho} \left(\frac{\pi d^2}{\pi d^3 / 6} \right) = \frac{6}{\rho d} \quad , \quad (3.2)$$

where ρ is the density (taken as 5.24 g/cm³) and d is the particle diameter (67 nm, as determined by TEM).

3.2.2 Surface Site Density

The synthesis procedure, mineral phase, size, and shape of the particles synthesized for this study are similar to those of the particles used by Liang (1988) (i.e.,

approximately spherical hematite particles with an average diameter of 70 nm). Liang (1988) studied the effect of surface chemistry on coagulation kinetics and was a valuable resource for this particle deposition study. Due to these similarities and the need to conserve particles so that the experimental program could be completed using the same batch of particles, the surface site density for the particles of this study was taken to be that measured for Liang's particles (4.98 ± 0.5 sites/nm²).

3.3 Granular Porous Medium

3.3.1 Porous Medium Physical and Chemical Composition

A silica sand (Ottawa 30 sand, U.S. Silica, Ottawa, IL) was used as the model collectors in this research. The chemical composition of Ottawa 30 sand, as reported by the manufacturer, is given in Table 3.2.

Sieve analysis of the sand, shown in Figure 3.2, was performed by Eylers (1994), who used the Ottawa 30 sand along with another sand to study the transport of metal ions between stream water and sediment bed. The geometric mean (d_g) and the geometric standard deviation (σ_g) for the grain size, computed for the middle 80% of the size distribution, are 500 μm and 1.25, respectively. Plate II shows a photograph of some Ottawa 30 sand grains magnified 5 times (Zeiss Axioplan 2 Imaging equipped with an Axiocam digital camera). The shape of the grains is prolate spheroidal with a nominal grain diameter of 520 μm . The nominal grain diameter was determined by averaging the minor and major axes of 25 sand grains.

Mineral	Ottawa 30 sand
SiO ₂	99.81%
Fe ₂ O ₃	0.015%
Al ₂ O ₃	0.042%
TiO ₂	0.013%
CaO	<0.01%
MgO	<0.01%
Na ₂ O	<0.01%

Table 3.2: Chemical composition of Ottawa 30 sand (as reported by the supplier).

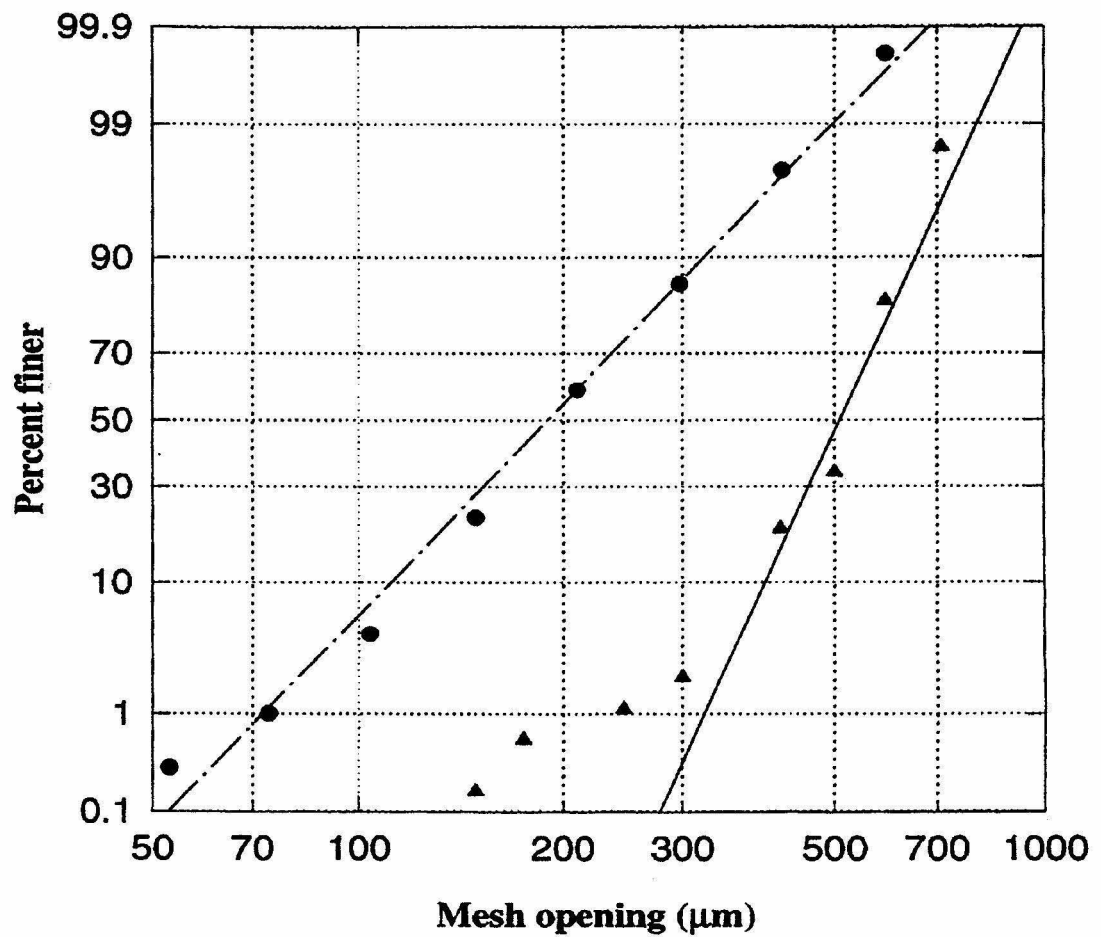


Figure 3.2: Sieve analyses of Ottawa 30 sand. From Eylers (1994).

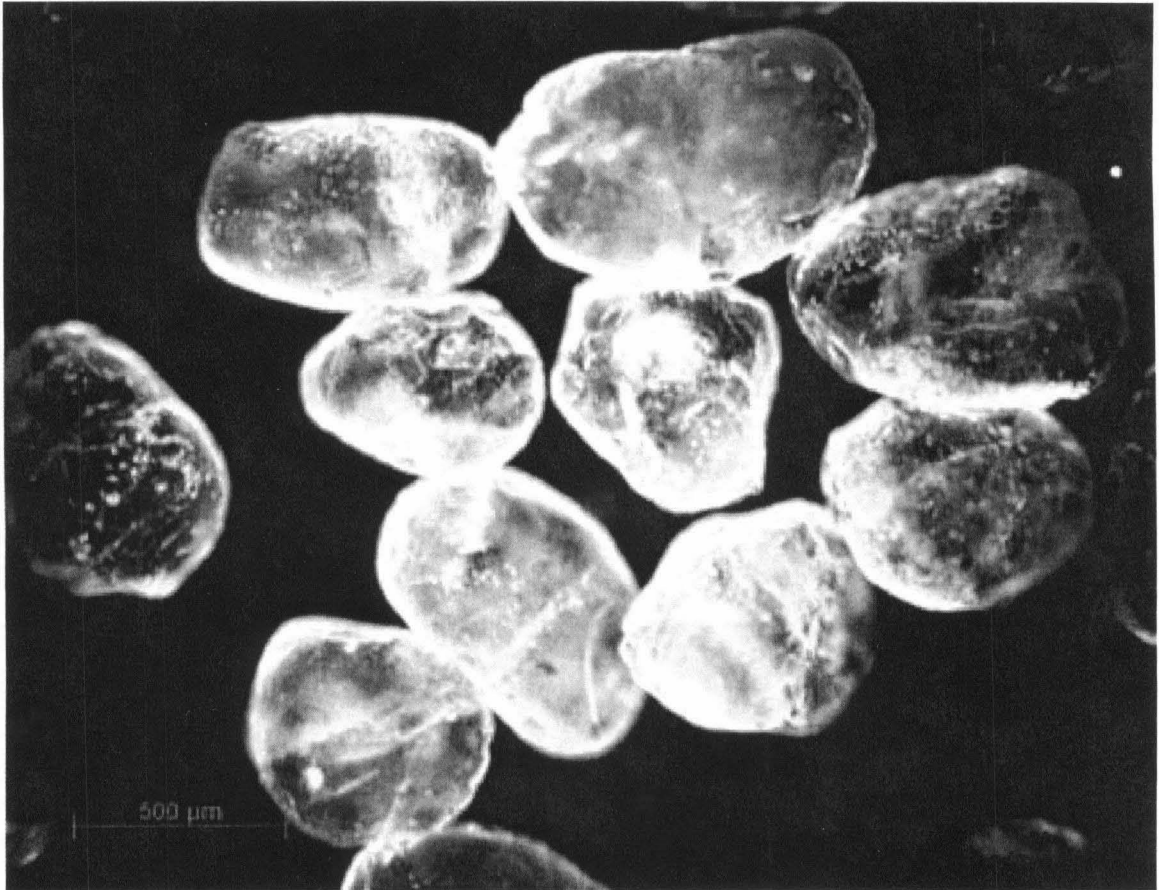


Plate II: Darkfield photograph (under 5x magnification) of the sand grains used in this research.

The porosity (pore space/total volume) of the Ottawa 30 sand was determined by measuring the volume of water required to fill the pore space of a sand bed packed by the “tap and fill” method which is the same way columns were packed for deposition experiments. In the tap and fill method, sand is slowly poured into a column containing water while the column is continuously tapped with a rubber mallet. Maintaining a free surface of water during the filling process keeps air bubbles from being incorporated in the sand bed, and continuous tapping allows for uniform packing. The porosity of Ottawa 30 sand determined in this manner was 0.34. The mineral density of the sand was found to be 2.63 g/cm^3 by placing a known amount of dry sand in a graduated cylinder and measuring the volume of water displaced.

3.3.2 Cleaning of Porous Medium

The sand cleaning procedure employed in this research was similar to that used by Elimelech et al. (2000). The steps are as follows:

1. Sonicate for 30 minutes in deionized water.
2. Soak in Sodium dithionite ($0.1 \text{ M Na}_2\text{S}_2\text{O}_4$) for 4 hours to remove surface impurities such as iron and manganese oxides.
3. Soak in chromic/sulfuric acid cleaning solution (Chromerge, Fisher Scientific, Pittsburgh, PA) for 12 hours.
4. Sonicate for 30 minutes in deionized water.
5. Soak in 5% hydrogen peroxide for 4 hours to remove organic impurities.
6. Soak in chromic/sulfuric acid cleaning solution for 12 hours.
7. Sonicate for 30 minutes in deionized water.
8. Soak in 12 N HCl for 12 hours.

9. Sonicate for 30 minutes in deionized water.

10. Dry at 50° C and store in sealed flask.

Between each of the above steps, the sand was repeatedly washed with deionized water until the conductivity of the supernatant was equal to that of deionized water ($\sim 2 \mu\text{S}/\text{cm}$).

3.4 Electrophoretic Mobility Measurements

3.4.1 Electrophoretic Mobility of Hematite Particles

Hematite particle mobilities were measured using a ZetaPALS instrument (Brookhaven Instruments, N.Y.). The ZetaPALS determines particles mobilities using Phase Analysis Light Scattering. Samples were prepared by adding appropriate amounts of Milli-Q water, NaCl stock, hematite stock, and specifically adsorbed ligand stock to a glass cuvette (total sample volume was 1.4 mL). The samples were ultrasonicated (in the glass cuvette) for 20 seconds (Bransonic model 1210 bath), the electrode assembly was inserted, and the mobility measurement was started.

It would have been ideal to use the same particle concentration as in the deposition experiments (influent concentration of 1 mg/L), since the particle mobility measurements were made to assist in the interpretation of the particle deposition results. However, preliminary measurements showed that a particle concentration of at least 10 mg/L was needed to give reproducible results. As the particle concentration approached 100 mg/L, the sample became too turbid for reproducible results. Therefore, the particle mobility measurements were made using 10 mg/L hematite. Some of the measurements were repeated using 50 mg/L, in order to elucidate the effect of particle concentration on mobility.

3.4.2 Electrophoretic Mobility of Sand Particles

For electrophoretic mobility studies, particles within the colloidal size range are needed so as to avoid settling. Therefore, whole sand grains can't be used in such measurements. Typically, sand grains are ground into particles suitable for electrophoretic mobility measurements using a mortar and pestle (Amirbahman and Olson, 1993) or rock mill (Johnson, 1999). To generate sub-micron sized sand particles for this research, the approach of Johnson et al. (1996) was used in which sand grains were ultrasonicated in deionized water for 10 minutes. Approximately 100 mL of sand and 200 mL of Milli-Q water were used. The supernatant becomes turbid as a result of sand particles being removed from the surface of the sand grains. This sand particle suspension was diluted by a factor of 25 to make electrophoretic mobility measurements in the same manner as the hematite particle mobility measurements. The size of the sand particles was also measured on the ZetaPALS instrument. A bi-modal distribution was observed with peaks at about 200 and 600 nm.

3.5 Particle Deposition Experiments

3.5.1 Experimental Apparatus for Particle Deposition

The model system for particle deposition was made up of the silica sand (Ottawa 30) packed in a cylindrical column. The experimental apparatus used in this research is described schematically in Figure 3.3 and is comprised of the following components:

- a) H₂O reservoir (pH 6.5 Milli-Q H₂O in 300 mL flask)
- b) Particle suspension (2 mg/L hematite, pH 6.5, in a 125 mL flask)
- c) Peristaltic pump with adjustable flow rate of 0-5 mL/min (Masterflex model U-07554-85, Cole-Parmer Instrument Co., Vernon Hills, IL) equipped with an

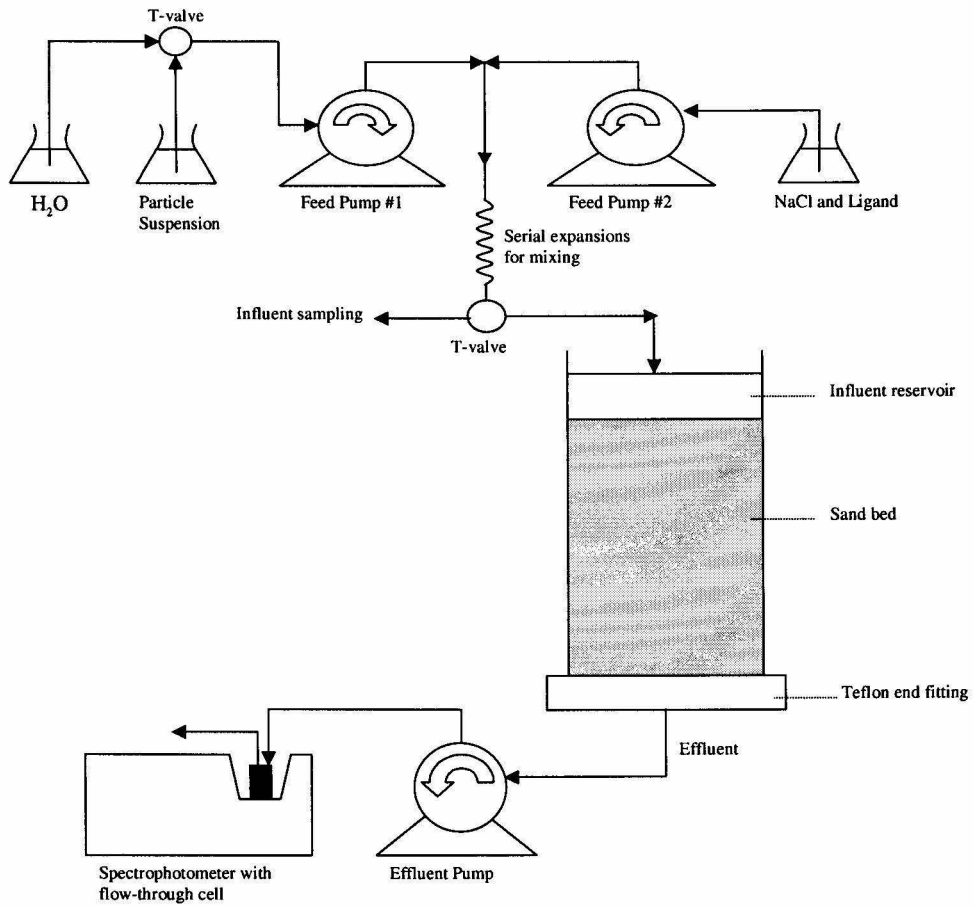


Figure 3.3: Schematic diagram of the particle deposition apparatus.

- eight-roller mini-cartridge pump head (Ismatec model 95600-36, Cole-Parmer Instrument Co.).
- d) NaCl/ligand solution (2 mM NaCl, variable ligand concentration, pH 6.5, in a 300 mL flask).
 - e) Isocratic pump with adjustable flow rate of 0-10 mL/min (Model G1310A, series 1100 iso-pump, Hewlett Packard).
 - f) Series of ten tubing expansions and contractions for mixing.
 - g) Cylindrical pyrex glass column of 3.07 cm inner diameter (7.4 cm²) with a teflon end fitting containing teflon support mesh (125 μ m pore size).
 - h) Peristaltic pump (similar to one previously described) to control effluent flow rate.
 - i) Spectrophotometer (diode array, model 8452A, Hewlett Packard) with a 2.5 cm flow-through cell used to quantify particle concentration.

Teflon tubing (0.8 mm i.d.) was used to transfer the solutions and suspensions in the model system, except at the peristaltic pumps where tygon tubing (1.5 mm i.d.) was used. The various valves and fittings were made of polypropylene. Four identical column assemblies were made so that the experimental program could be executed more rapidly. Each column was comprised of a 7.5 cm piece of pyrex tubing (3.07 cm i.d.) with a teflon end fitting attached to one end. The end fitting held the teflon mesh (125 μ m pore size) that supported the sand bed and collected the column effluent in grooves connected to the effluent tube. The end fittings for the columns and the 2.5 cm flow-through cell were machined by the researcher from solid teflon blocks. Quartz windows were used for the flow-through cell.

3.5.2 Particle Deposition Procedure

A typical particle deposition experiment consisted of measuring the concentration of particles leaving the column (described earlier) packed with silica sand as a function of time. The influent particle concentration is kept constant, by design. Here a list of the steps involved in a deposition run is given followed by a more detailed description:

Pre-run

- 1) Place column, filled with Milli-Q water, in vacuum chamber to remove air pockets below the support mesh.
- 2) Wet pack column with clean Ottawa 30 sand by tap and fill method (described earlier).
- 3) Condition column by flowing solution of the same chemistry (minus particles) as subsequent deposition experiment (10-15 pore volumes).
- 4) Adjust flow rate.
- 5) Measure influent particle concentration.

Actual deposition experiment

- 6) Start step input of particle suspension (defines $t=0$); measure effluent particle concentration at 5 second intervals (forward particle breakthrough).
- 7) Start step input of particle-free solution (reverse particle breakthrough).
- 8) Stop column flow.

Post-run

- 9) Remove sand from column.
- 10) Clean column, tubing, and flow-through cell.

All of the particle deposition data to be presented were obtained using a bed depth of 5 cm. The mass of sand required for this bed depth was 64.2 g, which was calculated using the total volume of the column ($\{\text{column cross-sectional area}\} \times \{\text{bed depth}\} = 7.4 \text{ cm}^2 \times 5 \text{ cm} = 37 \text{ cm}^3$), bed porosity (0.34), and mineral density of sand (2.63 g/cm^3). The column was packed with sand by slowly pouring clean, dried sand into the column filled with Milli-Q water while continuously tapping the side of the column with a rubber mallet. The sand bed was flushed with Milli-Q water to remove fines by allowing about 5 pore volumes to flow downward through the column unrestricted. The effluent tubing was then connected to the bottom of the column, thus placing the effluent flow rate under the control of the effluent pump. As Figure 3.3 illustrates, the top of the column is open to the atmosphere with a layer of solution (influent reservoir) over the surface of the sand bed. The influent reservoir must be maintained in order for saturated flow to continue. This design was chosen because it makes possible the sampling of influent during a particle deposition run.

The desired solution chemistry in the column influent was produced by combining the flow of two streams. This was done in order to avoid particle aggregation which would make the interpretation of deposition results untenable. One stream contained the appropriate amounts of NaCl and the specifically adsorbed solute under consideration, while the other stream contained the appropriate amount of hematite particles. The pH of the NaCl/ligand solution and the particle suspension was 6.5. After the two streams were mixed ahead of the column, by a series of 10 expansions and contractions, the pH of the column influent was 6.5 ± 0.05 . For all deposition experiments, the column influent contained 1 mM NaCl and 1 mg/L hematite particles.

Prior to the actual particle deposition phase of an experiment, a particle-free solution was directed through the sand bed in order to equilibrate the bed to the deposition experiment conditions. The solution had the same solution chemistry as that to be used in the particle deposition phase. This step was required to obtain reproducible results. Early in this step, the flow was adjusted to produce the desired approach velocity (also referred to as superficial velocity), which is defined as the volumetric flow rate divided by the inner cross-sectional area of the column. The approach velocity for all deposition experiments was 1.0 cm/min. This corresponds to a flow rate of 7.4 mL/min (the inner cross-sectional area of the column was given previously as 7.4 cm²). To ensure that the sand bed was equilibrated to the experimental conditions, the particle-free solution was allowed to flow until the effluent pH was equal to the influent pH (i.e., $\text{pH}_{\text{out}} = \text{pH}_{\text{in}} = 6.5 \pm 0.05$). A period of 30 minutes (approximately 18 pore volumes) was sufficient to achieve this condition.

After column equilibration, the flow was diverted from flowing to the influent reservoir by switching the T-valve just ahead of the column. The particle-free solution was replaced by the particle suspension of desired concentration by switching the T-valve ahead of feed pump #1 (see Figure 3.3) to draw the stock particle suspension instead of water. The influent particle concentration was measured, then the suspension was diverted to flow to the column by switching the T-valve. A step input of particles to the sand bed was accomplished by switching the T-valve precisely when the free surface of the influent reservoir (containing particle-free solution) reached the surface of the sand bed after being drawn down as a result of the effluent pump running. This time was defined as $t=0$ for the deposition experiment. The column influent flow rate was 8

mL/min (i.e., each feed pump was set at 4 mL/min), and since the effluent flow rate was 7.4 mL/min the influent reservoir could be established and maintained. The effluent particle concentration was measured at 5 second intervals. This allowed particle breakthrough curves to be constructed, from which the particle deposition rates could be calculated. Following the particle deposition phase, a reverse particle breakthrough was performed by displacing the particle suspension by a step input of particle-free solution. The purpose of this was to see if the effluent particle concentration returned to zero after the breakthrough front had passed. This was the case for all the deposition experiments performed, indicating that particle attachment was irreversible under constant flow conditions and solution chemistry. Table 3.3 summarizes the parameters for the particle deposition experiments.

3.5.3 Determination of Particle Concentration

Colloidal suspensions exhibit turbidity because they scatter light. The amount of scattering at a given wavelength depends on the size and shape of the particles, the number concentration of the particles, and the difference between the refractive indices of the particles and the medium (Kerker, 1969). A spectrophotometer can measure the total light extinction (also called optical density) of a particle suspension. In general, light extinction is a result of light scattering and light absorbance. The total light extinction for a monodisperse particle suspension is directly related to the particle number concentration. A UV/VIS diode array spectrophotometer (Hewlett Packard model 8452A) was used to measure the influent and effluent particle concentrations in deposition experiments.

Parameter	Value
Bed Depth	5 cm
Approach Velocity	1.0 cm/min
Influent Particle Conc. (C_0)	1.0 mg/L
pH	6.5 ± 0.05
NaCl concentration	1 mM
Specifically adsorbed ligand conc.	varied

Table 3.3: Summary of the conditions for particle deposition experiments.

The spectrum (190-820 nm) of a hematite suspension was measured in order to select a suitable wavelength for optical density measurements. No maximum was detected, but a shoulder was present at 370 nm. Therefore, particle concentrations were determined from optical density measurements at 370 nm. The optical density of hematite suspensions of known concentration was measured, and the resulting calibration curve is shown in Figure 3.4. A linear relationship between optical density and particle concentration is demonstrated. For this approach to measuring particle concentrations, it is necessary for the hematite suspension to be monodisperse since the optical density (total light extinction) changes with the degree of aggregation of a particle suspension (Liang, 1988).

3.5.4 Tracer Experiments

A conservative tracer should not interact with the porous medium. In theory, the flow properties of the particle deposition experimental apparatus can be characterized by using a conservative tracer. In our case, a 10 mM NaNO_3 solution was used as a

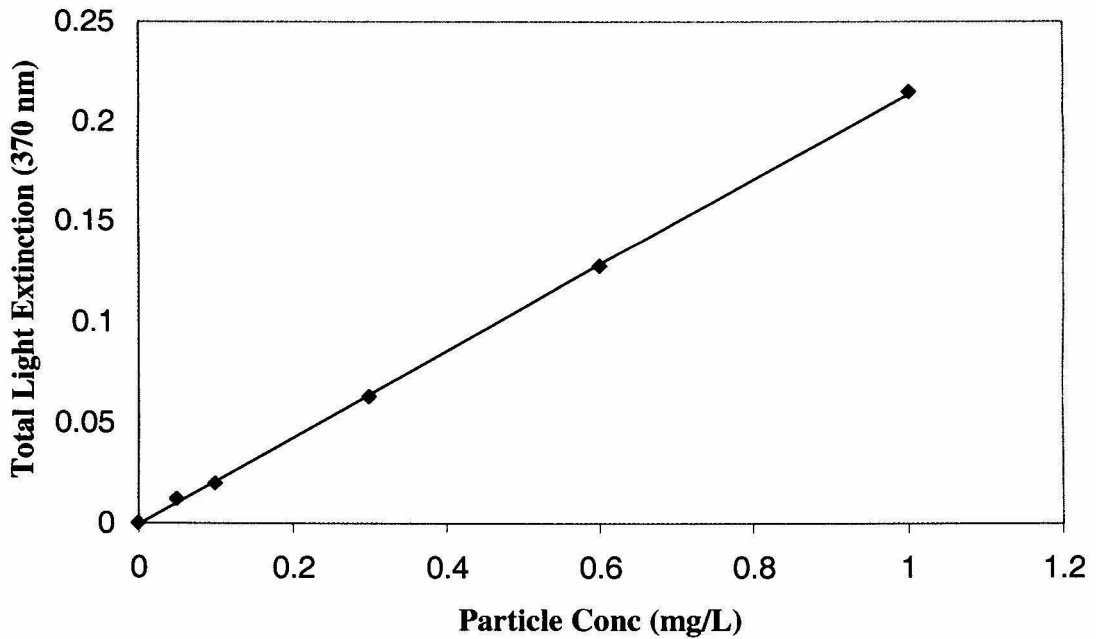


Figure 3.4: Total light extinction as a function of particle concentration.

tracer. A similar procedure to the one used for particle deposition experiments was used to determine the response of the packed sand bed to a step-function input of NaNO_3 . The influent and effluent concentration of NO_3^- was monitored by measuring the absorbance at 302 nm (Hewlett Packard UV/VIS spectrophotometer, model 8452A). The critical experimental parameter obtained from tracer experiments was the time corresponding to the initial particle removal rate.

Chapter 4. Experimental Results

4.0 Introduction

The principal experimental goal is to study the effects of small changes in the chemical composition of the aqueous phase on the kinetics of hematite deposition in a silica sand bed. The chemical changes consisted of adding solutes to the heterogeneous solid-water system that are capable of changing the surface chemistry of hematite particles. The effects of inorganic solutes, low molecular weight organic compounds, and polymeric organic compounds are studied at pH 6.5 and a background NaCl concentration of 1 mM. Electrokinetic mobility measurements were made to help in data interpretation.

4.1 Tracer Experiments

The experimental procedure is described in Section 3.5.2 and 3.5.4. Tracer breakthrough curves were obtained under the same flow conditions as particle deposition experiments. The results are presented in terms of Tr/Tr_0 as a function of time, where Tr and Tr_0 are the tracer effluent and influent concentrations, respectively. The initial time ($t = 0$) is defined as the time when the step input of tracer entered the packed bed. A representative tracer breakthrough curve is shown in Figure 4.1.

The results of the tracer experiments were used to determine the time of clean bed particle removal. During clean bed conditions, the particle deposition rate is not affected by particles attached to the collector surface. The clean bed removal time was chosen as

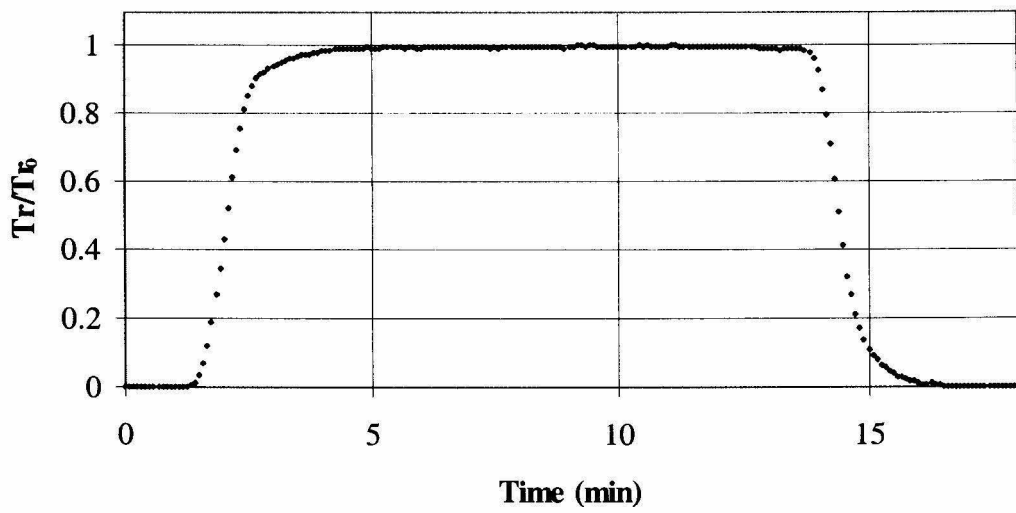


Figure 4.1: Tracer breakthrough curve (5 cm bed depth, 1 cm/min approach velocity).

the time corresponding to complete breakthrough of the tracer ($Tr/Tr_0 > 0.99$). This time was approximately 5 minutes. Therefore, the normalized effluent particle concentration (C/C_0) at 5 minutes was used in determining the single collector efficiencies (η_{exp}) and collision efficiencies (α_{exp}) for particle deposition experiments.

4.2 Particle Deposition Rates

All particle deposition experiments were conducted at room temperature (about 22° C), pH 6.5 ± 0.05 , and with an influent particle concentration of 1 mg/L. The procedure described in Section 3.5.2 was followed. Experiments were run in triplicate, and the standard deviation for the effluent particle concentration was less than 10%.

4.2.1 Effect of NaCl on Hematite Deposition

The effect of a variation in the NaCl concentration on hematite deposition was examined to determine the transport limited deposition rate (i.e., $\eta_{0,exp}$ of Section 2.2.3). Hematite deposition was studied at $[NaCl] = 0, 0.1, 1, \text{ and } 10 \text{ mM}$. The particle breakthrough curves are shown in Figure 4.2. The clean bed normalized effluent particle concentration (C/C_0 at 5 min) increases from 0.12 to 0.145 as NaCl is increased from zero to 0.1 mM. The C/C_0 ratio (5 min) increases to 0.16 when NaCl is increased to 1 mM. Increasing the NaCl to 10 mM gives similar results to the 1 mM case. This suggests that below 1 mM NaCl the particle deposition rate is enhanced beyond the transport limited case by electrostatic attraction between the hematite particles (positively charged at pH 6.5) and silica sand (negatively charged at pH 6.5). However, a 1.0 mM $[NaCl]$ is enough to reduce electrostatic attraction (by compression of the diffuse layers) to where particle deposition is transport limited. To summarize, the transport limited C/C_0 (5 min) value is 0.16.

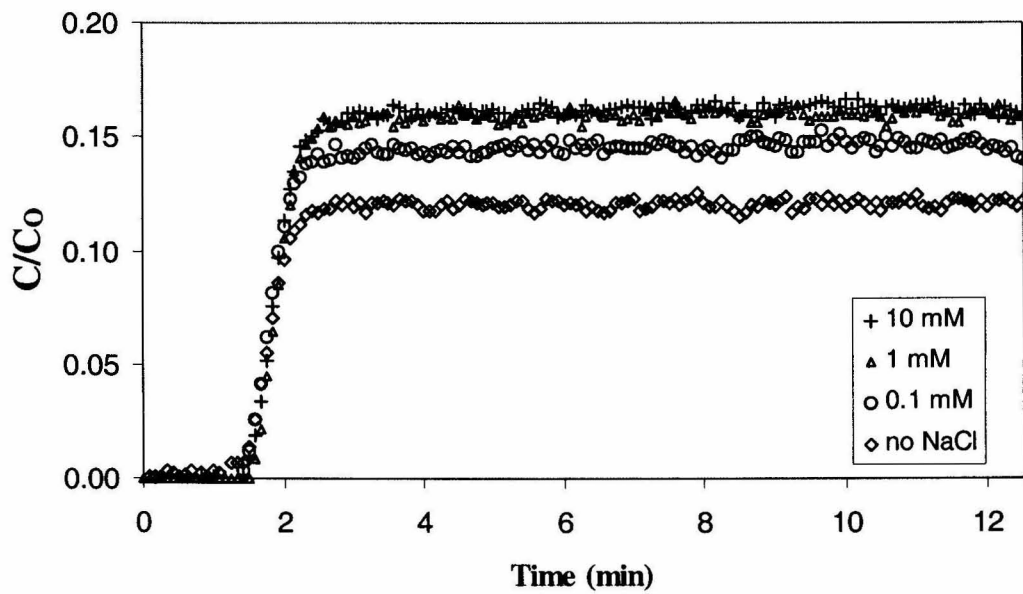


Figure 4.2: Hematite breakthrough curves with increasing concentrations of NaCl (5 cm bed depth, 1 cm/min approach velocity, pH 6.5, and $C_0 = 1$ mg/L).

4.2.2 Effect of Inorganic Compounds on Hematite Deposition

4.2.2.1 Effect of Phosphate and Arsenate on Hematite Deposition

The effect of phosphate on hematite deposition was studied at total phosphate concentrations ($[\text{PO}_4^{3-}]_T$) of 10, 25, 50, 75, 100, and 200 μM . Particle breakthrough curves in the presence of phosphate are shown in Figure 4.3. As the total phosphate concentration increases, the particle deposition rate decreases (i.e., C/C_0 (5 min) increases). Transport limited deposition results in a C/C_0 (5 min) value of 0.16 (Section 4.2.1). The addition of phosphate clearly results in an effective electrostatic repulsion.

As described in Chapter 2, the collision efficiency approaches unity when conditions are favorable for deposition and is much smaller than one when conditions are unfavorable for deposition. For the bed depth employed in this research (5 cm), the smallest collision efficiency that can be determined is around 0.01. Greater bed depths would have to be used in order to measure smaller collision efficiencies.

An expression for calculating the experimental collision efficiency is obtained by combining Equations (2.6) and (2.7) to give

$$\alpha_{\text{exp}} = \frac{\ln\left(\frac{C}{C_0}\right)}{-1.83}, \quad (4.1)$$

where C/C_0 is the clean bed normalized effluent particle concentration (i.e., taken at $t = 5$ min). Experimental collision efficiencies can be plotted as stability diagrams, that is, $\log \alpha_{\text{exp}}$ against $\log(\text{total solute concentration})$. The experimental collision efficiency is plotted as a function of total phosphate concentration in Figure 4.4. A total phosphate concentration of around 10 μM is needed to bring the collision efficiency below 1. The collision efficiency decreases as the total phosphate is increased, with a transition from

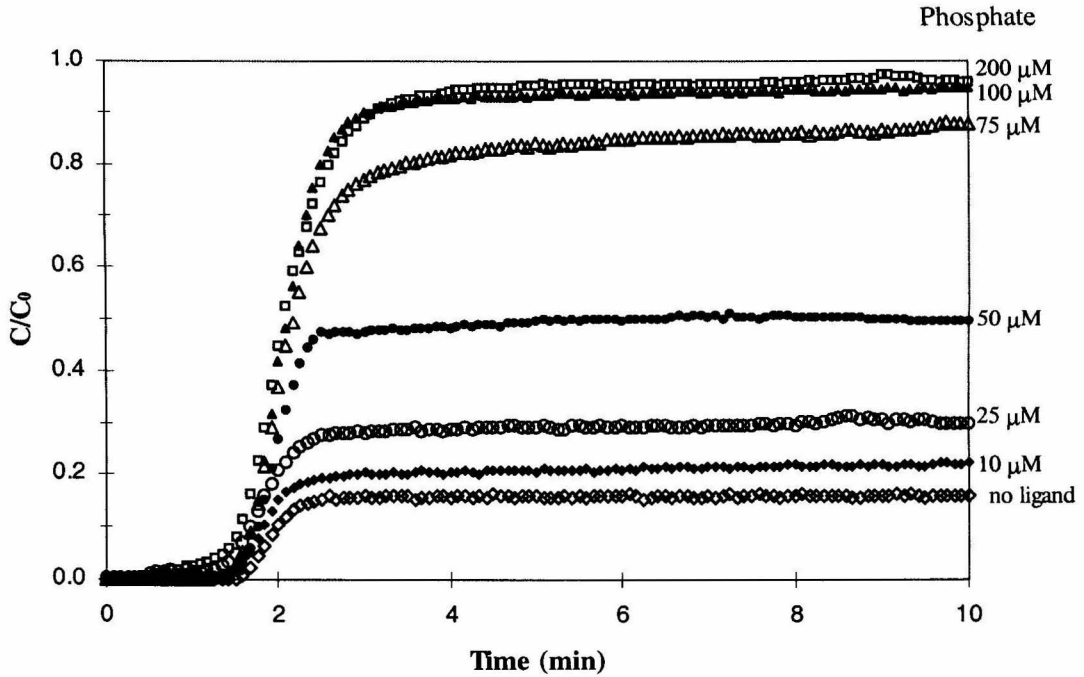


Figure 4.3: Hematite breakthrough curves in the presence of phosphate (5 cm bed depth, 1 cm/min approach velocity, pH 6.5, 1 mM NaCl, $C_0 = 1$ mg/L).

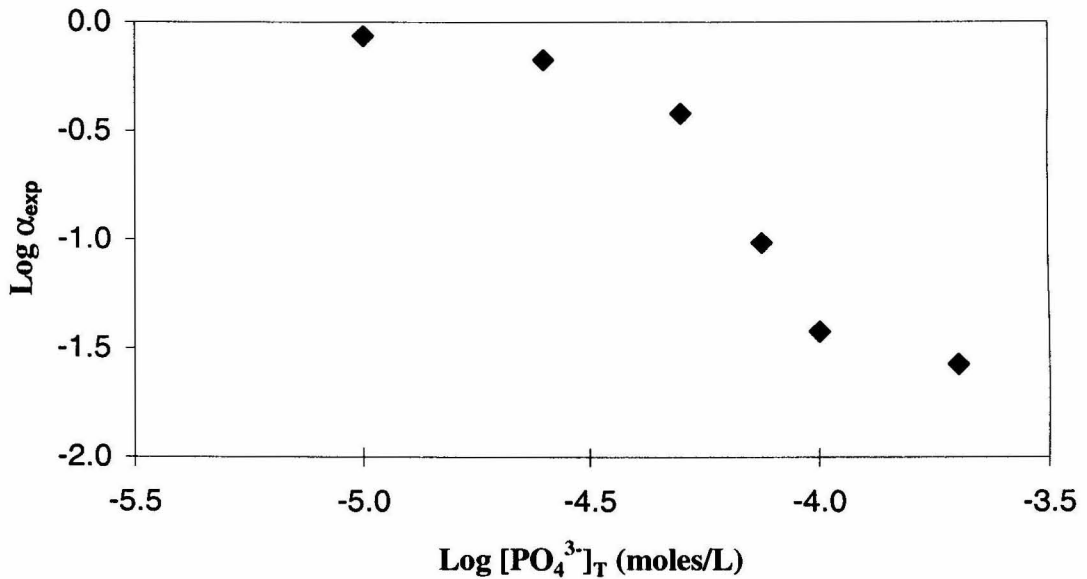


Figure 4.4: Experimental collision efficiency (α_{exp}) plotted as a function of total phosphate concentration (5 cm bed depth, 1 cm/min approach velocity, pH 6.5, 1 mM NaCl, $C_0 = 1$ mg/L).

relatively favorable deposition to relatively unfavorable deposition occurring between 50 and 75 μM $[\text{PO}_4^{3-}]_{\text{T}}$. This is the total phosphate needed to “stabilize” the hematite particles with respect to deposition. A collision efficiency of 2.69×10^{-2} is calculated for 200 μM $[\text{PO}_4^{3-}]_{\text{T}}$.

Arsenate was studied as a surface active ligand because arsenic species are present in some groundwaters (Davis et al., 2001). Since arsenate is chemically similar to phosphate, it is expected to have a similar effect on hematite deposition. Hematite breakthrough curves in the presence of arsenate are shown in Figure 4.5. Like phosphate, arsenate causes the particle deposition rate to decrease as its total concentration increases. In Figure 4.6, the collision efficiency is plotted against total arsenate concentration. The total arsenate concentration required to make the transition from favorable deposition (approximated by $\alpha_{\text{exp}} > 0.3$) to unfavorable deposition is between 37.5 and 50 μM . This “stabilizing” concentration is less than the phosphate case (i.e., 50 – 75 μM).

4.2.2.2 Effect of Fluoride on Hematite Deposition

Fluoride, F^- , is known to be specifically adsorbed on iron oxide surfaces. In fact, it has been used to experimentally determine the exchange capacity of hematite (Faust, 1985; Liang, 1988). Therefore, fluoride was chosen as a model monovalent anion. The hematite breakthrough curves presented in Figure 4.7 show that total fluoride concentrations as high as 3 mM do not affect the deposition rate appreciably. In the presence of 3 mM fluoride, the breakthrough curve has a hump at 2 to 3 minutes. This is probably a result of particle coagulation induced by the relatively high ionic strength and a reduction in surface charge. The independence of the collision efficiency on total fluoride concentration is shown in Figure 4.8.

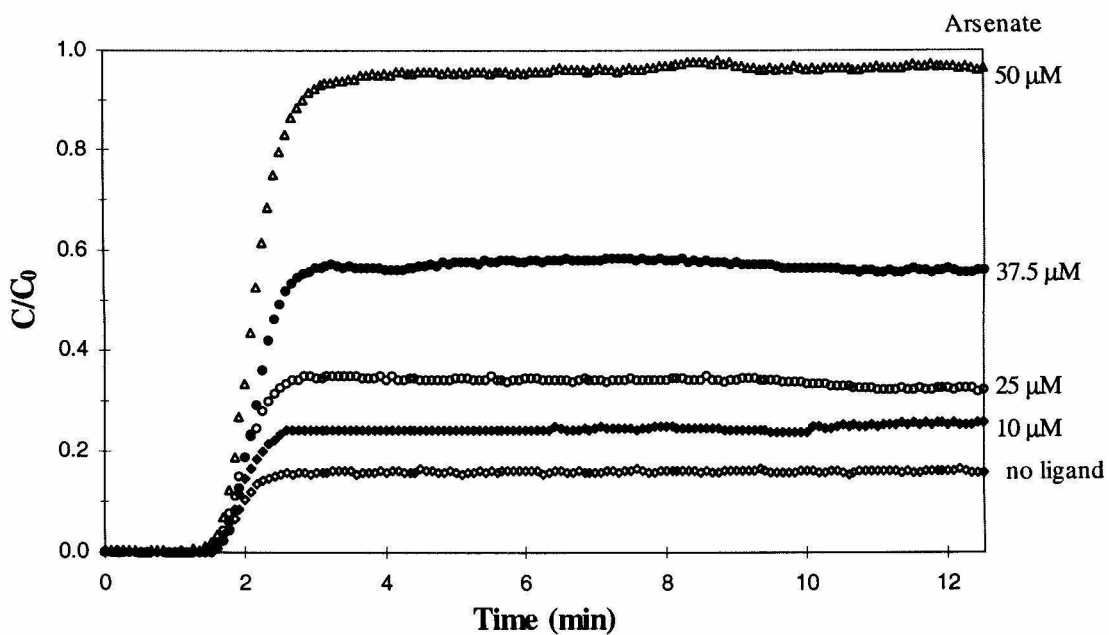


Figure 4.5: Hematite breakthrough curves in the presence of arsenate (5 cm bed depth, 1 cm/min approach velocity, pH 6.5, 1 mM NaCl, $C_0 = 1$ mg/L).

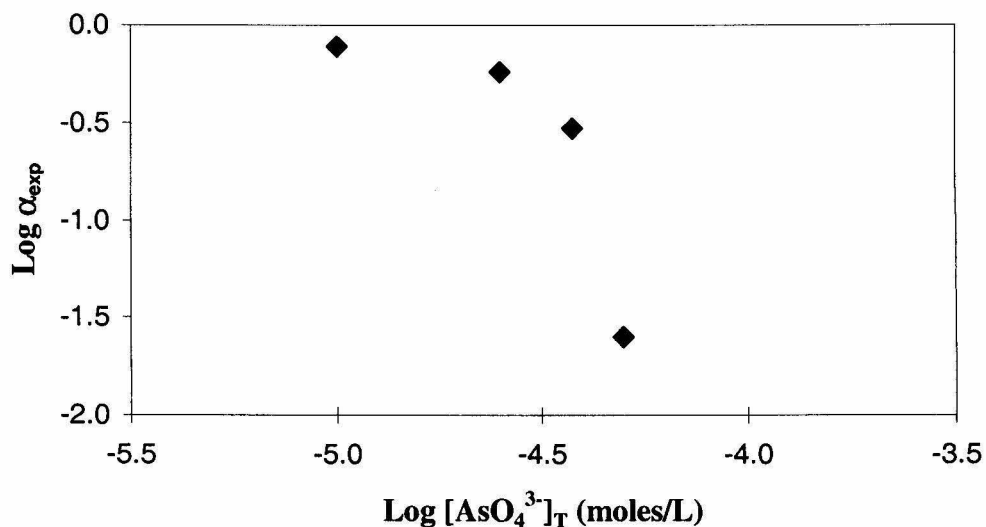


Figure 4.6: Experimental collision efficiency (α_{exp}) plotted as a function of total arsenate concentration (5 cm bed depth, 1 cm/min approach velocity, pH 6.5, 1 mM NaCl, $C_0 = 1$ mg/L).

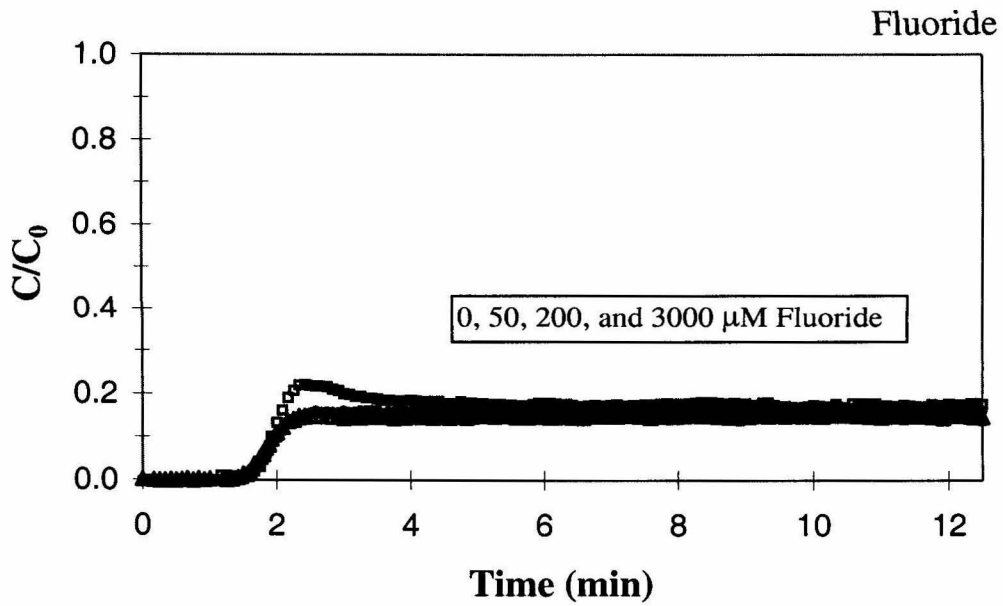


Figure 4.7: Hematite breakthrough curves in the presence of fluoride (5 cm bed depth, 1 cm/min approach velocity, pH 6.5, 1 mM NaCl, $C_0 = 1$ mg/L).

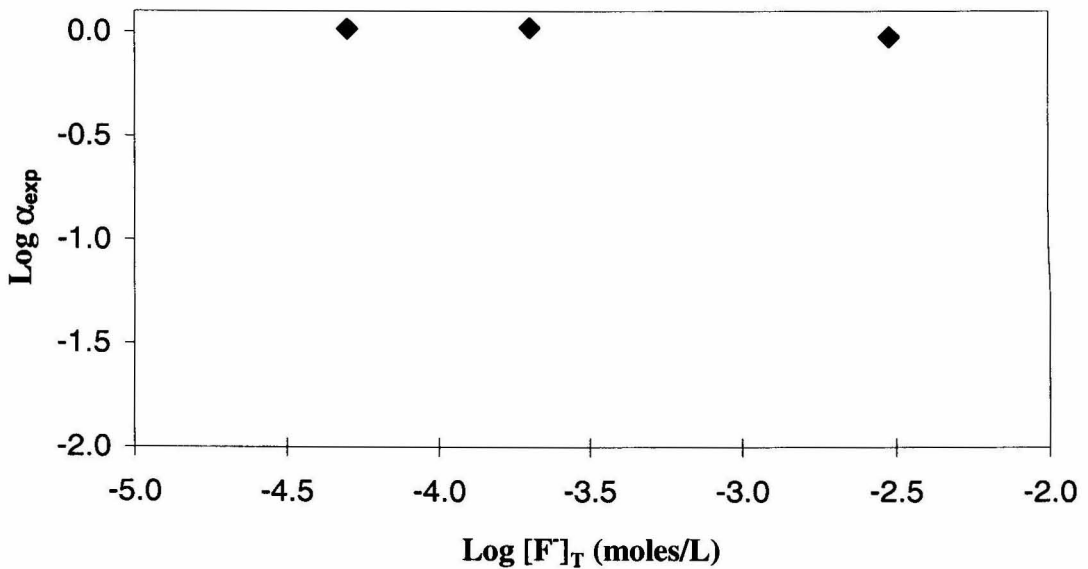


Figure 4.8: Experimental collision efficiency (α_{exp}) plotted as a function of total fluoride concentration (5 cm bed depth, 1 cm/min approach velocity, pH 6.5, 1 mM NaCl, $C_0 = 1$ mg/L).

4.2.3 Effect of Low Molecular Weight Organic Compounds on Hematite Deposition

4.2.3.1 Effect of Oxalate and Related Compounds on Hematite Deposition

Oxalic acid (HOOC-COOH), succinic acid (HOOC-(CH₂)₂-COOH), adipic acid (HOOC-(CH₂)₄-COOH), and suberic acid (HOOC-(CH₂)₆-COOH) were studied as model organic molecules. Adsorption studies have shown that carboxyl groups react chemically with surface hydroxyl groups of metal oxides (Kummert and Stumm, 1980). A related series of dicarboxylic acids was investigated to explore effects of a variation in the number of methylene groups, (-CH₂)_n, between the terminal carboxylate groups on the deposition behavior of hematite. The hematite breakthrough curves in the presence of each molecule are shown in Figure 4.9 (oxalate), Figure 4.10 (succinic acid), Figure 4.11 (adipic acid), and Figure 4.12 (suberic acid). The characteristic features of the breakthrough curves are the same for each of the dicarboxylic acids. In each case, a total concentration > 1 mM is needed to reduce the deposition rate below the transport-limited rate, and the rate of deposition remains favorable at total concentrations > 2 mM. The dependence of the collision efficiency on total dicarboxylic acid concentration is illustrated in Figure 4.13. Hematite particles are unstable with respect to deposition in the presence of the studied dicarboxylic acids over a wide range of concentrations (0 to 5 mM).

4.2.3.2 Effect of Phthalate and Related Compounds on Hematite Deposition

1,2-benzenedicarboxylic acid (phthalic acid), 1,2,4-benzenetricarboxylic acid (benzene-tri), and 1,2,4,5-benzenetetracarboxylic acid (benzene-tetra) were studied as model aromatic organic molecules. The related series of carboxylic acids was chosen to determine whether additional carboxylate groups on the benzene ring would affect

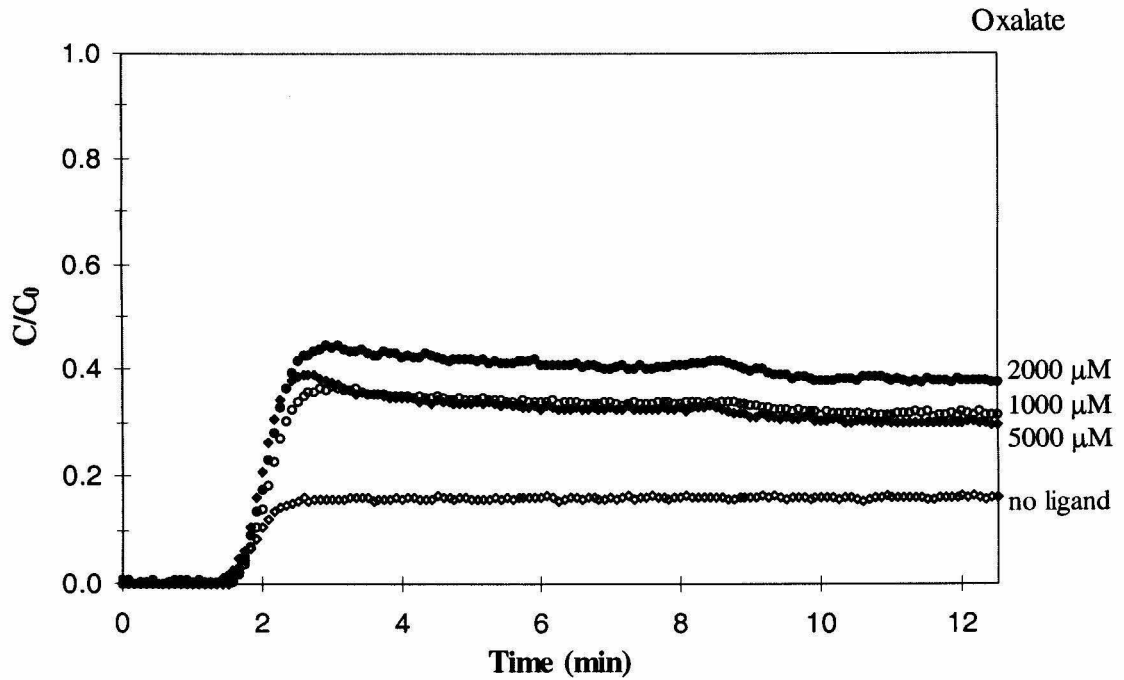


Figure 4.9: Hematite breakthrough curves in the presence of oxalic acid (C_2) (5 cm bed depth, 1 cm/min approach velocity, pH 6.5, 1 mM NaCl, $C_0 = 1$ mg/L).

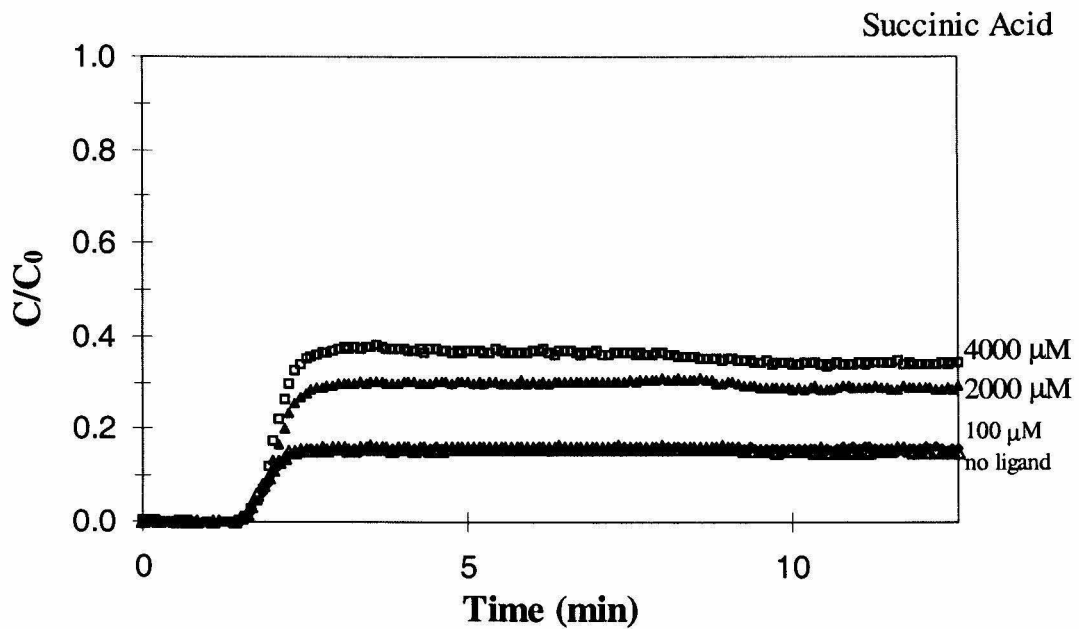


Figure 4.10: Hematite breakthrough curves in the presence of succinic acid (C_4) (5 cm bed depth, 1 cm/min approach velocity, pH 6.5, 1 mM NaCl, $C_0 = 1$ mg/L).

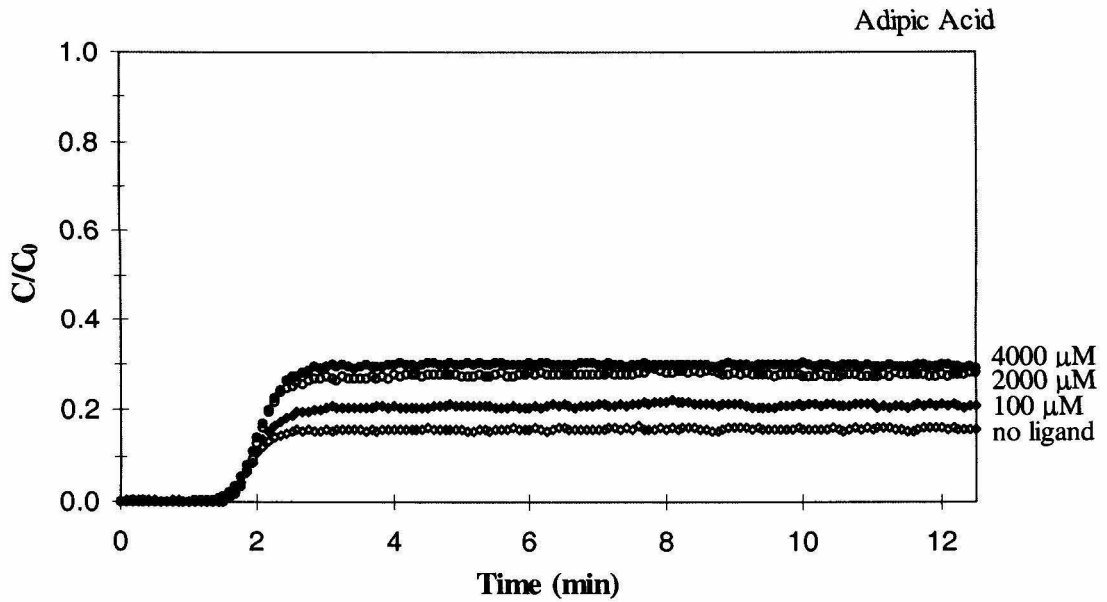


Figure 4.11: Hematite breakthrough curves in the presence of adipic acid (C_6) (5 cm bed depth, 1 cm/min approach velocity, pH 6.5, 1 mM NaCl, $C_0 = 1$ mg/L).

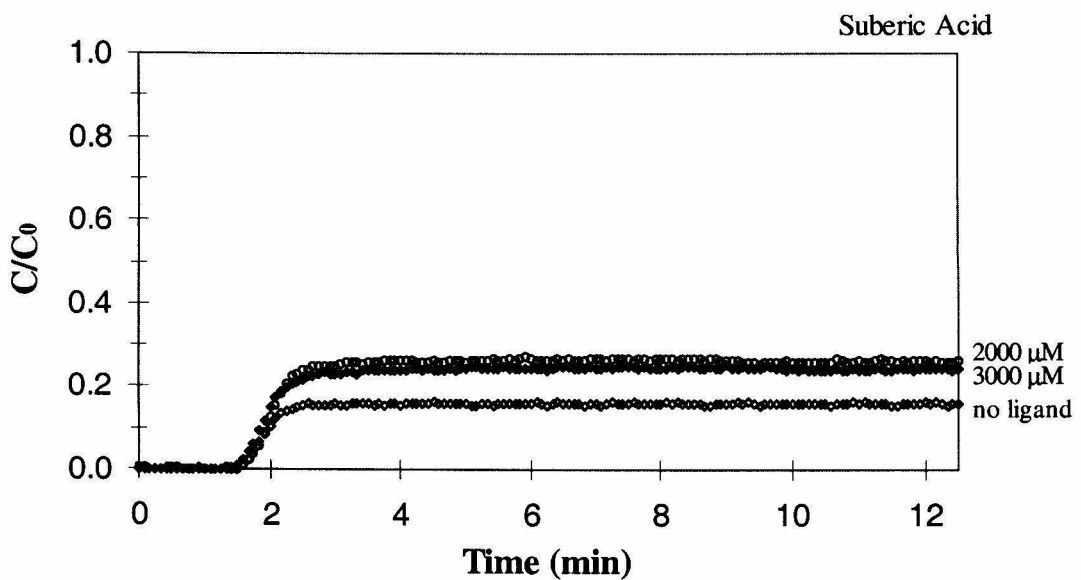


Figure 4.12: Hematite breakthrough curves in the presence of suberic acid (C_8) (5 cm bed depth, 1 cm/min approach velocity, pH 6.5, 1 mM NaCl, $C_0 = 1$ mg/L).

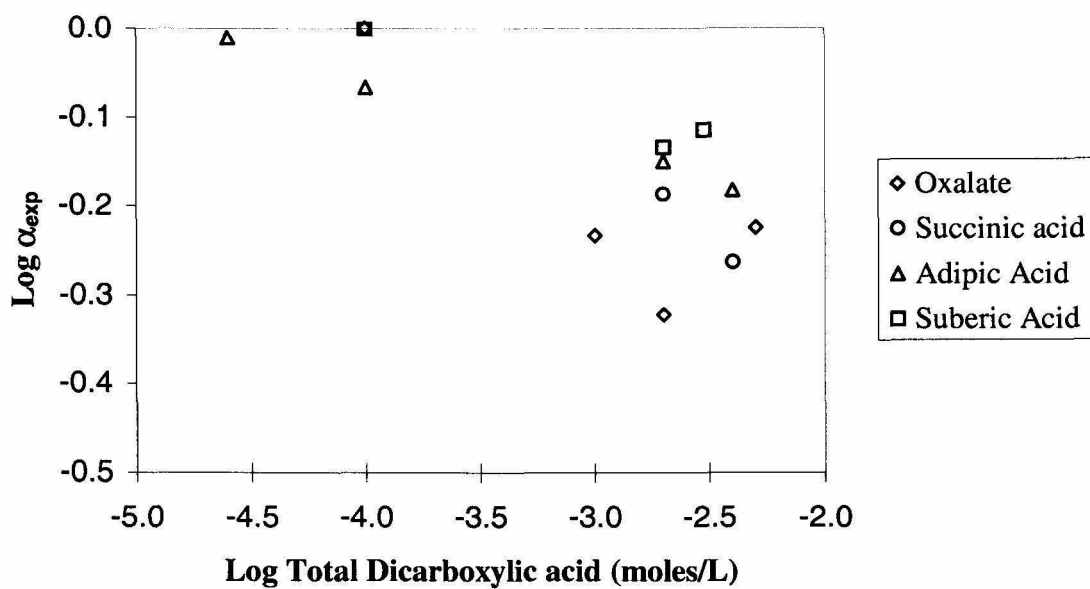


Figure 4.13: Experimental collision efficiency (α_{exp}) plotted as a function of total dicarboxylic acid concentration (5 cm bed depth, 1 cm/min approach velocity, pH 6.5, 1 mM NaCl, $C_0 = 1$ mg/L).

hematite deposition rates. Breakthrough curves in the presence of each compound are presented in Figure 4.14 (phthalate), Figure 4.15 (benzene-tri), and Figure 4.16 (benzene-tetra). In the case of phthalate, its effect on hematite deposition is similar to the effect of oxalate and its related compounds in that the deposition rate was only slightly reduced below the transport limited case at total phthalate concentrations of 1 and 2 mM. Conversely, benzene-tri and benzene-tetra cause a significant reduction in the hematite deposition rate at total concentrations less than 50 μM . The collision efficiencies as a function of total concentration of each carboxylic acid are compared in Figure 4.17. The transition to unfavorable deposition takes place at approximately 1 μM and 25 μM for benzene-tetra and benzene-tri, respectively. Phthalate does not produce unfavorable deposition over the concentration range studied.

4.2.3.3 Effect of Aspartic Acid on Hematite Deposition

Aspartic acid ($\text{HOOC-CH}_2\text{-CHNH}_2\text{-COOH}$), the monomer of polyaspartic acid, was also used in deposition experiments. Figure 4.18 shows hematite breakthrough curves in the presence of aspartic acid. Total concentrations of 2 and 4 mM produced significant reductions in the measured deposition rate. The collision efficiency is plotted as a function of total aspartic acid concentration in Figure 4.19. While aspartic acid is structurally similar to succinic acid, only aspartic acid shows an appreciable influence on the collision efficiency.

4.2.3.4 Effect of Butyric Acid on Hematite Deposition

Deposition experiments were conducted with butyric acid as a model compound for fatty acids. The particle breakthrough curves presented in Figure 4.20 illustrate that 3 mM total butyric acid only produces a small reduction in the deposition rate. The

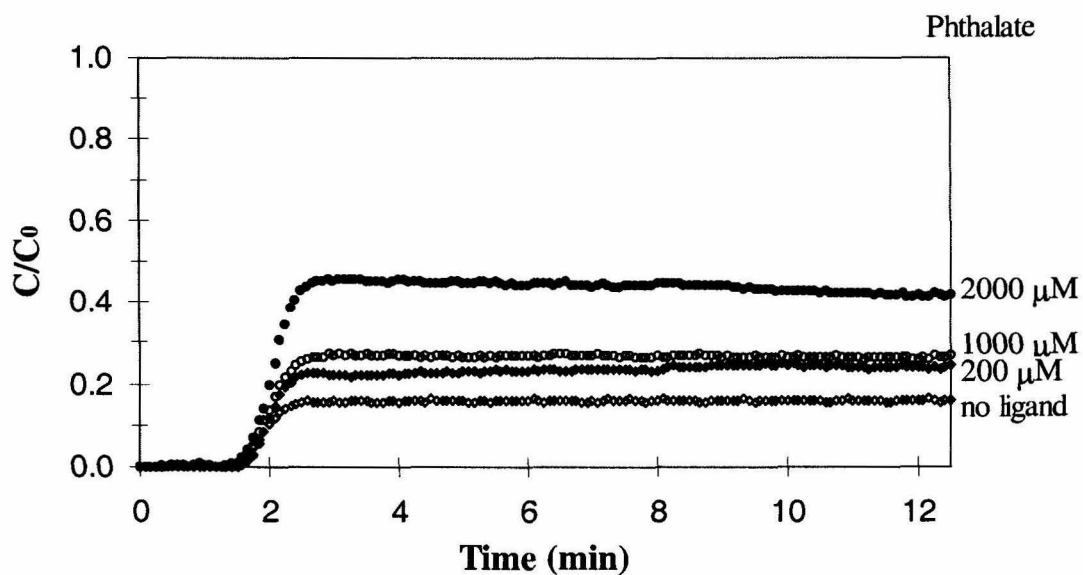


Figure 4.14: Hematite breakthrough curves in the presence of phthalate (5 cm bed depth, 1 cm/min approach velocity, pH 6.5, 1 mM NaCl, $C_0 = 1$ mg/L).

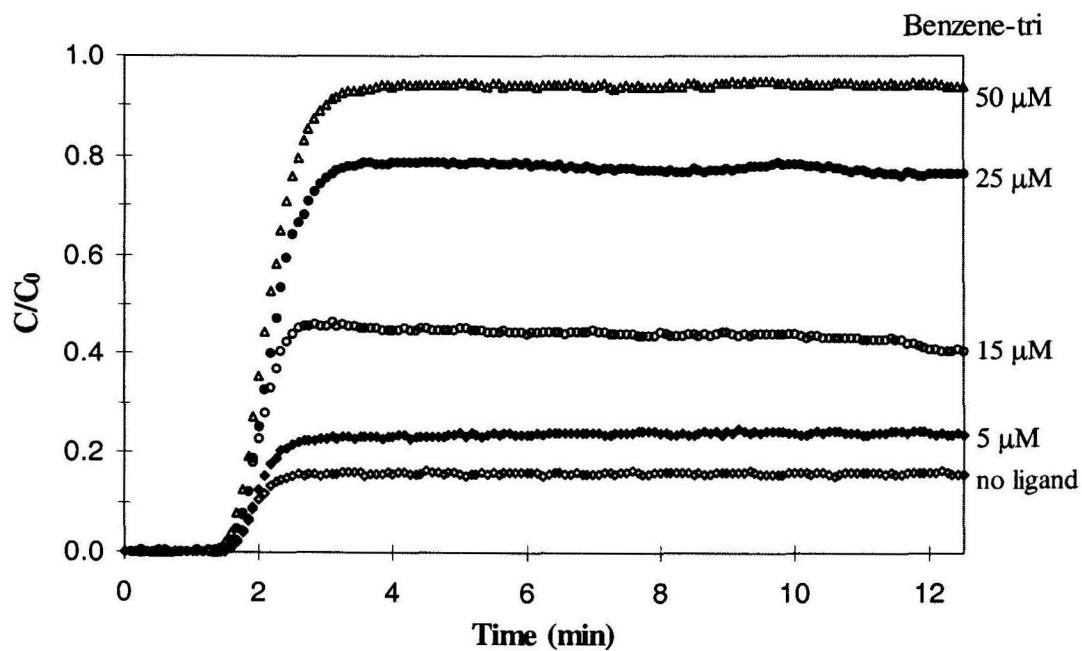


Figure 4.15: Hematite breakthrough curves in the presence of benzene-tri (5 cm bed depth, 1 cm/min approach velocity, pH 6.5, 1 mM NaCl, $C_0 = 1$ mg/L).

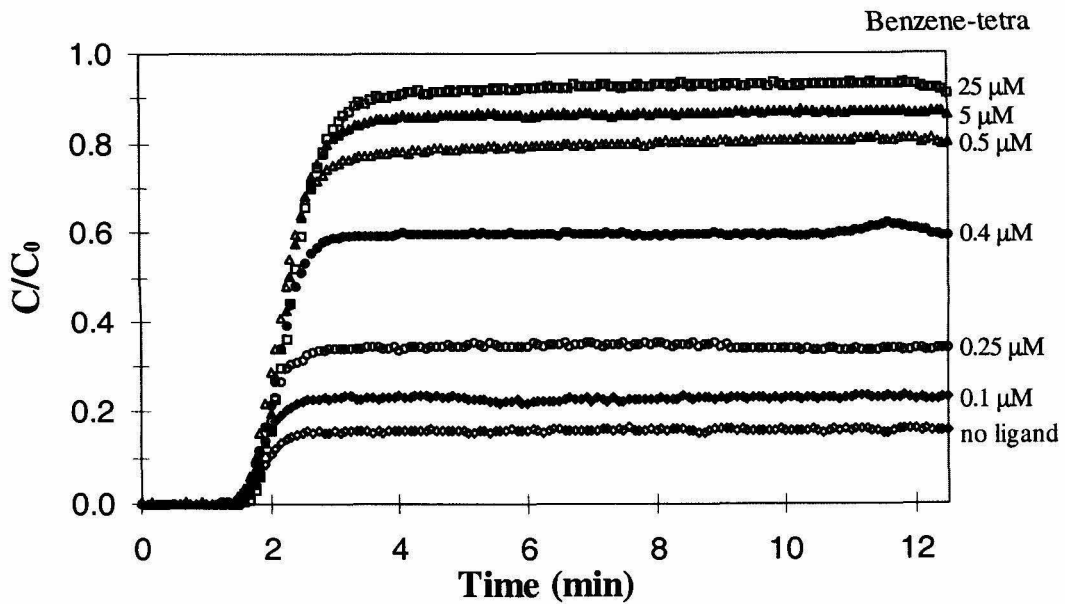


Figure 4.16: Hematite breakthrough curves in the presence of benzene-tetra (5 cm bed depth, 1 cm/min approach velocity, pH 6.5, 1 mM NaCl, $C_0 = 1$ mg/L).

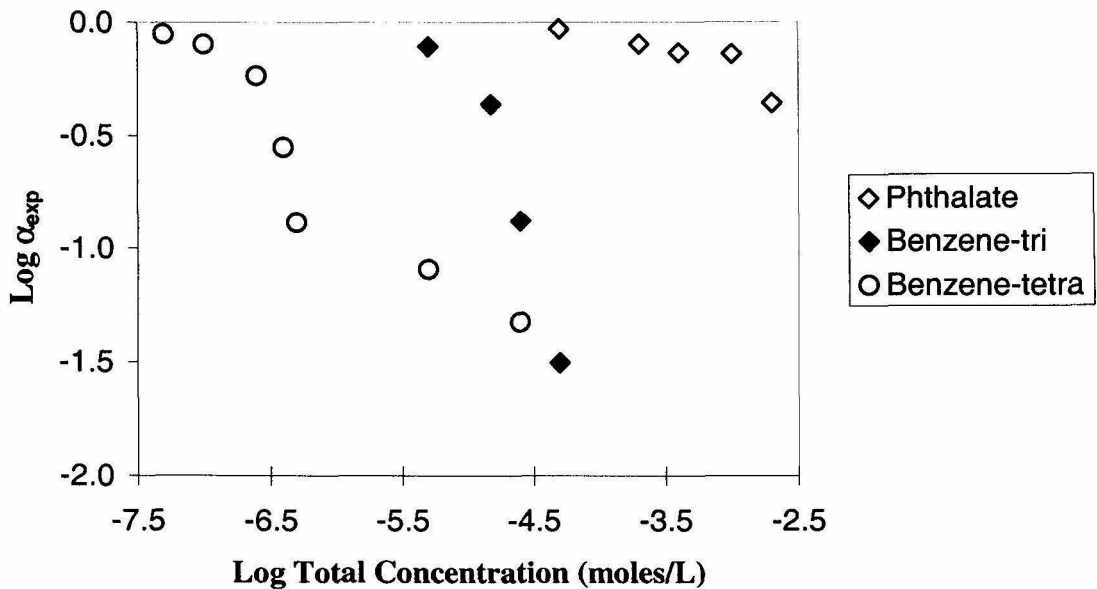


Figure 4.17: Experimental collision efficiency (α_{exp}) plotted as a function of total carboxylic acid concentration (5 cm bed depth, 1 cm/min approach velocity, pH 6.5, 1 mM NaCl, $C_0 = 1$ mg/L).

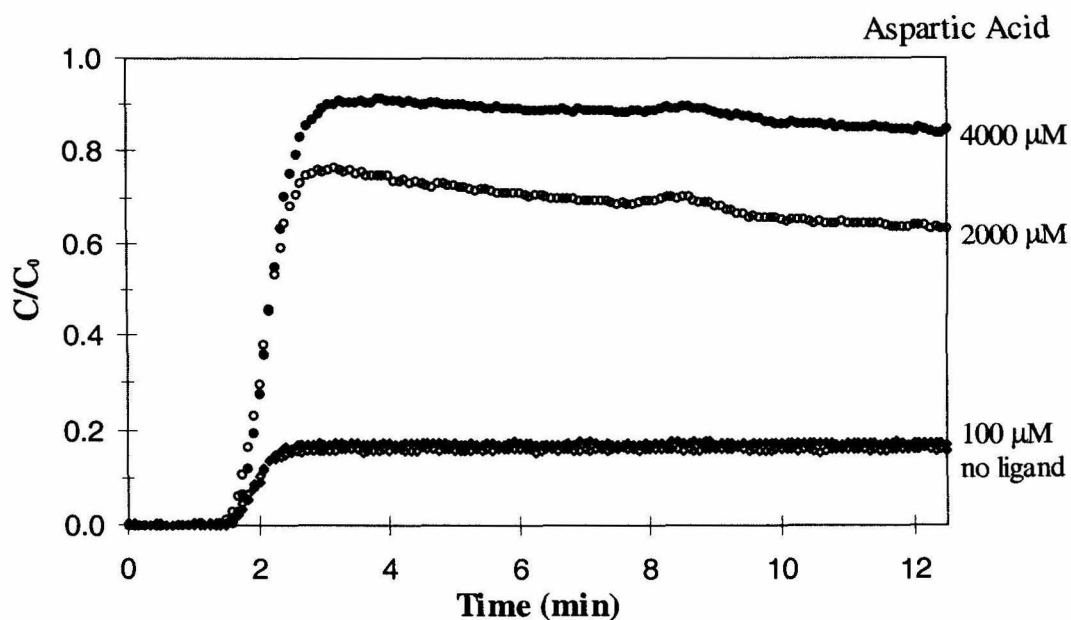


Figure 4.18: Hematite breakthrough curves in the presence of aspartic acid (5 cm bed depth, 1 cm/min approach velocity, pH 6.5, 1 mM NaCl, $C_0 = 1$ mg/L).

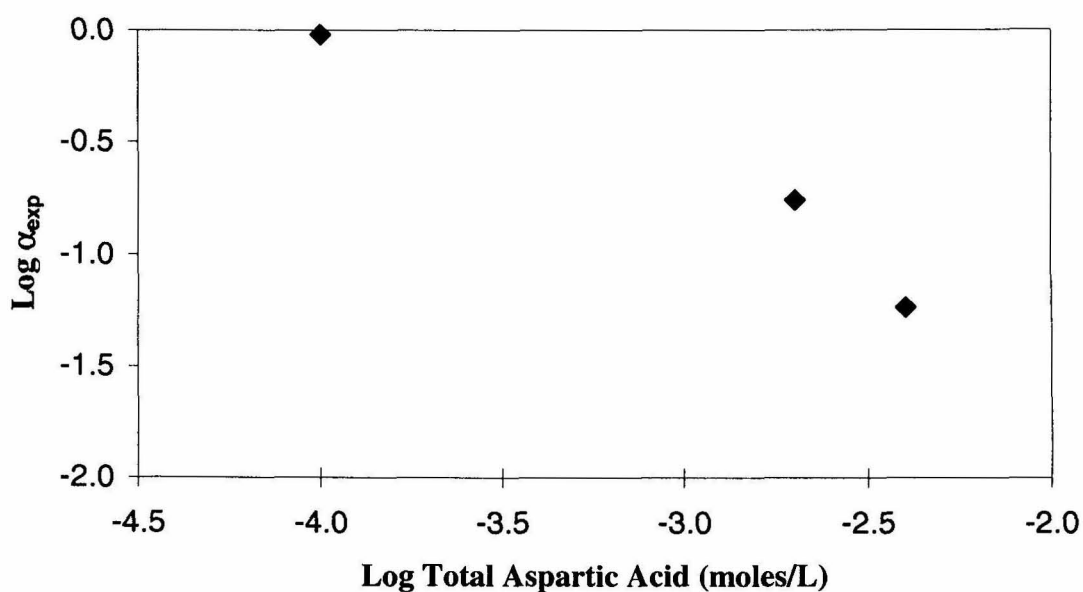


Figure 4.19: Experimental collision efficiency (α_{exp}) plotted as a function of total aspartic acid concentration (5 cm bed depth, 1 cm/min approach velocity, pH 6.5, 1 mM NaCl, $C_0 = 1$ mg/L).

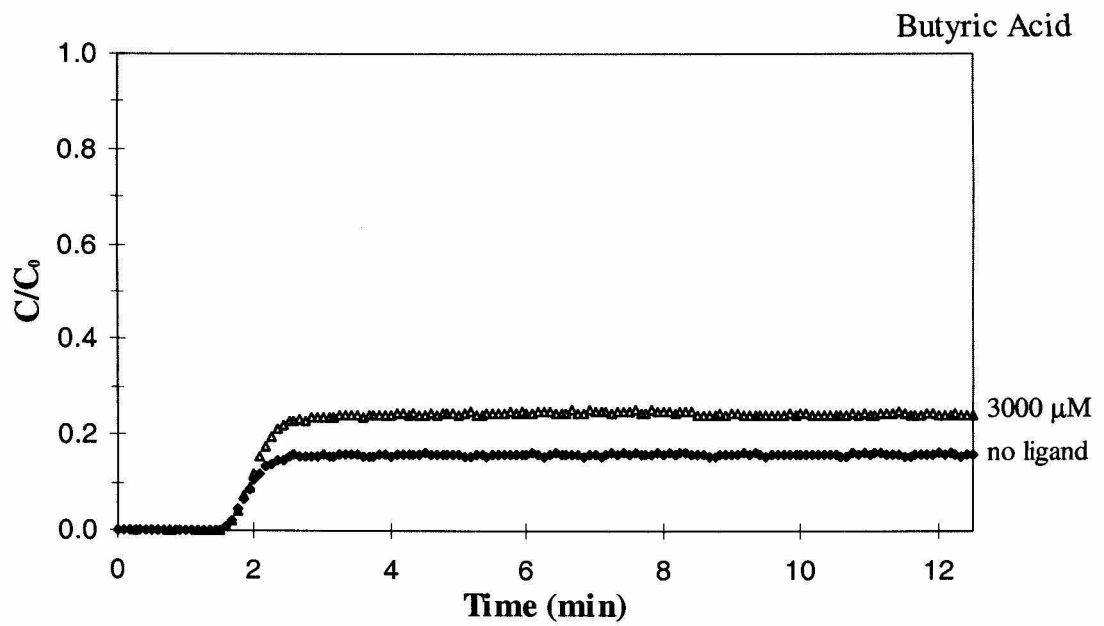


Figure 4.20: Hematite breakthrough curves in the presence of butyric acid (5 cm bed depth, 1 cm/min approach velocity, pH 6.5, 1 mM NaCl, $C_0 = 1$ mg/L).

breakthrough curves for 50 and 200 μM total butyric acid are not shown in Figure 5.20 because they are the same as the curve for no butyric acid. The apparent independence of the collision efficiency with respect to total butyric acid concentration is demonstrated in Figure 4.21.

4.2.3.5 Effect of Lauryl Sulfate on Hematite Deposition

The surfactant lauryl sulfate (also called “SDS” for sodium dodecyl sulfate) has been used in groundwater remediation projects to enhance the removal of organic pollutants (Tien et al., 2000). Therefore, the effect of lauryl sulfate on hematite deposition was studied. Hematite breakthrough curves in the presence of 0, 20, 40, and 50 μM total lauryl sulfate are shown in Figure 4.22. A small decrease in the deposition rate from the “no ligand” case to the 50 μM case is observed. The 40 and 50 μM experiments provide evidence for coagulation (i.e., humps in curves at 2 to 3 minutes). The collision efficiency is plotted as a function of total lauryl sulfate concentration in Figure 4.23.

4.2.4 Effect of Polymeric Organic Compounds on Hematite Deposition

Polyaspartic acid (PAA) (m.w. = 11,000) was used as a model compound for high-molecular weight, polymeric organic compounds. Naturally occurring organic matter (NOM) was also used in deposition experiments. McCarthy and co-workers (1993) observed the transport of natural organic matter in groundwater in field-scale injection studies. One fulvic acid (Suwannee River fulvic acid) and two humic acids (Suwannee River humic acid and Leonardite humic acid) from the International Humic Substances Society (IHSS) were used. The hematite breakthrough curves in the presence of each polyelectrolyte are shown in Figure 4.24 for polyaspartic acid (PAA), Figure 4.25

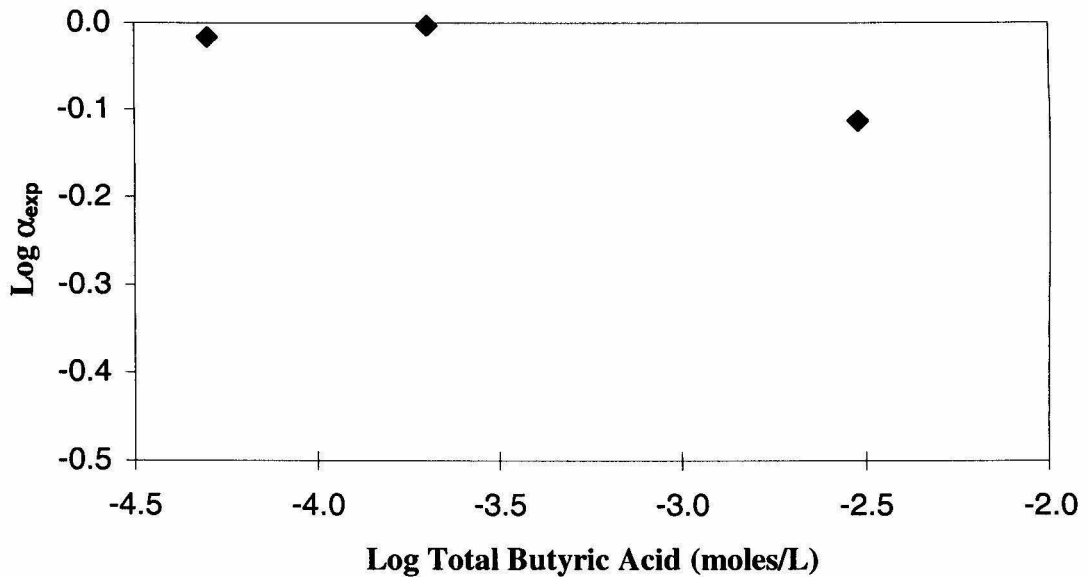


Figure 4.21: Experimental collision efficiency (α_{exp}) plotted as a function of total butyric acid concentration (5 cm bed depth, 1 cm/min approach velocity, pH 6.5, 1 mM NaCl, $C_0 = 1$ mg/L).

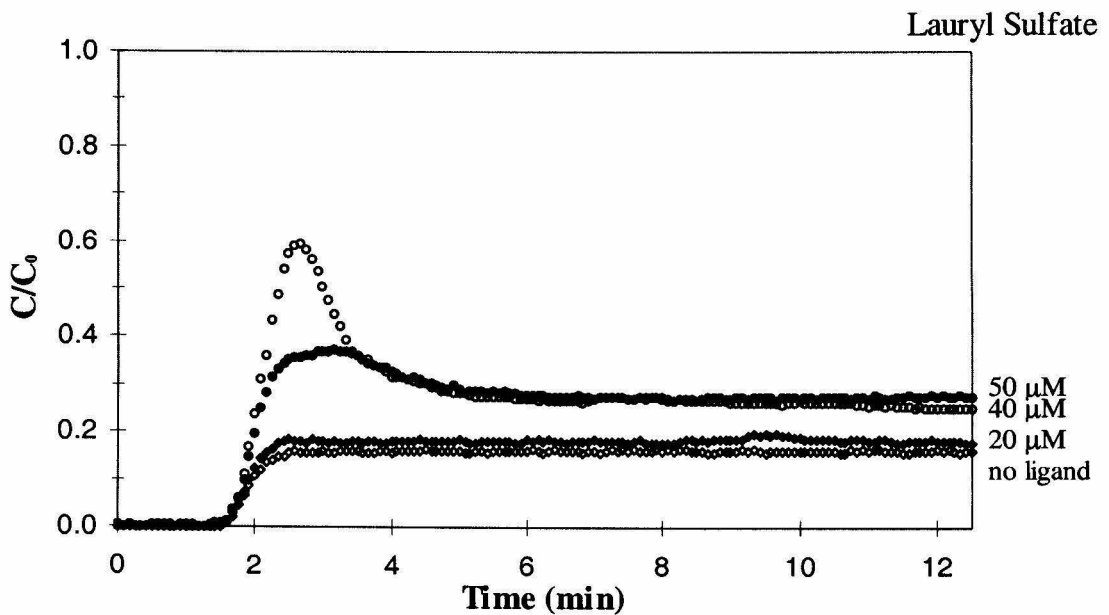


Figure 4.22: Hematite breakthrough curves in the presence of lauryl sulfate (5 cm bed depth, 1 cm/min approach velocity, pH 6.5, 1 mM NaCl, $C_0 = 1$ mg/L).

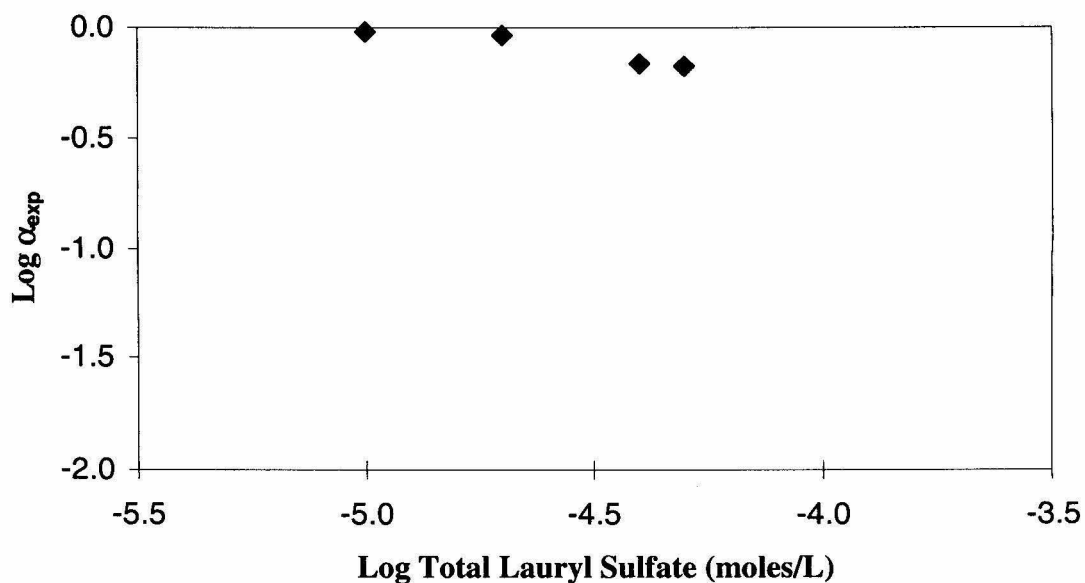


Figure 4.23: Experimental collision efficiency (α_{exp}) plotted as a function of total lauryl sulfate concentration (5 cm bed depth, 1 cm/min approach velocity, pH 6.5, 1 mM NaCl, $C_0 = 1$ mg/L).

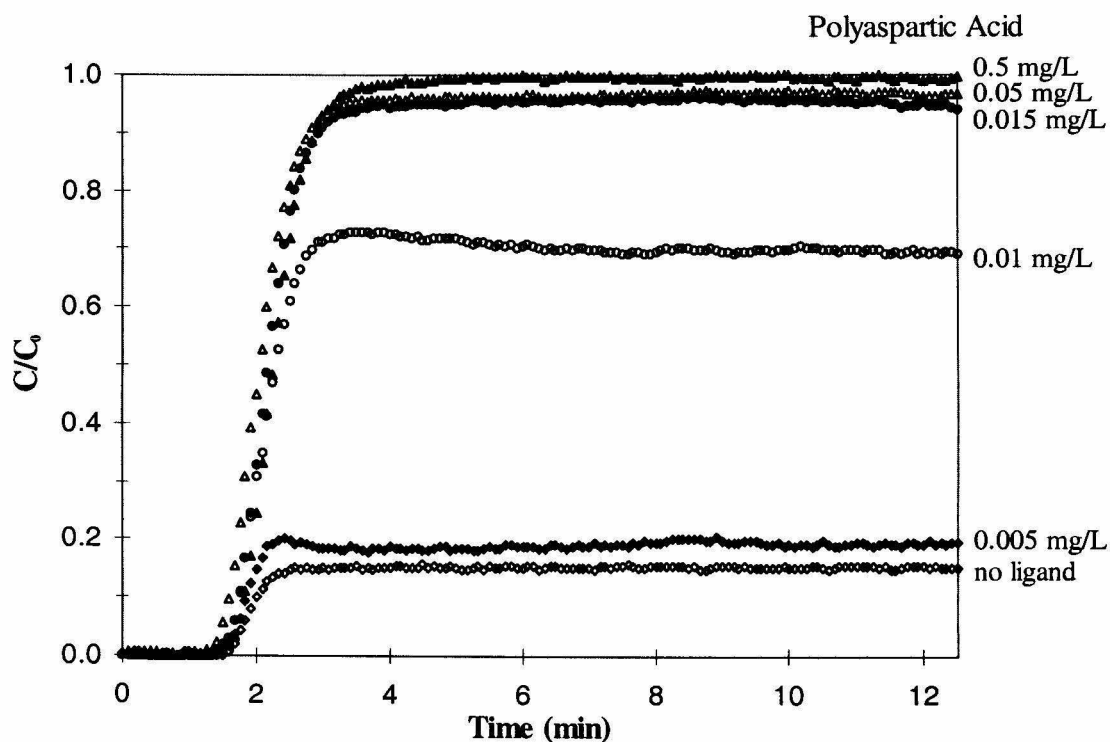


Figure 4.24: Hematite breakthrough curves in the presence of polyaspartic acid (5 cm bed depth, 1 cm/min approach velocity, pH 6.5, 1 mM NaCl, $C_0 = 1$ mg/L).

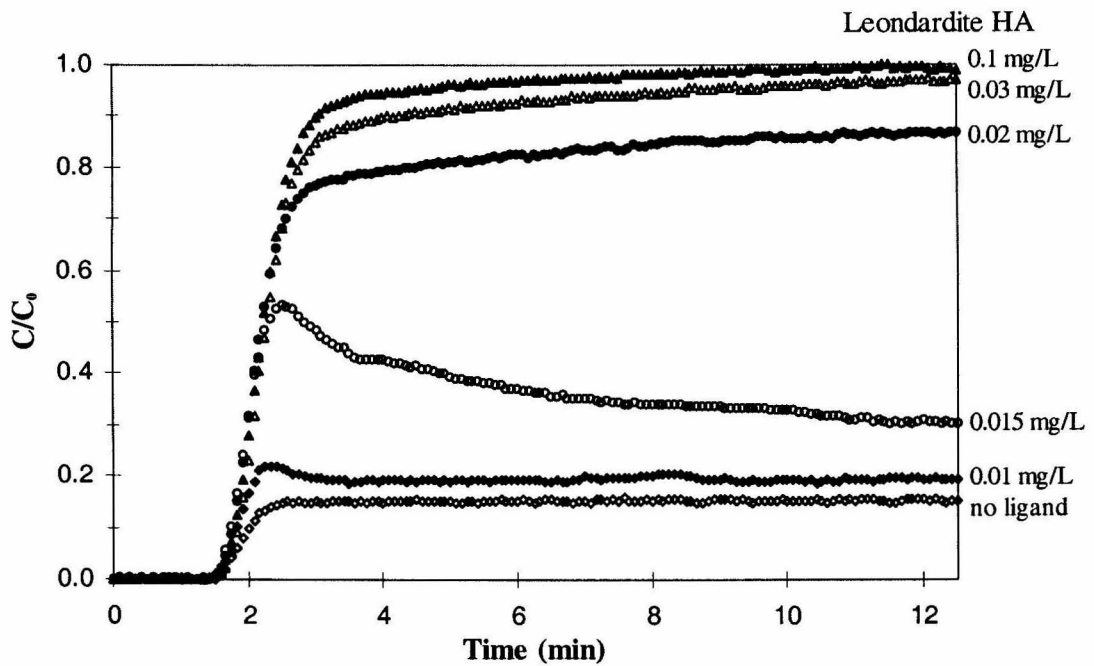


Figure 4.25: Hematite breakthrough curves in the presence of Leonardite humic acid (5 cm bed depth, 1 cm/min approach velocity, pH 6.5, 1 mM NaCl, $C_0 = 1$ mg/L).

for Leonardite humic acid (Leonardite HA), Figure 4.26 for Suwannee River fulvic acid (S.R. FA), and Figure 4.27 for Suwannee River humic acid (S.R. HA). The data are compared in Figure 4.28 where the collision efficiency is plotted as a function of total polyelectrolyte concentration. All four polyelectrolytes had a similar effect on hematite deposition, producing unfavorable deposition at total concentrations of 2×10^{-5} g/L or lower. The order of effectiveness in causing unfavorable deposition is

$$\text{PAA} > \text{S.R. HA} > \text{S.R. FA} \sim \text{Leonardite HA}$$

4.3 Electrokinetic Measurements

Proton exchange at amphoteric metal hydroxy groups on metal oxide surfaces results in either positively or negatively charged surfaces. Other specifically adsorbed ions are able to reduce the surface charge, and even cause charge reversal at sufficient concentrations. Electrophoretic mobility data provide independent information on the sign and magnitude of the surface charge.

The procedure for the electrophoretic mobility measurements is described in Section 3.4. The chemical conditions (e.g., pH, NaCl concentration, and presence of specifically adsorbed species) were the same as in the hematite deposition experiments except for the particle concentration. In order to achieve enough signal for mobility measurements, 10 mg/L hematite was used instead of 1 mg/L (C_0 in deposition experiments). Some of the electrophoretic mobility measurements were repeated using 50 mg/L hematite in an attempt to understand the effect of relative particle concentration on mobility. The standard deviation for the mobility measurements was less than 15%.

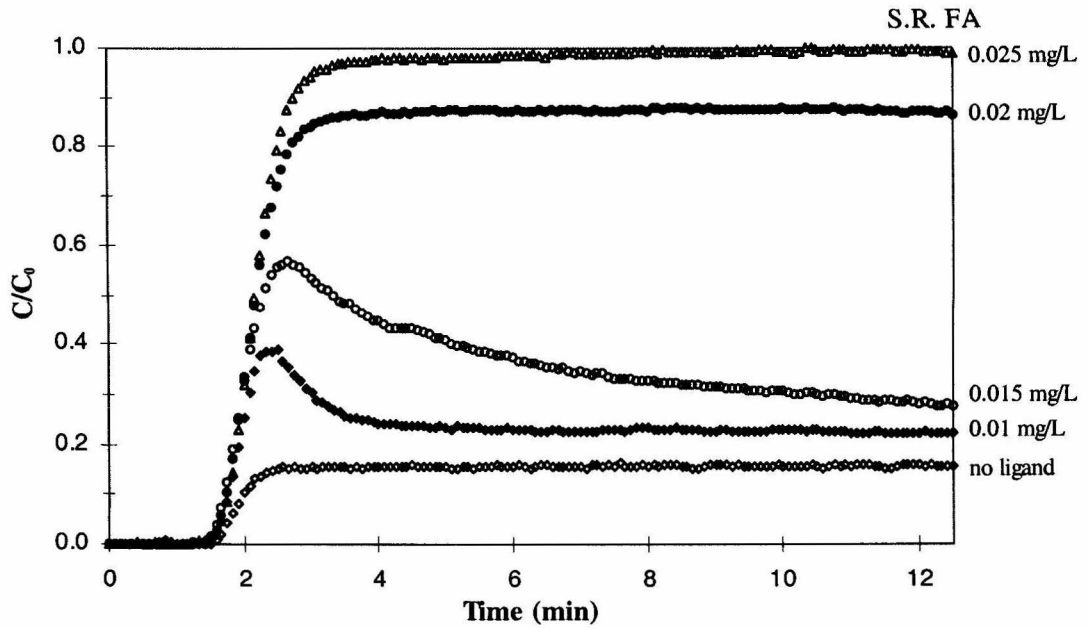


Figure 4.26: Hematite breakthrough curves in the presence of Suwannee River fulvic acid (5 cm bed depth, 1 cm/min approach velocity, pH 6.5, 1 mM NaCl, $C_0 = 1$ mg/L).

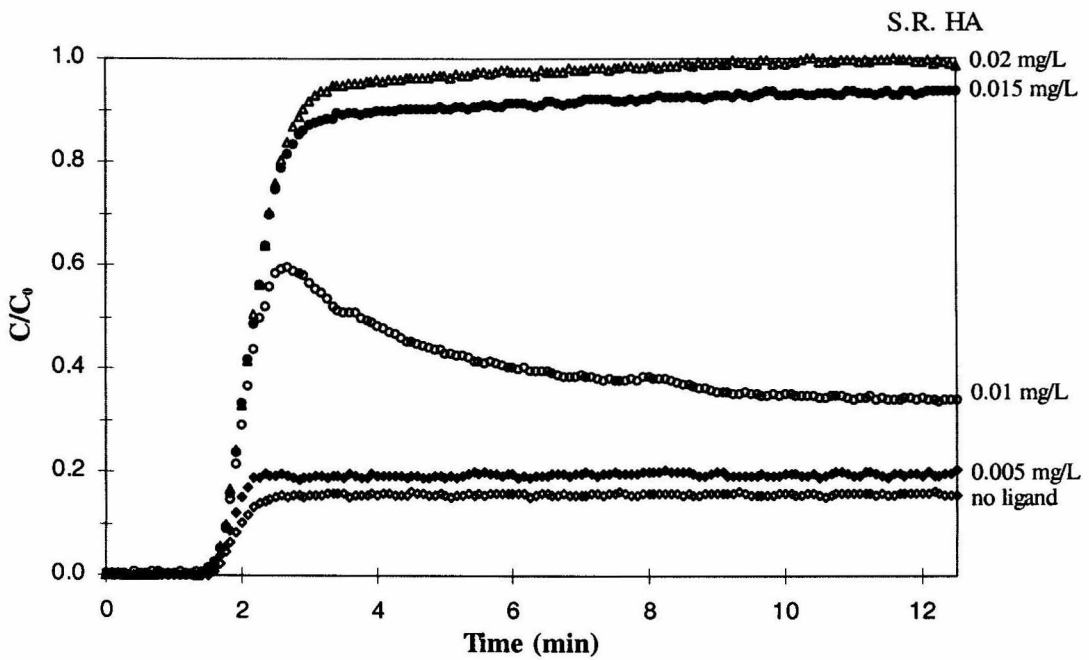


Figure 4.27: Hematite breakthrough curves in the presence of Suwannee River humic acid (5 cm bed depth, 1 cm/min approach velocity, pH 6.5, 1 mM NaCl, $C_0 = 1$ mg/L).

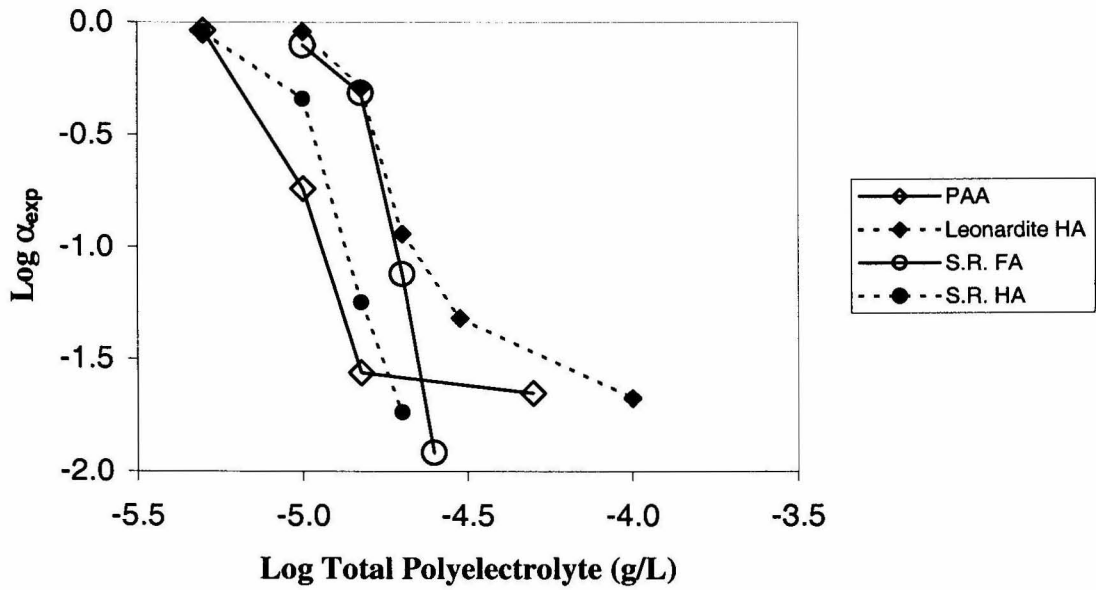


Figure 4.28: Experimental collision efficiency (α_{exp}) plotted as a function of total polyelectrolyte concentration (5 cm bed depth, 1 cm/min approach velocity, pH 6.5, 1 mM NaCl, $C_0 = 1$ mg/L).

4.3.1 Effect of pH on Silica Sand Mobility

The electrophoretic mobility of silica sand (Ottawa 30) particles was measured over the pH range of 1 to 8. These results are plotted in Figure 4.29 and show that the pH_{zpc} is ~ 2.2 , which is similar to reported values for other silica and quartz sands. At pH 6.5, where deposition experiments were conducted, the silica sand is highly negatively charged with a mobility of $-3 \mu\text{m}\cdot\text{sec}^{-1}/\text{V}\cdot\text{cm}^{-1}$.

4.3.2 Effect of pH on Hematite Mobility

The electrophoretic mobility of the hematite particles used in this research was measured as a function of pH. The results are plotted in Figure 4.30. The pH_{zpc} determined by electrophoretic mobility is approximately 7.5. The reported pH_{zpc} values for hematite range from 6.5 to 9.5. Figure 5.30 shows hematite mobility to be insensitive to pH below pH 6.5 and above pH 8.5 with a sharp decrease in mobility (from positive to negative) between pH 7 and 8. At the pH of the deposition experiments (6.5), hematite has a net positive surface charge and a mobility of about $2 \mu\text{m}\cdot\text{sec}^{-1}/\text{V}\cdot\text{cm}^{-1}$.

4.3.3 Hematite Mobility in the Presence of Inorganic Compounds

The electrophoretic mobility of hematite particles was measured as a function of phosphate, arsenate, and fluoride concentrations. The results are plotted in Figure 4.31 (phosphate), Figure 4.32 (arsenate), and Figure 4.33 (fluoride). The data show that phosphate and arsenate are both able to reduce hematite mobility as their concentrations increase. The sign of the mobility changes to negative as the concentration of phosphate and arsenate is increased further. The point of zero mobility is reached at $\sim 20 \mu\text{M}$ for phosphate and $\sim 10 \mu\text{M}$ for arsenate. Figure 4.33 shows that fluoride is able to reduce the

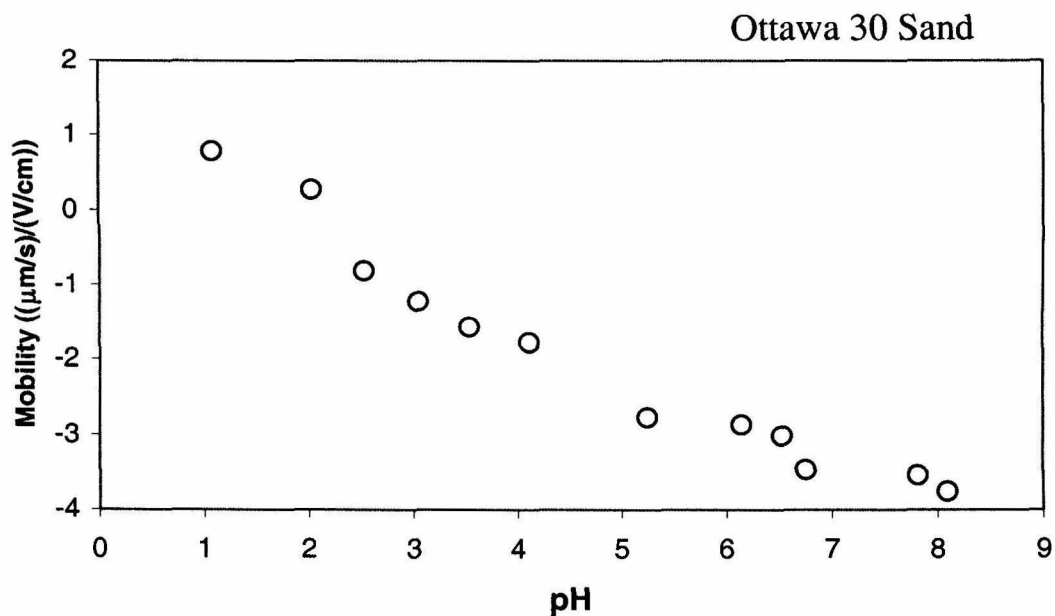


Figure 4.29: Electrophoretic mobility of silica sand (Ottawa 30) particles as a function of pH (1 mM NaCl).

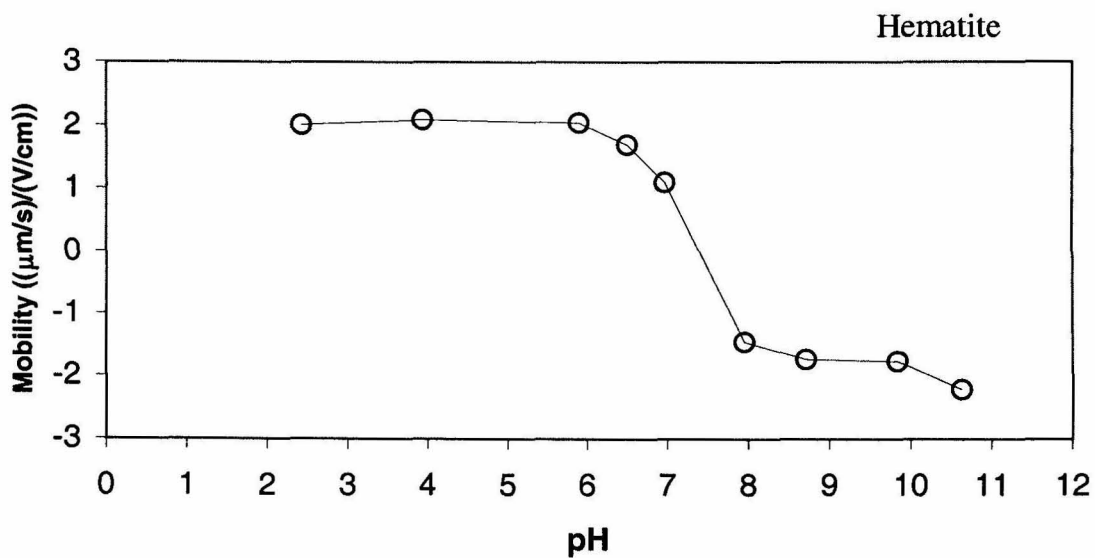


Figure 4.30: Electrophoretic mobility of hematite particles as a function of pH (1 mM NaCl).

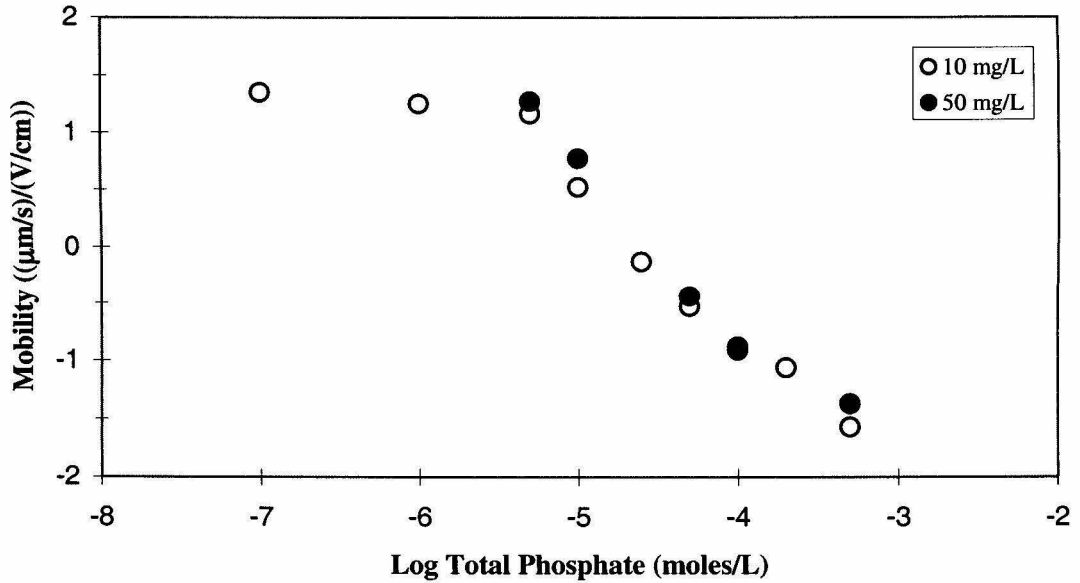


Figure 4.31: Electrophoretic mobility of hematite particles as a function of total phosphate concentration (pH 6.5, 1 mM NaCl).

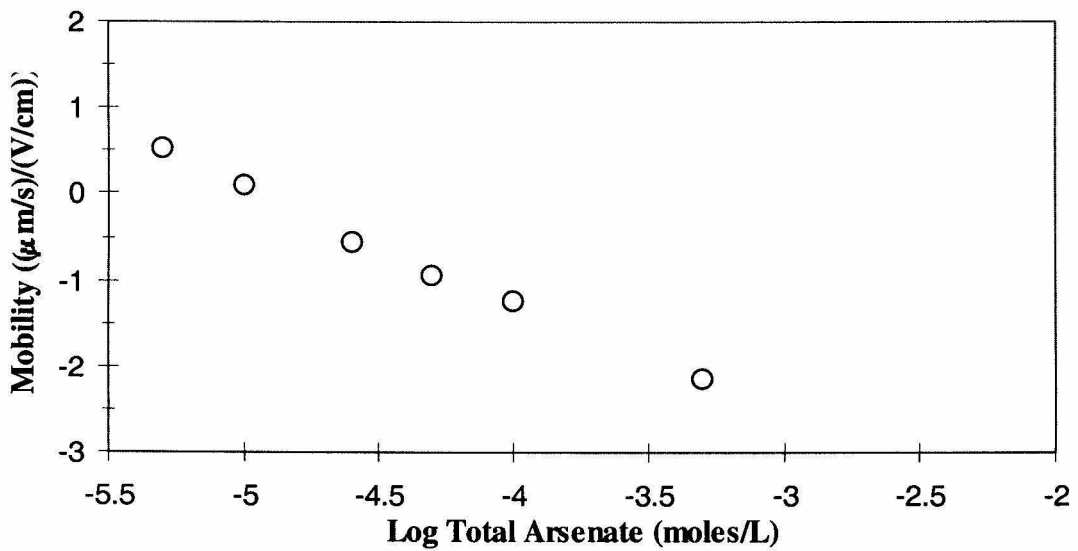


Figure 4.32: Electrophoretic mobility of hematite particles as a function of total arsenate concentration (pH 6.5, 1 mM NaCl, 10 mg/L hematite).

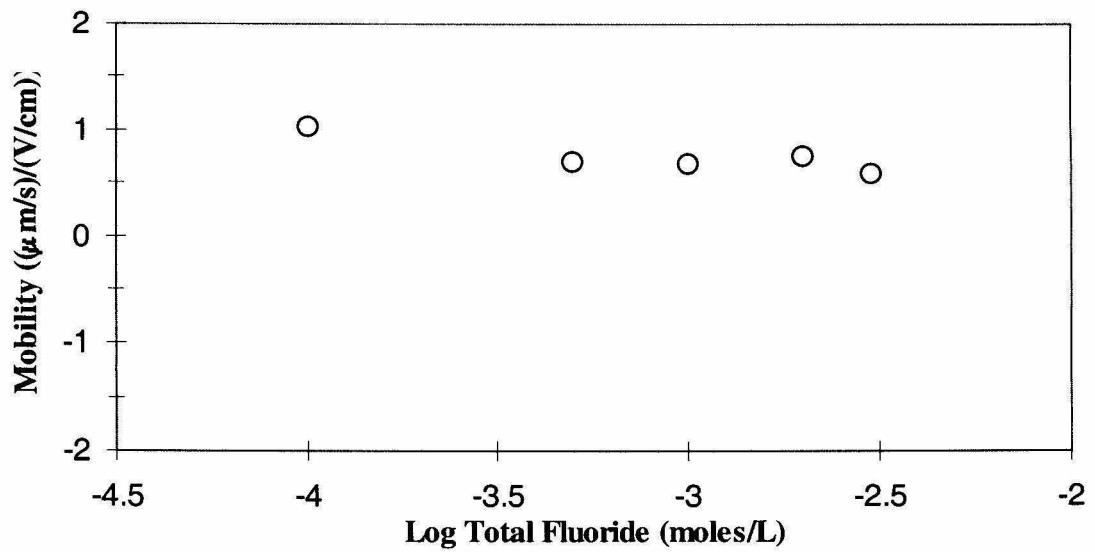


Figure 4.33: Electrophoretic mobility of hematite particles as a function of total fluoride concentration (pH 6.5, 1 mM NaCl, 10 mg/L hematite).

hematite mobility as concentration increases, but the hematite mobility remains positive at fluoride concentrations as high as 2 mM.

Phosphate was chosen as a representative case to study the effect of particle concentration on hematite mobility. In this case, hematite concentrations of 10 mg/L and 50 mg/L were used for mobility measurements in the presence of phosphate. These results are shown in Figure 4.31 for the 10 mg/L hematite data; they show no apparent effect of hematite particle concentration on mobility.

4.3.4 Hematite Mobility in the Presence of Oxalate and Related Compounds

The electrophoretic mobility of hematite is influenced by the addition of oxalic acid (C_2), succinic acid (C_4), adipic acid (C_6), and suberic acid (C_8), as illustrated in Figure 4.34. The dicarboxylic acids have a similar effect on the mobility of hematite, in that the mobility is reduced with an increase in concentration. In each case, zero mobility is reached at approximately 1 mM.

4.3.5 Hematite Mobility in the Presence of Phthalate and Related Compounds

Hematite mobility was studied as a function of 1,2-benzenedicarboxylic acid (phthalic acid), 1,2,4-benzenetricarboxylic acid (benzene-tri), and 1,2,4,5-benzenetetracarboxylic acid (benzene-tetra). These results are plotted in Figure 4.35. The obvious features are that (1) hematite mobility is reduced as the concentration of each compound increases, (2) benzene-tetra is more effective than benzene-tri at reducing mobility, (3) while benzene-tri is more effective than phthalate at reducing mobility, and (4) zero mobility is achieved at about 0.3 μM for benzene-tetra, 10 μM for benzene-tri, and 300 μM for phthalate.

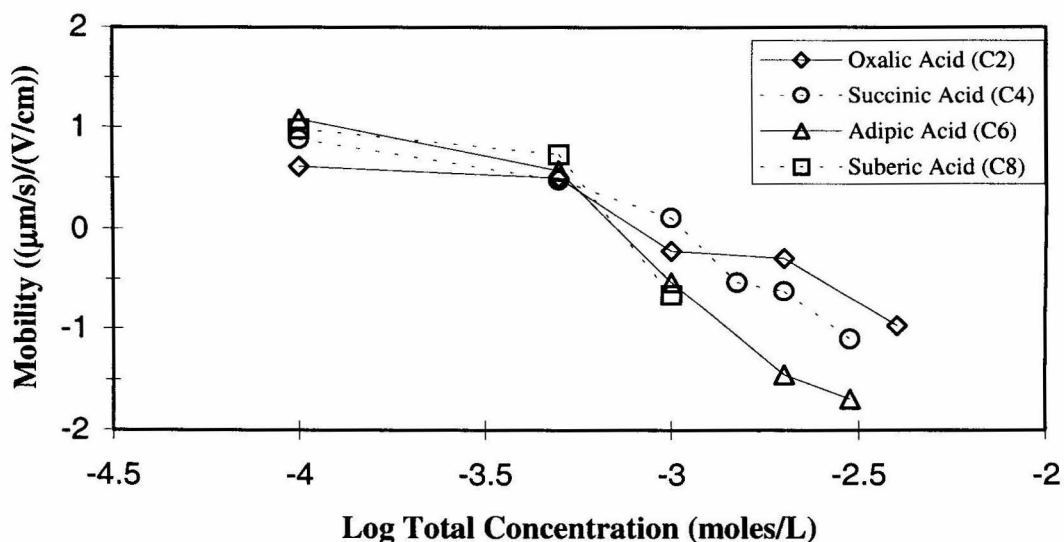


Figure 4.34: Electrophoretic mobility of hematite particles as a function of total concentration of oxalate and other dicarboxylic acids (pH 6.5, 1 mM NaCl, 10 mg/L hematite).

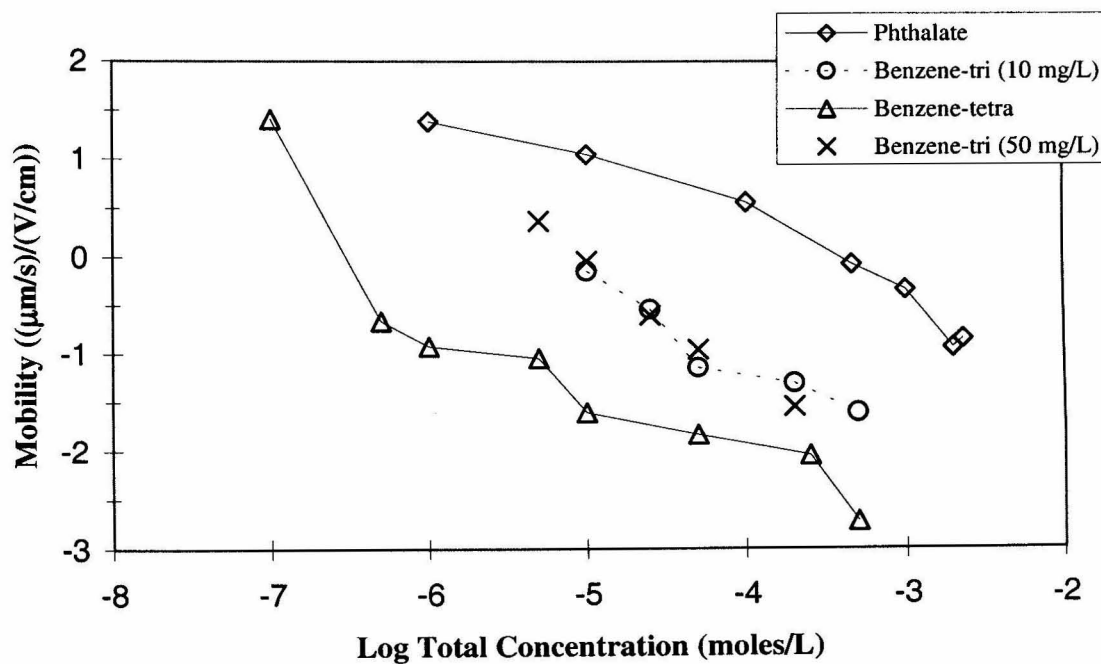


Figure 4.35: Electrophoretic mobility of hematite particles as a function of total concentration of phthalate and other aromatic carboxylates (pH 6.5, 1 mM NaCl, 10 mg/L hematite unless stated otherwise).

The effect of particle concentration on hematite mobility was studied for the benzene-tri case. The mobility measurements for 50 mg/L suspensions of hematite are shown in Figure 4.35 along with similar measurements at 10 mg/L. These results show that particle concentration does not influence hematite mobility in the presence of benzene-tri.

4.3.6 Hematite Mobility in the Presence of Aspartic Acid

The electrophoretic mobility of hematite as a function of the aspartic acid concentration is shown in Figure 4.36. Hematite mobility decreases with increasing total concentration, with mobility changes being most rapid near zero mobility. The total aspartic acid concentration needed to produce zero mobility is approximately 8×10^{-4} molar.

4.3.7 Hematite Mobility in the Presence of Butyric Acid

Hematite mobility was not influenced by the addition of butyric acid, as illustrated in Figure 4.37. Total butyric acid concentrations as high as 3 mM were unable to alter the mobility of hematite.

4.3.8 Hematite Mobility in the Presence of Lauryl Sulfate

In Figure 4.38, hematite mobility as a function of lauryl sulfate concentration is shown. The addition of lauryl sulfate decreased the mobility to zero at about 67 μ M.

4.3.9 Hematite Mobility in the Presence of Polymeric Organic Compounds

Hematite mobility was studied as a function of polyaspartic acid (PAA), Leonardite humic acid (Leonardite HA), Suwannee River fulvic acid (S.R. FA), and Suwannee River humic acid (S.R. HA). These results are compared in Figure 4.39. The most obvious features of the data are that (1) the NOM samples decrease hematite

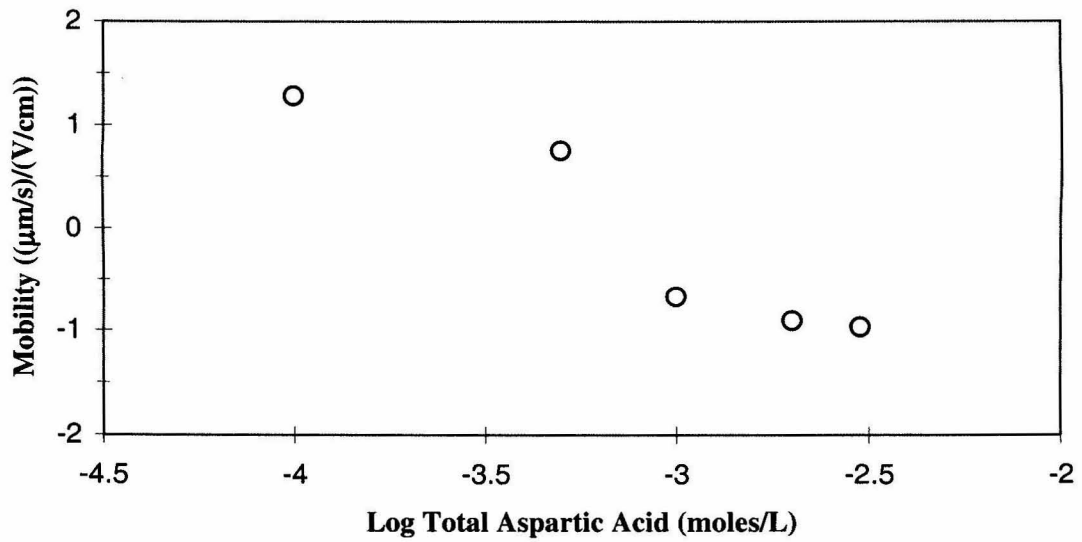


Figure 4.36: Electrophoretic mobility of hematite particles as a function of total aspartic acid concentration (pH 6.5, 1 mM NaCl, 10 mg/L hematite).

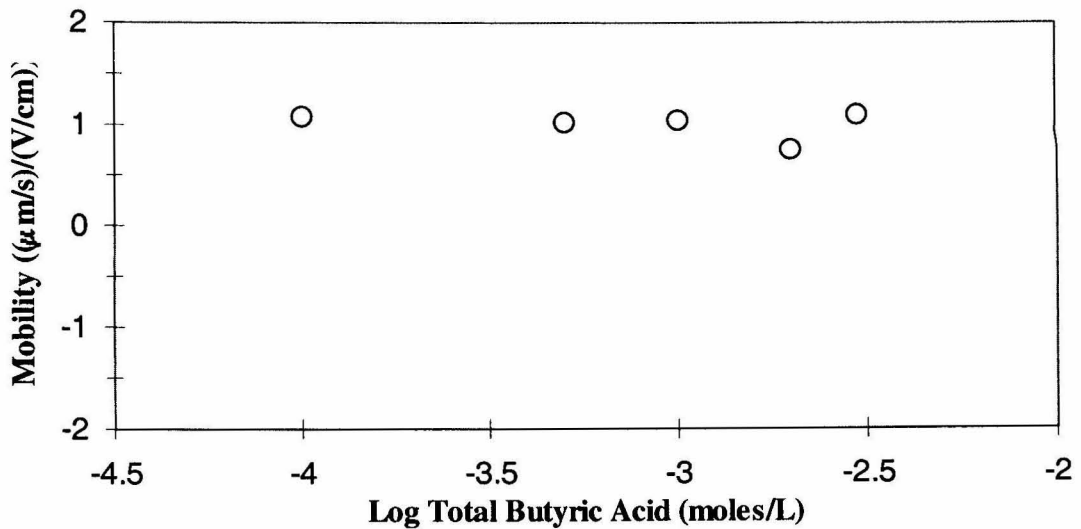


Figure 4.37: Electrophoretic mobility of hematite particles as a function of total butyric acid concentration (pH 6.5, 1 mM NaCl, 10 mg/L hematite).

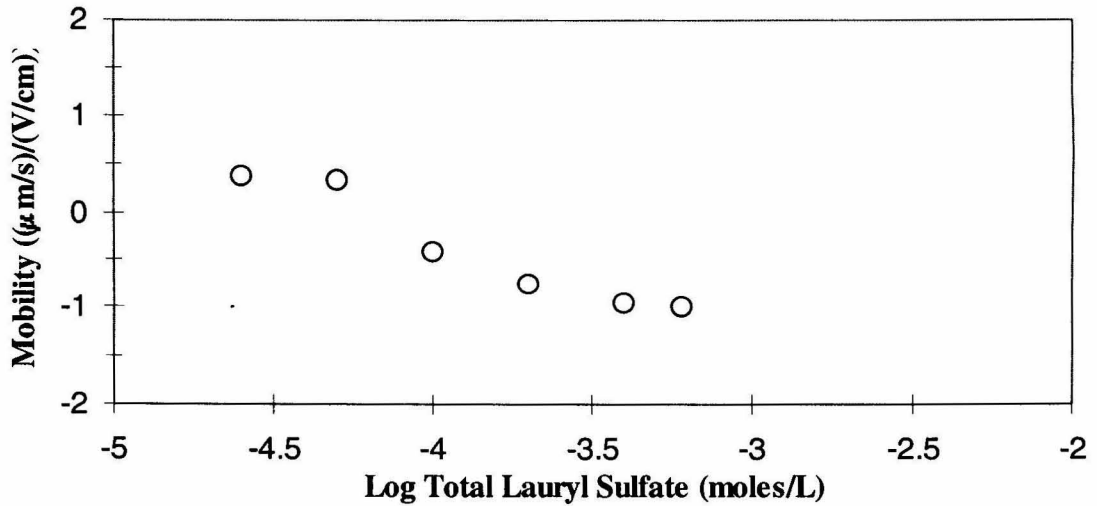


Figure 4.38: Electrophoretic mobility of hematite particles as a function of total lauryl sulfate concentration (pH 6.5, 1 mM NaCl, 10 mg/L hematite).

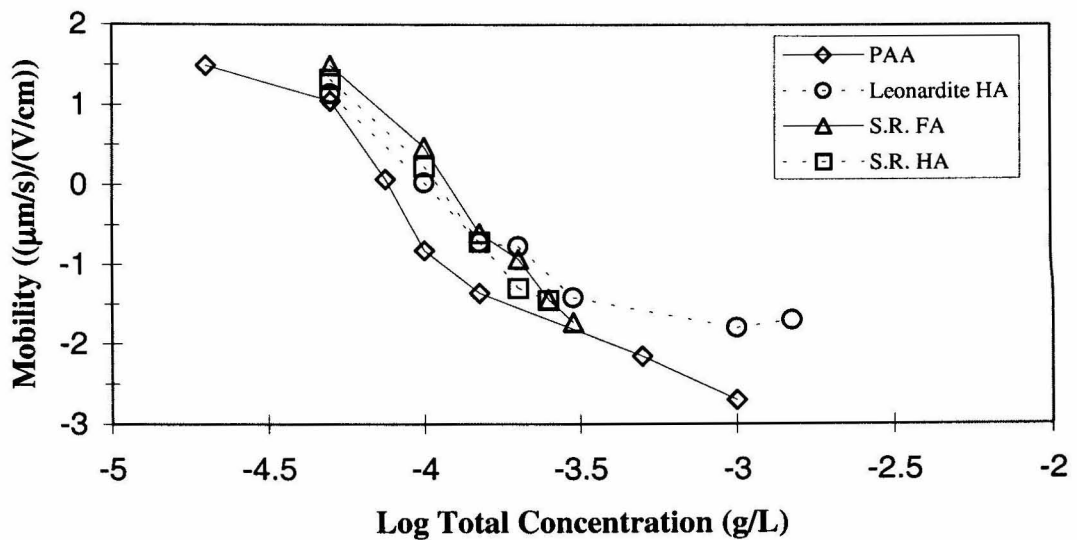


Figure 4.39: Electrophoretic mobility of hematite particles as a function of total concentration of polyelectrolyte (pH 6.5, 1 mM NaCl, 10 mg/L hematite).

mobility as their total concentration increases in a similar fashion, and (2) that zero mobility is achieved at approximately 10^{-4} g/L for each compound.

Mobility measurements using a 50 mg/L suspension of hematite in the presence of PAA were made and compared to a 10 mg/L hematite suspension (Figure 4.40). Similar measurements were made for S.R. HA and this comparison is shown in Figure 4.41. Unlike the cases for phosphate and benzene-tri, the hematite particle concentration appears to influence the measured hematite mobility in the presence of PAA and S.R. HA. For PAA (Figure 4.39) with 50 mg/L hematite, the mobility measurements are shifted to the right (i.e., to higher total PAA concentration) compared to the 10 mg/L hematite suspensions. In these cases, the mobility measurements are shifted approximately by a factor of 5, which corresponds to the relative difference in the hematite particle concentrations. The same trend is true for the S.R. HA data (i.e., the measurements with 50 mg/L hematite are shifted to higher total S.R. HA concentrations by a factor of 5 relative to the measurements made with 10 mg/L hematite).

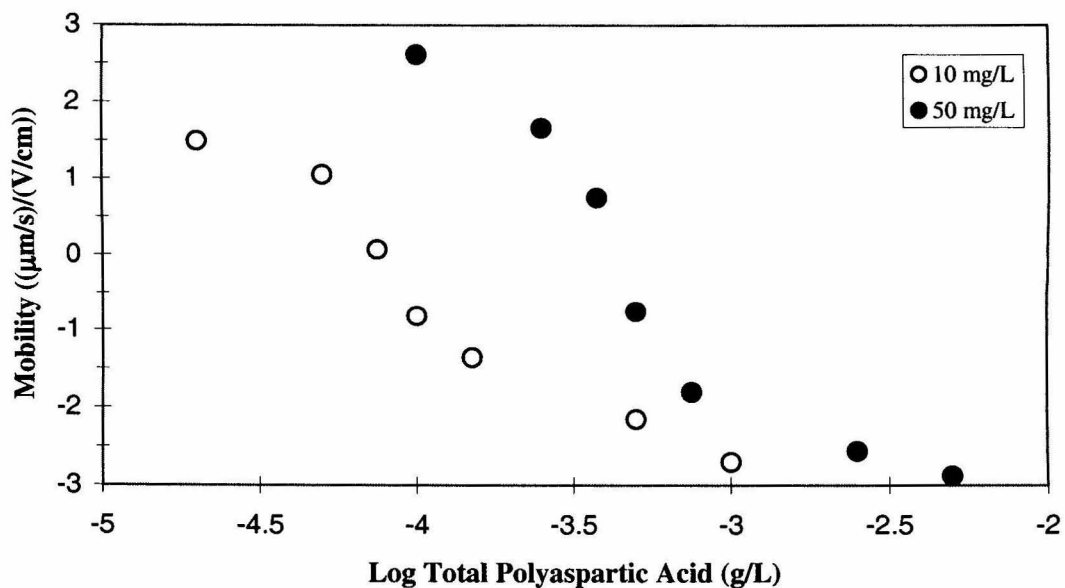


Figure 4.40: Electrophoretic mobility of hematite particles as a function of total polyaspartic acid (PAA) concentration (pH 6.5, 1 mM NaCl).

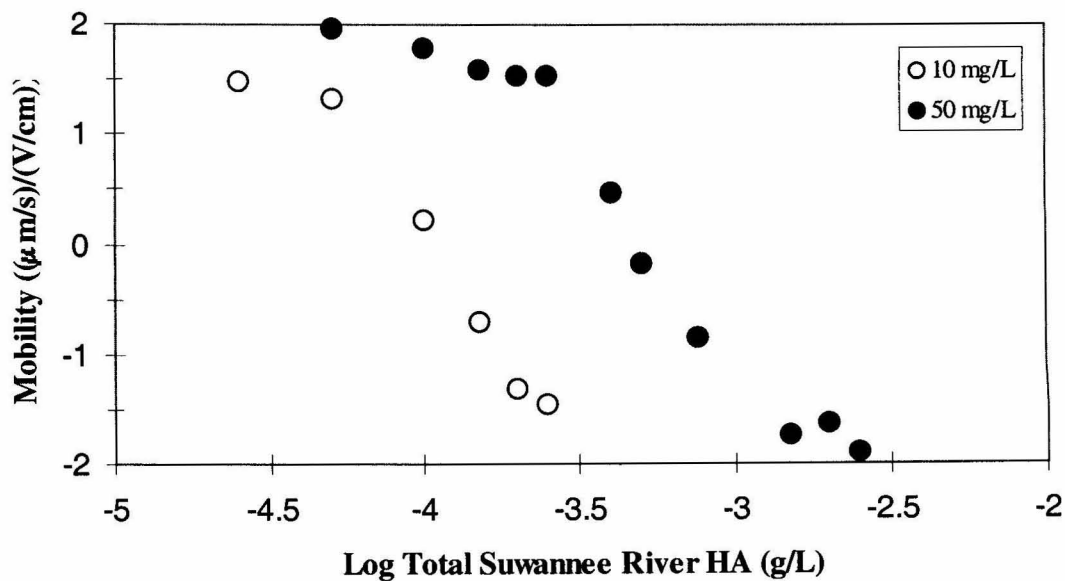


Figure 4.41: Electrophoretic mobility of hematite particles as a function of total Suwannee River HA concentration (pH 6.5, 1 mM NaCl).

Chapter 5. Discussion of Results

5.0 Introduction

The results presented in Chapter 4 are discussed in this chapter. Hematite surface charge and potential change as aqueous chemical conditions are varied. The changes are a result of the adsorption of aqueous species on the surface of hematite, and electrophoretic mobility is a direct measure of the ζ -potential produced by the adsorption process. In the absence of specifically adsorbed species at pH 6.5 and 1 mM NaCl, hematite deposition in a silica sand bed is favorable due to attractive electrostatic interactions. The experimental results (Chapter 4) clearly showed that the addition of specifically adsorbed solutes can produce unfavorable deposition conditions by changing the magnitude and sign of the surface charge on hematite.

5.1 Particle Mobility, ζ -Potential and Surface Potential

In particle electrophoresis, the particle drags some liquid with it as it moves. The slipping plane separates the bulk liquid from the liquid moving with the particle. The ζ -potential is defined as the electrostatic potential on the slipping plane, and it is proportional to the electrophoretic mobility. Wiersema et al. (1966) described a procedure for converting mobility data into ζ -potential values for a spherical particle.

The surface potential is used in calculating the electrostatic interaction energy. Since the ζ -potential is defined at a finite distance from the surface, it is usually less than the surface potential. The surface potential can be related to the ζ -potential by employing

a physical model of the interface (e.g., the Gouy-Chapman diffuse layer model). In particle deposition studies, the assumption that the ζ -potential equals the effective surface potential is often made.

5.2 Hematite Deposition in the Presence of Inorganic Solutes

5.2.1 Hematite Deposition in the Presence of Phosphate and Arsenate

Phosphate and arsenate were shown to control hematite deposition and mobility at pH 6.5 and 1 mM NaCl. Figure 5.1 compares the collision efficiency and electrophoretic mobility as a function of total phosphate concentration, and Figure 5.2 shows the comparison as a function of total arsenate concentration. In both cases (phosphate and arsenate), the collision efficiency is near 1 at 10 μM total concentration and lower. For phosphate, the collision efficiency decreases gradually as the total concentration increases from 10 to 50 μM with a sharp decrease in the collision efficiency to unfavorable deposition ($\log \alpha_{\text{exp}} \leq -1.5$, or $\alpha_{\text{exp}} \leq 0.03$) as the total concentration increases to about 100 μM . The collision efficiency data for arsenate are similar, but the transition from favorable deposition ($0.2 \leq \alpha_{\text{exp}} \leq 1$) to unfavorable deposition ($\alpha_{\text{exp}} \leq 0.03$) is sharper than in the phosphate case, with unfavorable deposition occurring at around 50 μM .

The mobility data is shown in Figures 5.1 and 5.2 suggest that electrostatic interactions control the hematite deposition rate (α_{exp}) in the presence of phosphate and arsenate. The decreasing trend in the collision efficiency with increasing total concentration is accompanied by a decreasing trend in the hematite mobility. Collision efficiencies near 1 correspond to positive hematite mobility values (attractive electrostatics). The departure of the collision efficiency from near 1 to lower values takes

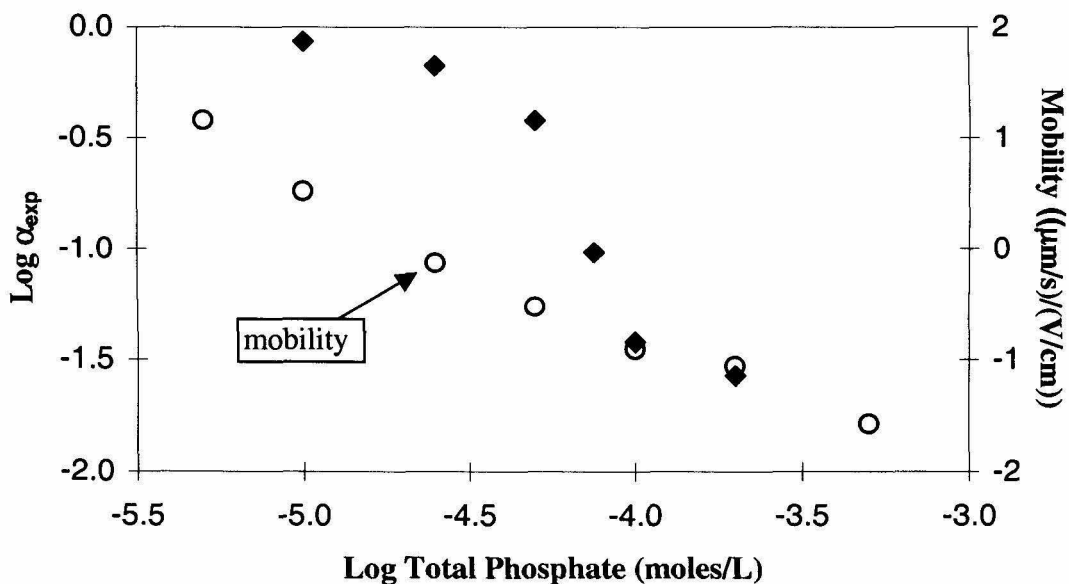


Figure 5.1: Comparison of collision efficiency, α_{exp} , and hematite mobility as a function of total phosphate concentration at pH 6.5 and 1 mM NaCl.

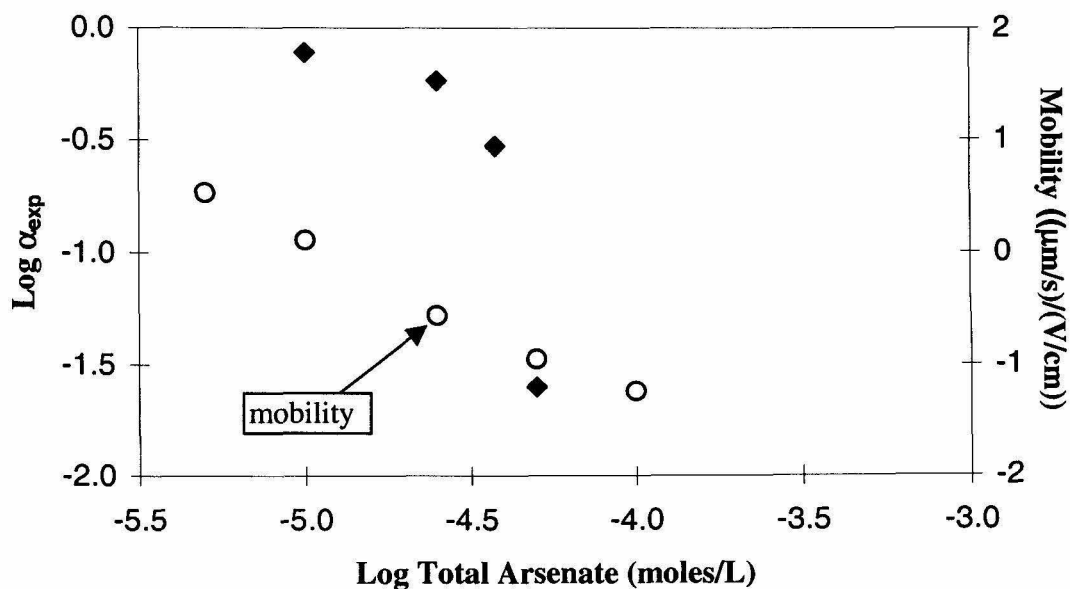
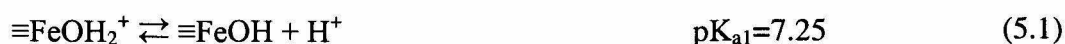


Figure 5.2: Comparison of collision efficiency, α_{exp} , and hematite mobility as a function of total arsenate concentration at pH 6.5 and 1 mM NaCl.

place at the total concentration that results in the change of the hematite mobility from positive to negative. Therefore, the onset of repulsive electrostatics results in the decrease of hematite deposition rates below the transport limited rate. Unfavorable deposition ($\alpha_{\text{exp}} \leq 0.03$) is achieved when the hematite mobility reaches $-1 \mu\text{m}\cdot\text{s}^{-1}/\text{V}\cdot\text{cm}^{-1}$ for both phosphate and arsenate.

A description of phosphate adsorption on hematite can illustrate how surface chemical reactions are able to influence hematite mobility by changing the surface speciation. The surface speciation determines the surface charge, which in turn (along with ionic strength) determines the surface potential. The surface potential is proportional to the ζ -potential, which is proportional to the electrophoretic mobility. Liang (1988) was able to model the adsorption of phosphate on hematite by assuming that the surface species were $\equiv\text{FeOH}_2^+$, $\equiv\text{FeOH}$, $\equiv\text{FeO}^-$, $\equiv\text{FePO}_4\text{H}_2$, $\equiv\text{FePO}_4\text{H}^-$, and $\equiv\text{FePO}_4^{2-}$. A good fit to her data was achieved by using the following reactions and equilibrium constants:



The pH_{zpc} of the hematite used in this research was 7.5. (Liang's hematite had a pH_{zpc} of 8.5) The deposition and mobility experiments were conducted at pH 6.5, therefore, $\equiv\text{FeOH}_2^+$ and $\equiv\text{FeOH}$ would dominate over $\equiv\text{FeO}^-$. Reactions (5.4) and (5.5) show how negatively charged surface species can be produced by phosphate reacting

with the uncharged $\equiv\text{FeOH}$ site. Charge-altering reactions involving $\equiv\text{FeOH}_2^+$ can be obtained by combining reactions (5.1) and (5.4) as well as combining reactions (5.1) and (5.5) to give



Reactions (5.6) and (5.7) illustrate how negatively charged surface species can be produced by phosphate reacting with the positively charged $\equiv\text{FeOH}_2^+$ site. Hence, it is evident that adding phosphate to a hematite suspension dominated by $\equiv\text{FeOH}_2^+$ and $\equiv\text{FeOH}$ produces negatively charged surface species ($\equiv\text{FePO}_4\text{H}^-$ and $\equiv\text{FePO}_4^{2-}$) that decrease the surface charge and potential. At sufficient concentrations, phosphate results in charge reversal. Hematite mobility in the presence of phosphate can be explained simply by invoking surface complexation as illustrated above.

5.2.2 Hematite Deposition in the Presence of Fluoride

Figure 5.3 compares the collision efficiency and hematite mobility as a function of total fluoride concentration. The fact that fluoride shows little influence the collision efficiency can be explained by fluoride's inability to alter the mobility of hematite. Only a slight decrease in the mobility is observed as fluoride is added and the total concentration is increased beyond 2 mM. Since the hematite mobility remains positive over the entire range of concentrations studied, deposition remains favorable (attractive electrostatics).

5.2.3 Effect of Particle Concentration on Hematite Mobility

The results of this research are presented in terms of the "total" concentration of solute added, as was the case in related work done on hematite coagulation (Liang, 1988;

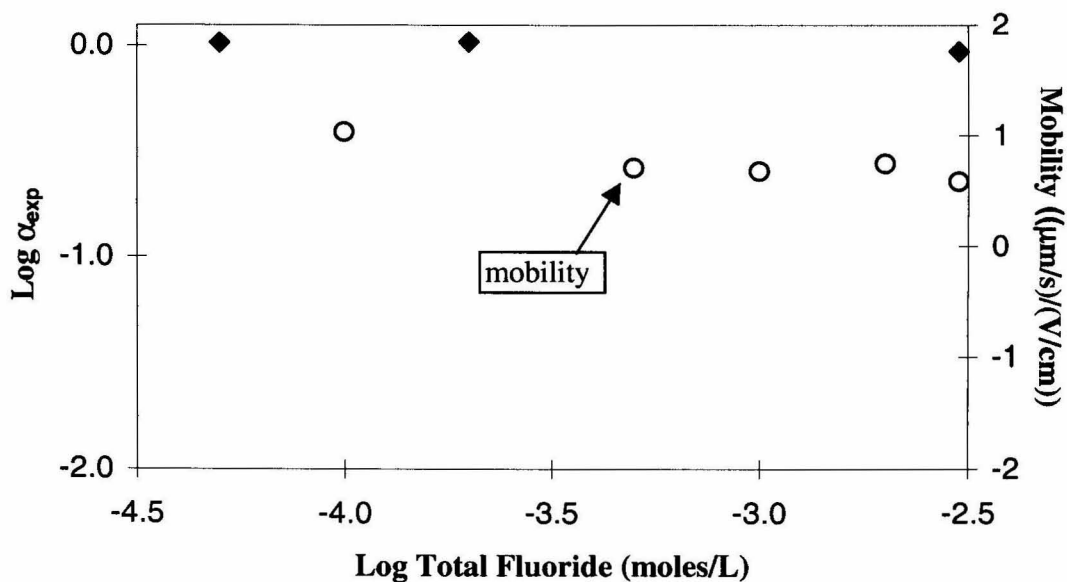


Figure 5.3: Comparison of collision efficiency, α_{exp} , and hematite mobility as a function of total fluoride concentration at pH 6.5 and 1 mM NaCl.

Tiller, 1993). This is a practical matter because expressing the mobility (or collision efficiency) as a function of the aqueous concentration of the solute (or adsorbed concentration) would require separate adsorption studies to be performed. Consequently, one must consider the possible influence of particle concentration.

While the deposition experiments had an influent particle concentration (C_0) of 1 mg/L, the mobility measurements required 10 mg/L hematite for reproducible results. The influence of particle concentration was investigated for the case of phosphate by making another set of mobility measurements using 50 mg/L hematite. Suspensions with higher particle concentrations were too turbid for mobility measurements to be made. Figure 4.31 shows that hematite mobility as a function of total phosphate concentration is the same for 10 mg/L and 50 mg/L hematite. The absence of a particle concentration

effect suggests that the mobility for 1 mg/L hematite (C_0) is the same as the mobility for 10 mg/L hematite. Therefore, the hematite mobility data for 10 mg/L can be used to interpret the hematite deposition data ($C_0 = 1$ mg/L) without correction.

Another approach for investigating the influence of particle concentration on hematite mobility in the presence of phosphate is to make chemical equilibrium calculations using different particle concentrations. The software program MINEQL+ was used to model the adsorption of phosphate on hematite at pH 6.5 and 1 mM NaCl. The calculations utilized reactions (5.1) through (5.5). In order to make the results more pertinent to the hematite used in this research (pH_{zpc} of 7.5), a $\text{pK}_{\text{a}1}$ of 6.25 was assumed for reaction (5.1) and a $\text{pK}_{\text{a}2}$ of 8.75 was assumed for reaction (5.2). The results of the calculations are presented in Figure 5.4 where the surface potential is plotted as a function of total phosphate concentration for hematite concentrations of 1, 10, and 17 mg/L. The evident features of the calculation results are (1) the surface potentials for the three hematite concentrations are different at a total phosphate concentration of 0.1 μM , (2) the surface potentials converge as the total phosphate increases, and (3) the surface potentials are basically the same at total phosphate concentrations of 0.5 μM and higher. The surface potential calculations give additional evidence of hematite mobility being independent of particle concentration in the presence of phosphate.

5.3 Hematite Deposition in the Presence of Small Organic Molecules

5.3.1 Hematite Deposition in the Presence of Oxalate and Related Compounds

The hematite deposition and electrophoretic mobility results for oxalic acid (C_2), succinic acid (C_4), adipic acid (C_6), and suberic acid (C_8) are all very similar (Figures 4.13 and 4.34). As a representative case, the collision efficiency and mobility are

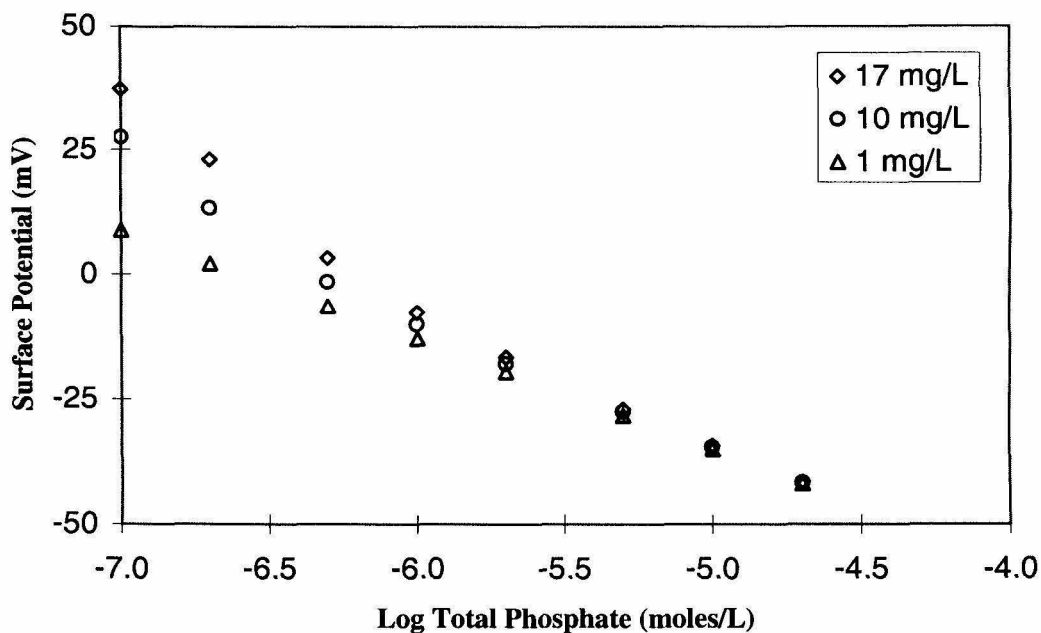


Figure 5.4: Calculated hematite surface potential as a function of total phosphate concentration for different hematite particle concentrations (pH 6.5 and 1 mM ionic strength). Model calculations were made using MINEQL+.

compared as a function of total succinic acid concentration in Figure 5.5. Succinic acid fails to produce unfavorable deposition ($\alpha_{\text{exp}} \leq 0.03$) at total concentrations as high as 4 mM. However, the mobility measurements show hematite mobility being reversed (from positive to negative) at around 1 mM. In addition, near 4 mM total succinic acid concentration, the value of the mobility is around $-1 \mu\text{m}\cdot\text{s}^{-1}/\text{V}\cdot\text{cm}^{-1}$, which resulted in unfavorable deposition in the case of phosphate and arsenate. Based on electrostatic considerations, one would expect the dicarboxylic acids to cause unfavorable deposition at total concentrations around 4 mM.

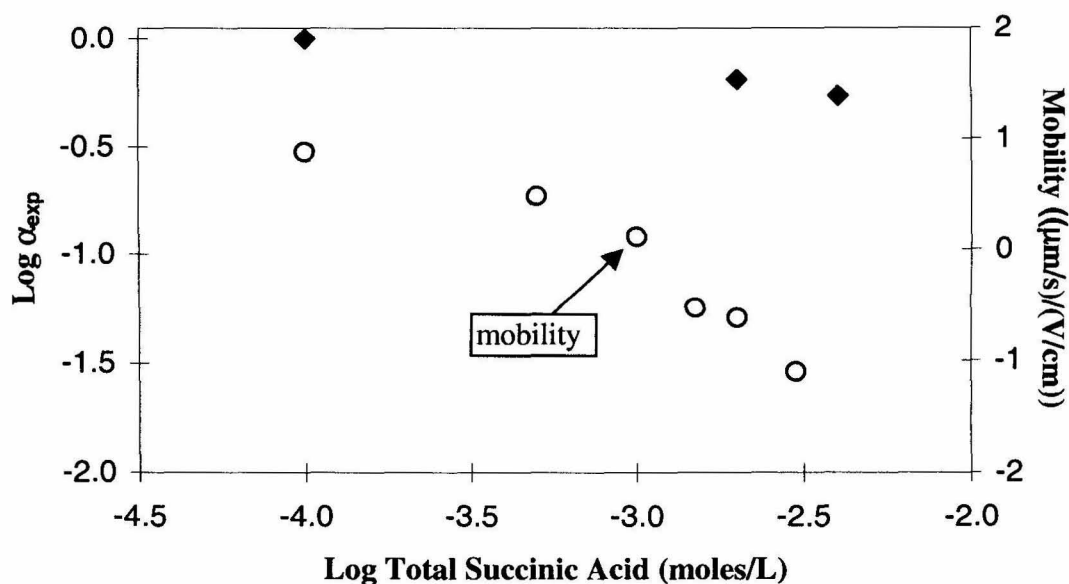


Figure 5.5: Comparison of collision efficiency, α_{exp} , and hematite mobility as a function of total succinic acid concentration at pH 6.5 and 1 mM NaCl.

When considered separately, the deposition and mobility data in the presence of oxalate are consistent with results reported for coagulation and adsorption studies. Liang (1988) observed that the addition of oxalate increased hematite coagulation rates as the total oxalate concentration increased. The coagulation rate reached a maximum (near transport limited coagulation) at a total oxalate concentration of 10^{-4} molar, but the coagulation rate remained constant as the total oxalate concentration was increased to 2 mM. The fact that the coagulation rate did not decrease as the total oxalate was increased beyond 100 μM , suggests that the hematite surface charge was not reversed by the surface complexation of oxalate (Liang didn't measure the hematite mobility in the presence of oxalate). This is consistent with the deposition rates observed in this research, where only a slight decrease in the deposition rate is observed as the total

oxalate is increased beyond 1 mM. Zhang and co-workers (1985) studied the adsorption of oxalic acid on hematite. At 1 mM total oxalate (pH 6.5), an electrophoretic mobility of $-1.5 \mu\text{m}\cdot\text{s}^{-1}/\text{V}\cdot\text{cm}^{-1}$ was measured. This is consistent with our measured hematite mobility of around $-1 \mu\text{m}\cdot\text{s}^{-1}/\text{V}\cdot\text{cm}^{-1}$ for 4 mM total oxalate. This significant reversal in mobility was also observed by Djafer and co-workers (1991) who investigated the adsorption of oxalate on goethite ($\alpha\text{-FeOOH}$).

The production of negative surface charge by the adsorption of a dicarboxylic acid on a metal oxide surface dominated by positive and uncharged sites can be explained by a surface complexation approach (Kummert and Stumm, 1980) analogous to the one described previously for phosphate adsorption.

5.3.2 Hematite Deposition in the Presence of Phthalate and Related Compounds

Figure 5.6 compares the collision efficiency and mobility as a function of total phthalate concentration. The results are similar to those for succinic acid (and its related compounds) (Figure 5.5). Only a slight decrease in the collision efficiency is observed at total phthalate concentrations corresponding to mobility values near $-1 \mu\text{m}\cdot\text{s}^{-1}/\text{V}\cdot\text{cm}^{-1}$. Therefore, one would expect unfavorable deposition ($\alpha_{\text{exp}} \leq 0.03$) at total phthalate concentrations around 2 mM based on electrostatic considerations.

The collision efficiency and hematite mobility as a function of total benzene-tri (1,2,4-benzenetricarboxylic acid) concentration are compared in Figure 5.7. It is evident that the collision efficiency is determined by electrostatic interactions. Favorable deposition takes place when hematite mobility is positive (attractive electrostatics). The collision efficiency starts to decrease when the mobility is reversed (from positive to negative), and continues to decrease as the hematite mobility becomes more negative.

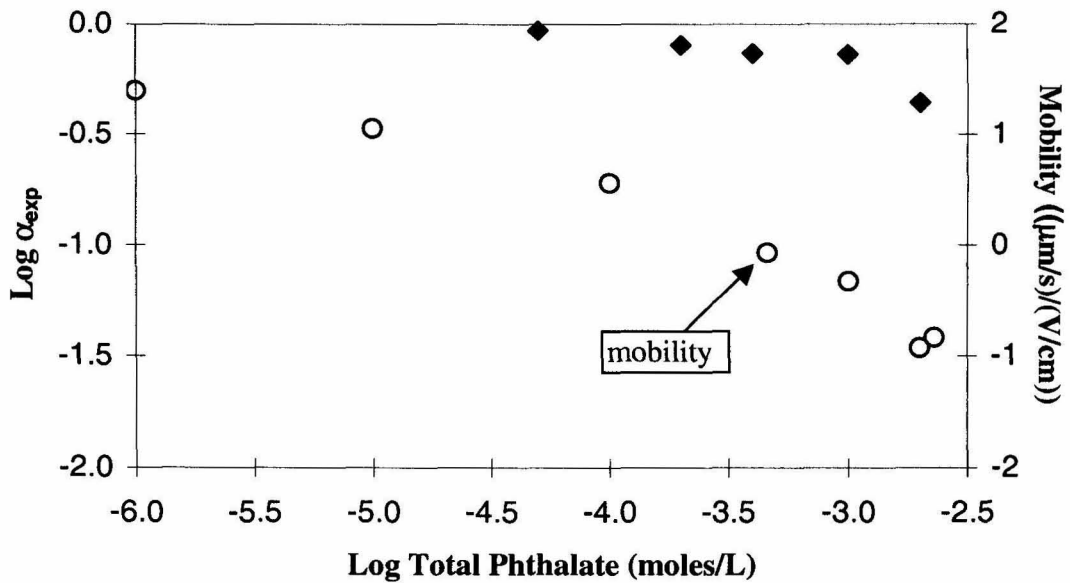


Figure 5.6: Comparison of collision efficiency, α_{exp} , and hematite mobility as a function of total phthalate concentration at pH 6.5 and 1 mM NaCl.

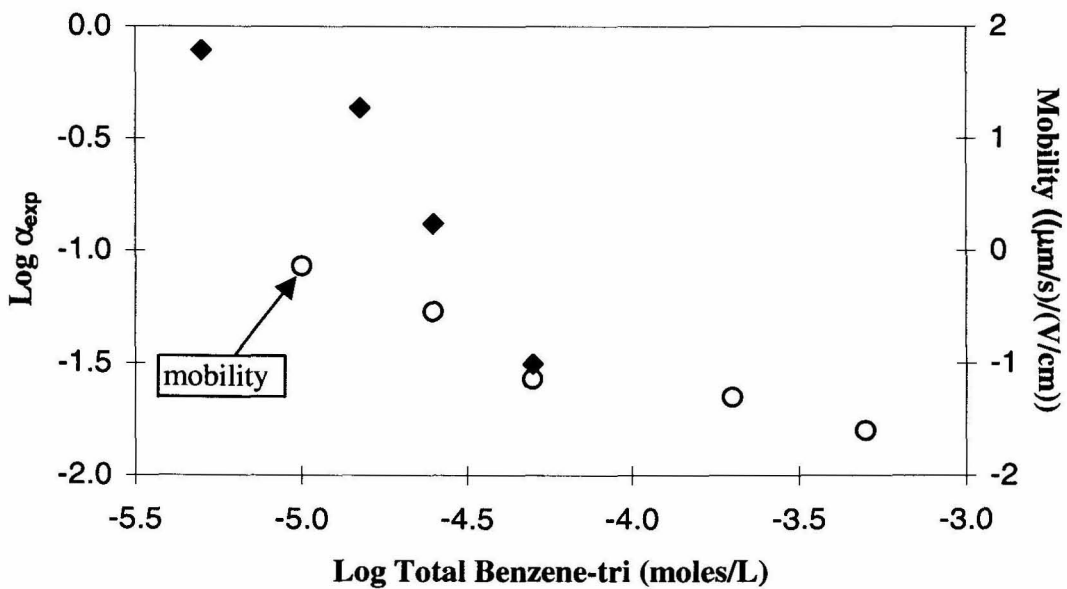


Figure 5.7: Comparison of collision efficiency, α_{exp} , and hematite mobility as a function of total benzene-tri concentration at pH 6.5 and 1 mM NaCl.

Unfavorable deposition ($\alpha_{\text{exp}} \leq 0.03$) coincides with a mobility of $-1 \mu\text{m}\cdot\text{s}^{-1}/\text{V}\cdot\text{cm}^{-1}$, as was the case with phosphate and arsenate.

The control of hematite deposition by electrostatic interactions is also apparent when benzene-tetra (1,2,4,5-benzenetetracarboxylic acid) is added to the system. Figure 5.8 compares the collision efficiency and hematite mobility as a function of total benzene-tetra concentration. The change in the collision efficiency as it relates to changes in hematite mobility is similar to the benzene-tri case. Benzene-tetra is able to facilitate the transition from favorable to unfavorable deposition at a lower total concentration than benzene-tri. For benzene-tetra, the transition takes place around $1 \mu\text{M}$ while approximately $20 \mu\text{M}$ is the total benzene-tri concentration needed to produce the transition.

5.3.3 Hematite Deposition in the Presence of Aspartic Acid

Aspartic acid is succinic acid with an amine group on one of the methylene groups. The collision efficiency and mobility are compared as a function of total aspartic acid concentration in Figure 5.9. The evident features are (1) aspartic acid affects hematite mobility in a similar fashion as succinic acid, (2) aspartic acid is able to significantly reduce the collision efficiency at a total concentration around 4 mM while succinic acid only reduces the collision efficiency slightly at similar concentrations, and (3) hematite deposition in the presence of aspartic acid can be explained in terms of electrostatic interactions (unlike the succinic acid case).

5.3.4 Hematite Deposition in the Presence of Butyric Acid

The independence of the collision efficiency and hematite mobility with respect to the addition of butyric acid is shown in Figure 5.10. Hematite mobility remains

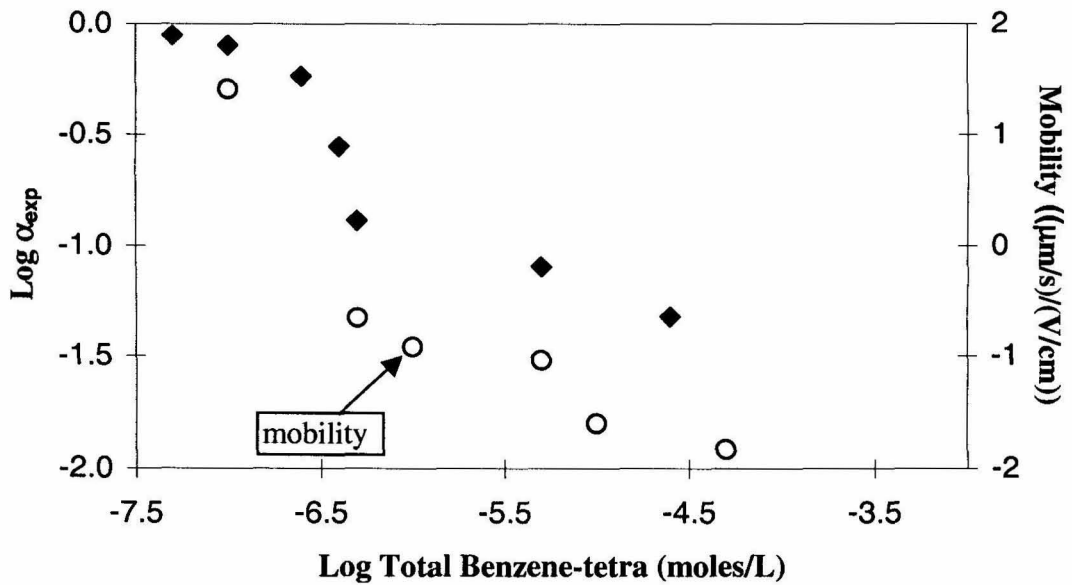


Figure 5.8: Comparison of collision efficiency, α_{exp} , and hematite mobility as a function of total benzene-tetra concentration at pH 6.5 and 1 mM NaCl.

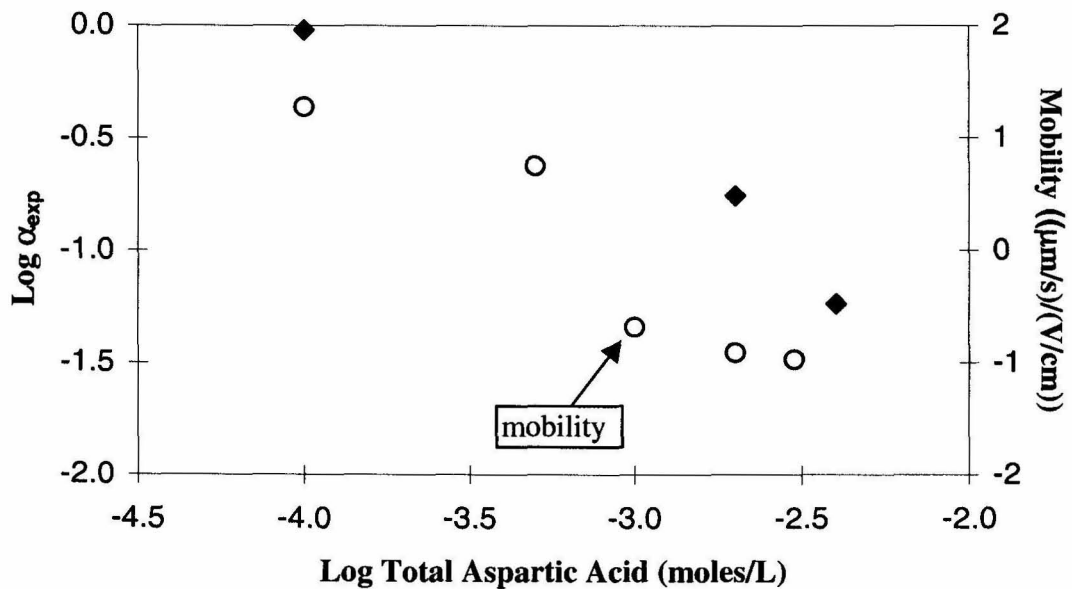


Figure 5.9: Comparison of collision efficiency, α_{exp} , and hematite mobility as a function of total aspartic acid concentration at pH 6.5 and 1 mM NaCl.

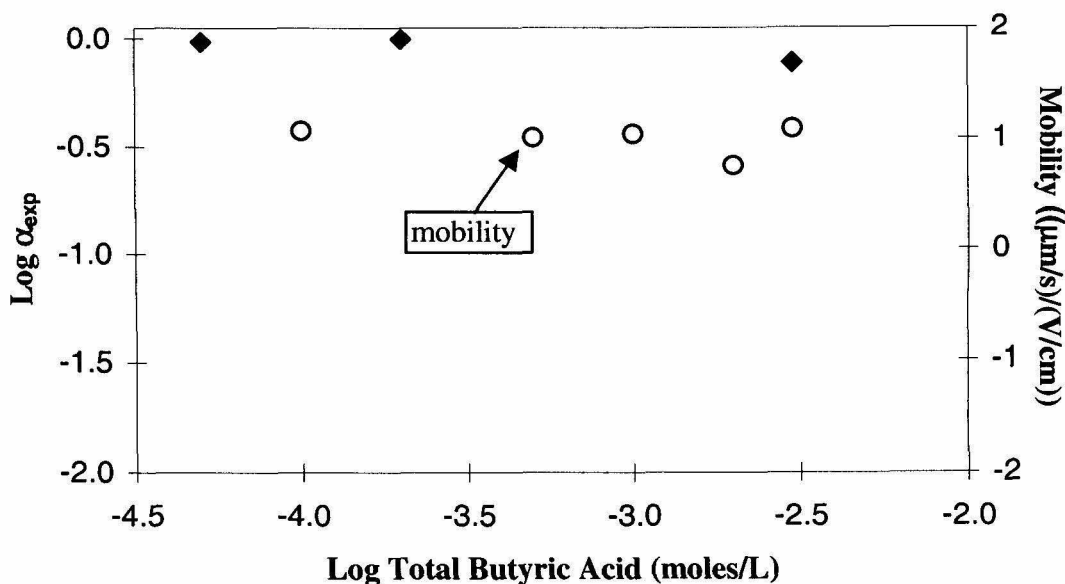


Figure 5.10: Comparison of collision efficiency, α_{exp} , and hematite mobility as a function of total butyric acid concentration at pH 6.5 and 1 mM NaCl.

approximately $1 \mu\text{m}\cdot\text{s}^{-1}/\text{V}\cdot\text{cm}^{-1}$ at total concentrations up to 3 mM. Therefore, deposition remains favorable (attractive electrostatics) and the collision efficiency stays near 1 as total butyric acid concentration is increased.

5.3.5 Effect of Particle Concentration on Hematite Mobility

Benzene-tri was selected as a representative case to study the influence of particle concentration on hematite mobility in the presence of small organic molecules. The motivation for doing so is discussed in Section 5.2.3. The approach was the same as the phosphate case, in that hematite mobility measurements were repeated using 50 mg/L hematite and compared to the measurements made using 10 mg/L. The comparison (presented in Figure 4.35) shows the measurements to be the same, indicating that particle concentration does not influence hematite mobility in the presence of benzene-tri.

Hence, hematite mobility as a function of total benzene-tri concentration (or other small organics) at 1 mg/L hematite (C_0 in deposition experiments) is expected to be the same as with 10 mg/L hematite. This allows the mobility data for 10 mg/L hematite to be used without correction in interpreting deposition data ($C_0 = 1$ mg/L).

Chemical equilibrium calculations, similar to those described earlier for phosphate (Section 5.2.3), were also made to investigate the influence of particle concentration on hematite mobility in the presence of a diprotic organic acid. The modeling results for organic acid adsorption were almost identical to the results for phosphate adsorption (Figure 5.4). In agreement with the observations from hematite mobility measurements, the calculated hematite surface potential as a function of total organic acid concentration is essentially the same for 1, 10, and 17 mg/L hematite.

5.4 Hematite Deposition in the Presence of Polymeric Organic Compounds

5.4.1 Comparison of Deposition Results and Mobility Measurements

The collision efficiency and hematite mobility are compared as a function of total polyelectrolyte concentration in Figure 5.11 for polyaspartic acid (PAA), Figure 5.12 for Leonardite humic acid (Leonardite HA), Figure 5.13 for Suwannee River fulvic acid (S.R. FA), and Figure 5.14 for Suwannee River humic acid (S.R. HA). The data for all four polyelectrolytes suggest that the hematite mobility measurements, as shown, cannot explain the changes in the collision efficiency as each polyelectrolyte is added to the system. This is in contrast to most of the specifically adsorbed solutes considered to this point. However, unlike the other solutes studied, the hematite mobility in the presence of polyelectrolytes is influenced by particle concentration. This is shown in Figure 4.40 (for PAA) and Figure 4.41 (for S.R. HA) where mobility measurements using 10 and 50 mg/L

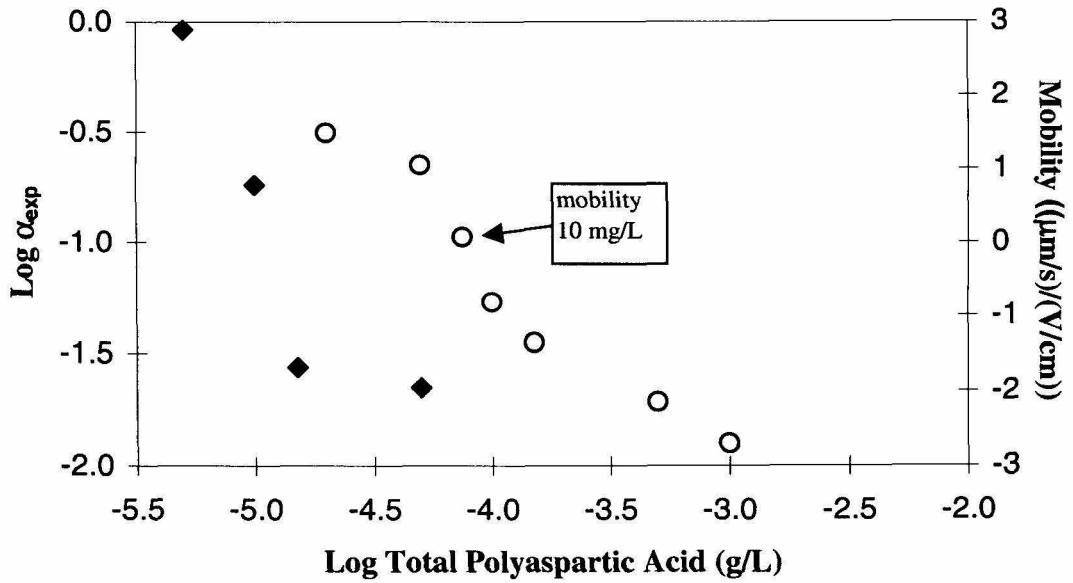


Figure 5.11: Comparison of collision efficiency, α_{exp} , and hematite mobility as a function of total polyaspartic acid concentration at pH 6.5 and 1 mM NaCl.

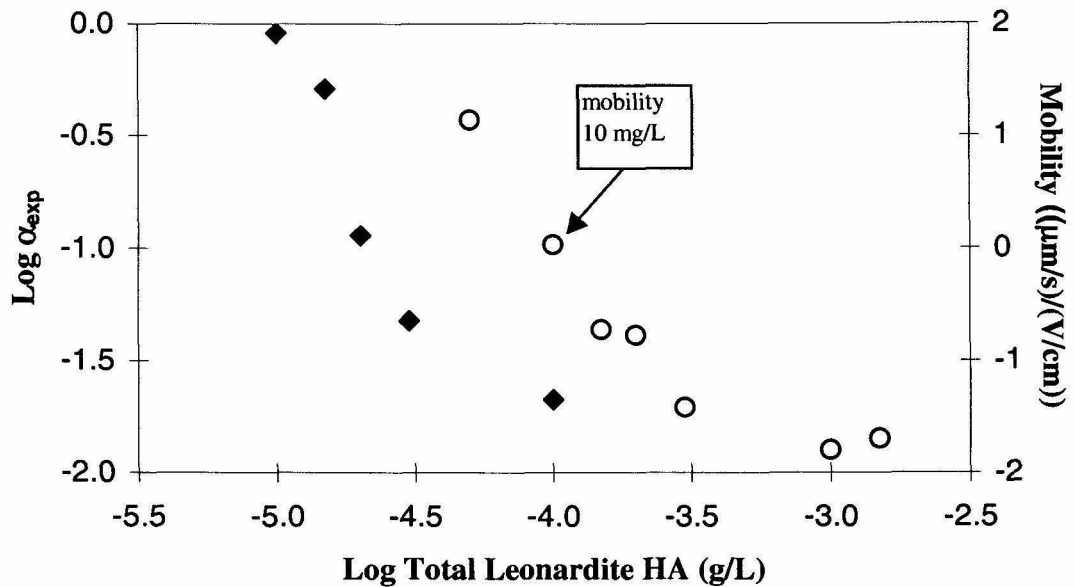


Figure 5.12: Comparison of collision efficiency, α_{exp} , and hematite mobility as a function of total Leonardite humic acid concentration at pH 6.5 and 1 mM NaCl.

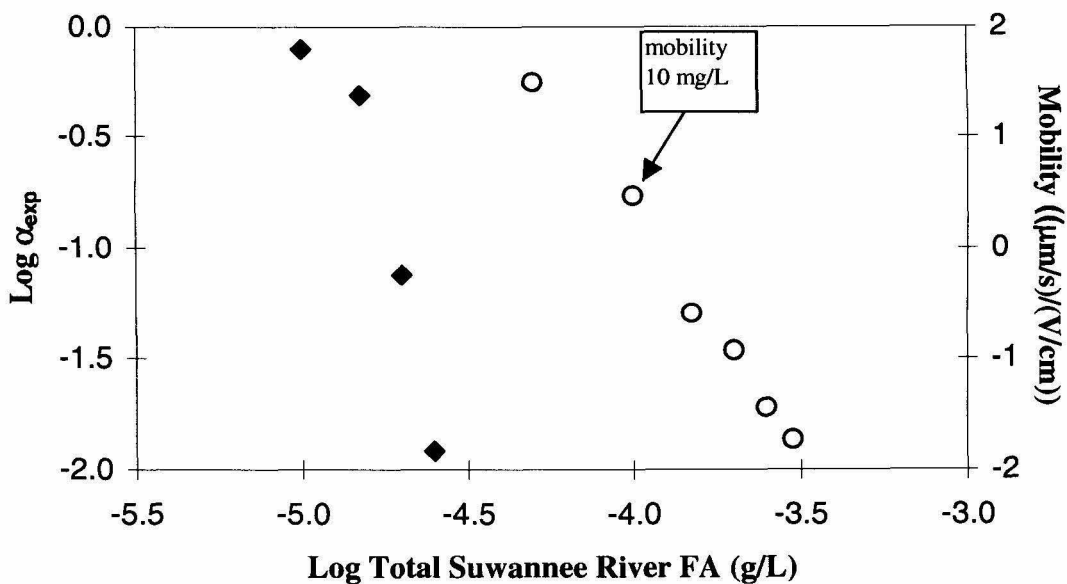


Figure 5.13: Comparison of collision efficiency, α_{exp} , and hematite mobility as a function of total Suwannee River FA concentration at pH 6.5 and 1 mM NaCl.

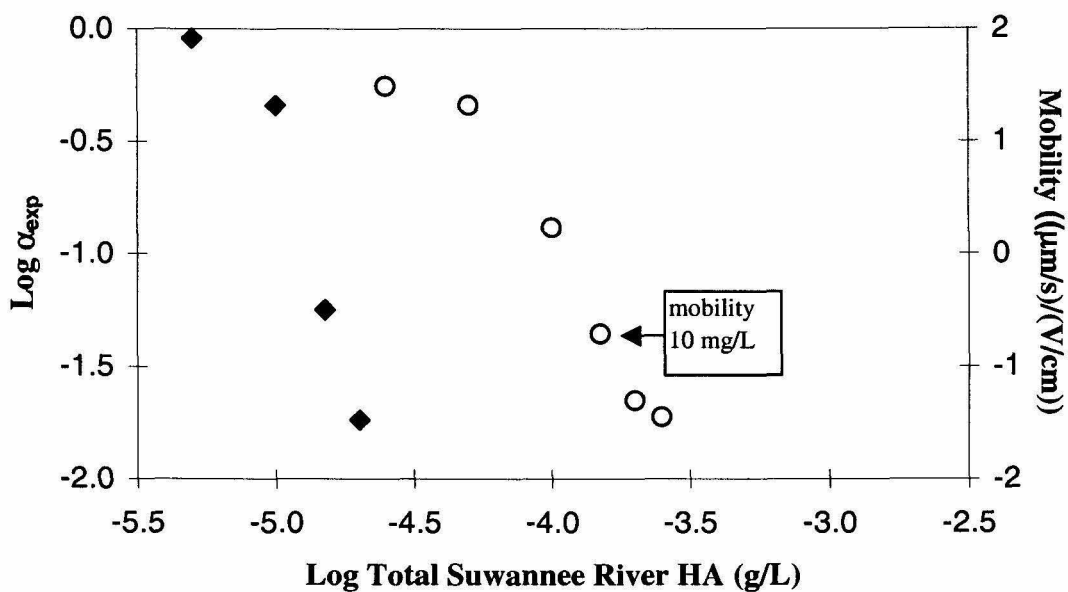


Figure 5.14: Comparison of collision efficiency, α_{exp} , and hematite mobility as a function of total Suwannee River HA concentration at pH 6.5 and 1 mM NaCl.

hematite are compared. The 50 mg/L measurements are shifted, relative to the 10 mg/L measurements, to higher total concentrations of polyelectrolyte by a factor of 5, which is the same factor relating the particle concentrations.

For mobility measurements to be useful in the interpretation of hematite deposition results, the adsorbed concentration of solute on the hematite particles must be the same in both cases. Consequently, one must be able to adjust hematite mobility measurements so as to match the adsorbed concentration present during the corresponding deposition experiment. The form of the adjustment can be determined from the mobility measurements made using different particle concentrations (10 and 50 mg/L hematite). Since the adsorbed concentration of the solute of interest determines the hematite mobility (at a given pH and ionic strength), matching the hematite mobility measurements taken at different particle concentrations would approximate the matching of adsorbed concentrations of solute. The adjustment necessary to match the mobility measurements using 50 mg/L hematite with the 10 mg/L measurements is to divide the total polyelectrolyte concentration of each mobility measurement (at 50 mg/L) by 5.

The data shown in Figure 4.40 (for PAA) is presented again in Figure 5.15 along with the “adjusted” 50 mg/L data. Also, the data shown in Figure 4.41 (for S.R. HA) is presented again in Figure 5.16 along with the “adjusted” 50 mg/L data. There is good agreement between the 10 mg/L hematite measurements and the adjusted 50 mg/L measurements. This suggests that mobility measurements using 10 mg/L hematite in the presence of polyelectrolytes should be adjusted to lower total concentrations of polyelectrolyte by a factor of 10 in order to make the mobility measurements comparable for the interpretation of deposition results obtained using 1 mg/L hematite (C_0).

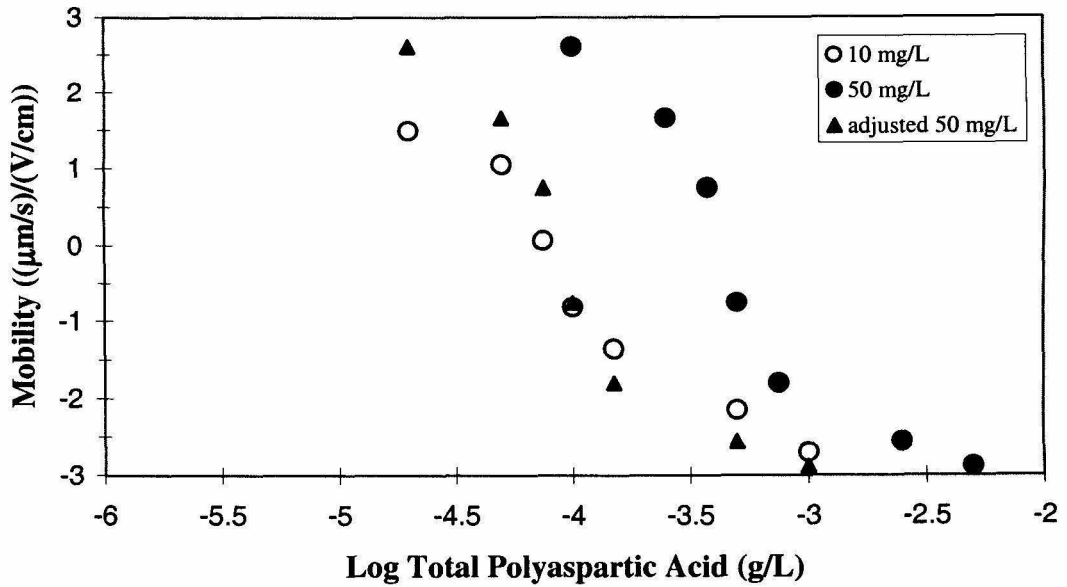


Figure 5.15: Hematite mobility as a function of total polyaspartic acid concentration at pH 6.5 and 1 mM NaCl. Note that the 50 mg/L measurements are shifted to lower PAA concentrations by a factor of 5 to give the “adjusted 50 mg/L” measurements.

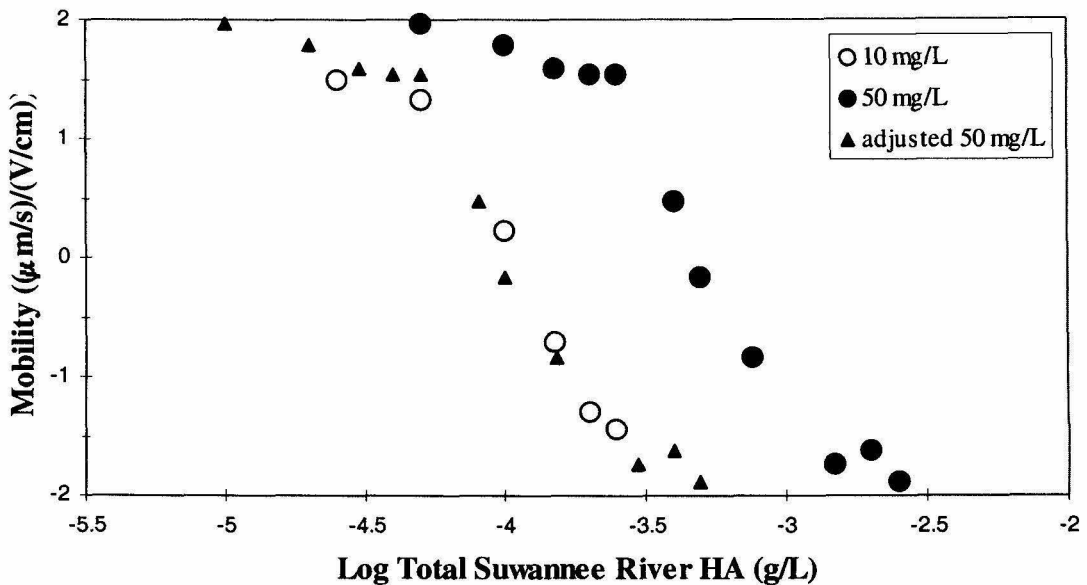


Figure 5.16: Hematite mobility as a function of total S.R. HA concentration at pH 6.5 and 1 mM NaCl. Note that the 50 mg/L measurements are shifted to lower S.R. HA concentrations by a factor of 5 to give the “adjusted 50 mg/L” measurements.

The collision efficiency and the “adjusted” hematite mobility are compared as a function of total polyelectrolyte concentration in Figure 5.17 for PAA, Figure 5.18 for Leonardite HA, Figure 5.19 for S.R. FA, and Figure 5.20 for S.R. HA. The adjusted mobility measurements make it clear that the collision efficiency is controlled by electrostatic interactions. For all four polyelectrolytes, the decrease in the collision efficiency coincides with the reversal (from positive to negative) of the hematite mobility. In addition, unfavorable deposition ($\alpha_{\text{exp}} \leq 0.03$) takes place at hematite mobility values of around $-1 \mu\text{m}\cdot\text{s}^{-1}/\text{V}\cdot\text{cm}^{-1}$ (similar to previous observations).

5.4.2 The Langmuir Equation and Total Adsorbate Concentration

The Langmuir equation will be used as the basis for a discussion on the influence of particle concentration on hematite mobility as a function of “total” polyelectrolyte concentration. The adsorption of dissolved humic substances (HS) on mineral surfaces has been observed to follow Langmuir-type isotherms (Tipping, 1981; McCarthy et al., 1993; and Schlautman and Morgan, 1994). The Langmuir equation is as follows:

$$\Gamma = \Gamma_m \frac{K_{\text{ads}} C}{1 + K_{\text{ads}} C}, \quad (5.8)$$

where Γ is the adsorption density (mg HS adsorbed/g particles), Γ_m is the maximum adsorption density, C is the concentration of free HS remaining in solution (mg HS/L), and K_{ads} is an adsorption constant (L/mg HS). If the adsorption density in one situation (e.g., a deposition experiment) is to be the same as the adsorption density in another situation (e.g., a hematite mobility measurement using a 10-fold greater particle concentration), then C_1 (the free concentration of adsorbate in solution for the deposition experiment) must equal C_2 (the free concentration of adsorbate in solution for the mobility measurement). The mass balance of adsorbate gives

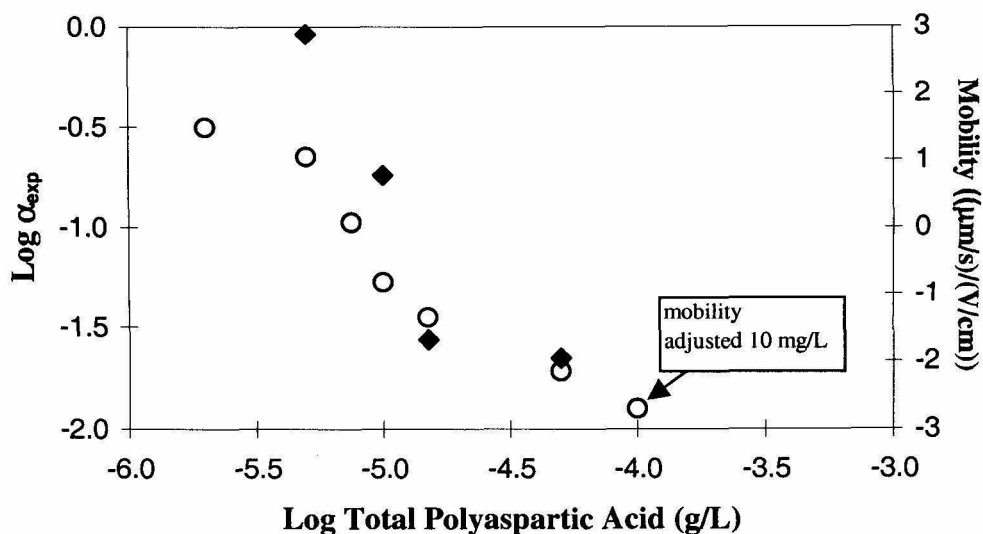


Figure 5.17: Comparison of collision efficiency, α_{exp} , and “adjusted” hematite mobility as a function of total polyaspartic acid concentration at pH 6.5 and 1 mM NaCl. Note that the 10 mg/L mobility measurements are shifted to lower PAA concentrations by a factor of 10 to give the “adjusted 10 mg/L” measurements.

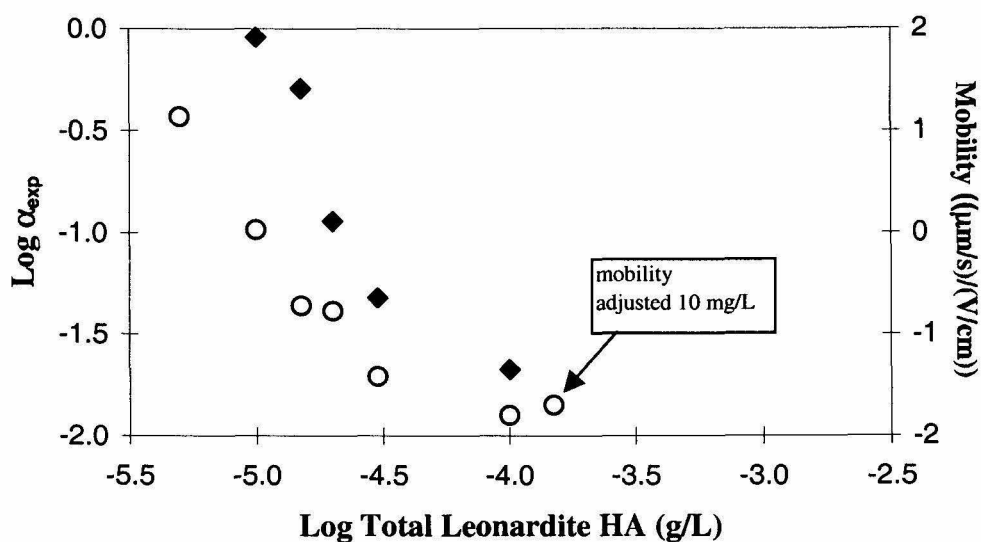


Figure 5.18: Comparison of collision efficiency, α_{exp} , and “adjusted” hematite mobility as a function of total Leonardite HA concentration at pH 6.5 and 1 mM NaCl. Note that the 10 mg/L mobility measurements are shifted to lower Leonardite HA concentrations by a factor of 10 to give the “adjusted 10 mg/L” measurements.

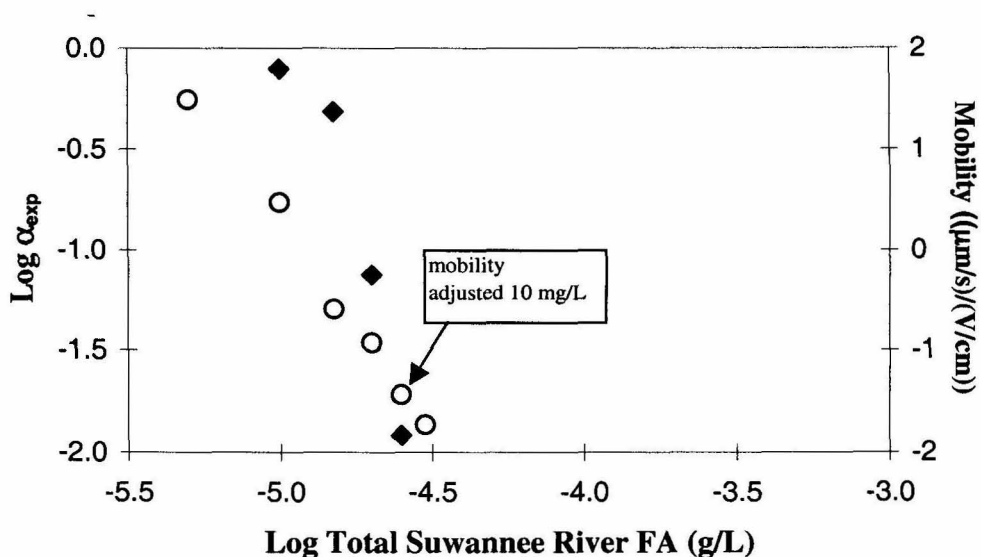


Figure 5.19: Comparison of collision efficiency, α_{exp} , and “adjusted” hematite mobility as a function of total S.R. FA concentration at pH 6.5 and 1 mM NaCl. Note that the 10 mg/L mobility measurements are shifted to lower S.R. FA concentrations by a factor of 10 to give the “adjusted 10 mg/L” measurements.

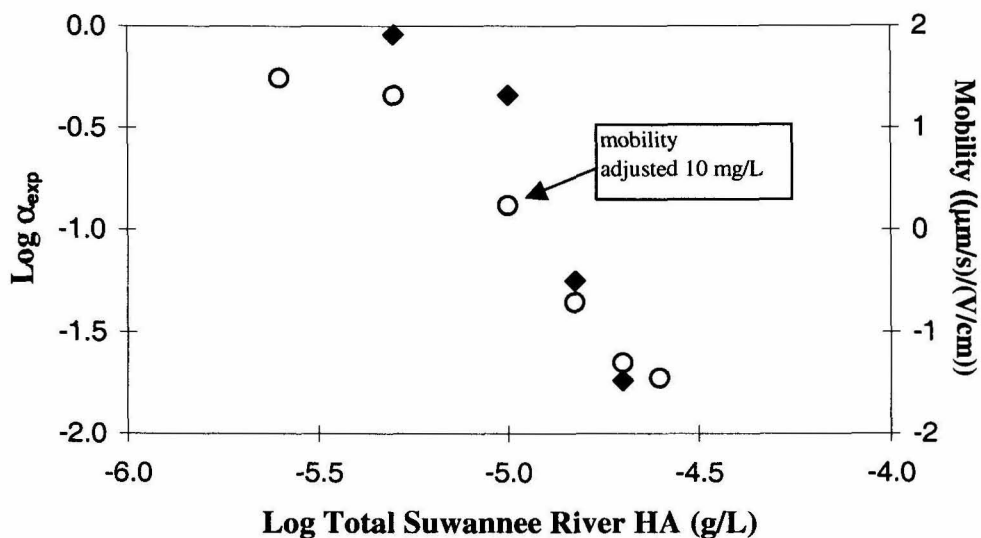


Figure 5.20: Comparison of collision efficiency, α_{exp} , and “adjusted” hematite mobility as a function of total S.R. HA concentration at pH 6.5 and 1 mM NaCl. Note that the 10 mg/L mobility measurements are shifted to lower S.R. HA concentrations by a factor of 10 to give the “adjusted 10 mg/L” measurements.

$$C_t = (\text{dissolved conc.}) + (\text{adsorbed conc.}) = C + \Gamma S \quad , \quad (5.9)$$

where C_t is the total adsorbate concentration (mg adsorbate/L) and S is the particle concentration (g particles/L). Setting $C_1 = C_2$ and substituting gives

$$\frac{C_{t,2}}{C_{t,1}} = \frac{\Gamma S_1}{C_{t,1}} \left(\frac{S_2}{S_1} - 1 \right) + 1 \quad (5.10)$$

Recall our initial stipulation of $\Gamma_1 = \Gamma_2 = \Gamma$. Physically, $\Gamma S_1/C_{t,1}$ is the ratio of the adsorbed concentration to the total concentration of the solute of interest. For $C_{t,2}/C_{t,1}$ to be close to S_2/S_1 (as was observed for hematite mobility measurements in the presence of polyelectrolytes), $\Gamma S_1/C_{t,1}$ must be close to 1. This means that almost all of the adsorbate added to the system would end up adsorbed to the particles.

To explain how $\Gamma S_1/C_{t,1}$ (adsorbed conc./total conc.) could approach 1, consider a flexible polymer. The loss of conformational degrees of freedom upon attachment to the surface makes polymer adsorption entropically unfavorable. Instead, the free energy of binding polymer segments (e.g., carboxyl groups) to the surface is what drives polymer adsorption (Lyklema, 1985). A small surface/segment affinity is usually sufficient to induce strong adsorption. Once adsorbed, polymers don't easily desorb because a polymer has many opportunities to bind with a surface and it is unlikely that all of the bound segments will desorb at the same time.

6. Summary and Conclusions

6.0 Introduction

The deposition kinetics of hematite particles in packed beds of silica sand has been studied in the presence of various electrolytes. The collision efficiencies determined from column experiments, combined with the results from electrophoretic mobility measurements, show the importance of specific adsorption on hematite deposition and electrophoretic mobility. In particular, the adsorption of ions known as “potential determining ions” because of (1) the formation of chemical bonds with surface groups, and (2) the alteration of surface potential due to the adsorption of these ions. The critical point in understanding how aqueous chemistry influences deposition kinetics is the adsorption of ions on hematite surfaces causes a change in the surface charge and potential, which in turn alters the total interaction energy between particles and collectors.

6.1 The Collision Efficiency and Electrostatic Repulsion

6.1.1 Theory and Observations

Figure 6.1 presents the results for most of the deposition experiments conducted for this research. The collision efficiency is plotted against the corresponding hematite mobility measured at the same chemical conditions of the deposition experiment. The data reveal the significance of electrostatic interaction in determining the hematite deposition rate (collision efficiency). At positive hematite mobilities,

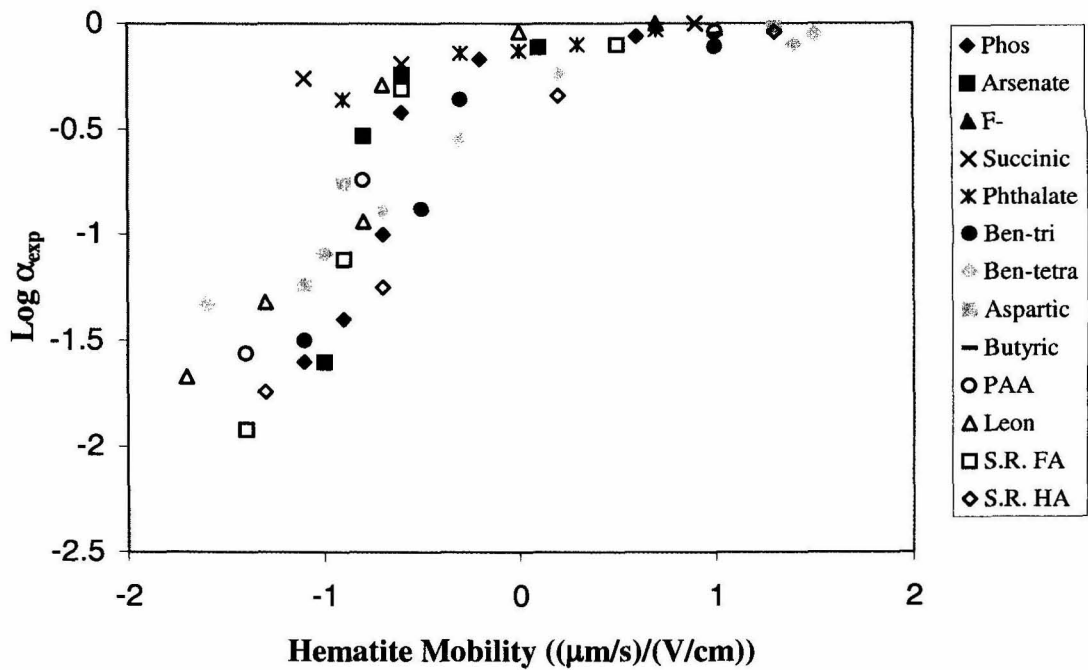


Figure 6.1: Collision efficiency, α_{exp} , as a function of the hematite mobility measured at the same chemical conditions of the deposition experiment.

electrostatic attraction between hematite particles and silica sand grains result in collision efficiencies near 1 (favorable deposition). As hematite mobility changes from positive to negative, a decreasing trend in the collision efficiency begins. The decreasing trend in the collision efficiency continues as hematite mobility becomes more negative.

DLVO theory predicts a drastic decrease in the collision efficiency at the onset of electrostatic repulsion. Figure 6.2 shows a comparison of theoretical and experimental collision efficiencies of negatively charged latex particles in beds of glass beads (negatively charged) as a function of $[KCl]$ (Elimelech and O'Melia, 1990). The $[KCl]$ is a measure of the amount of electrostatic repulsion in the system since the particles and collectors remain negatively charged and higher $[KCl]$ would result in decreased electrostatic repulsion by compression of the diffuse layers. Therefore, Figures 6.1 and 6.2 both show the collision efficiency as a function of electrostatic repulsion. In Figure 6.1, electrostatic repulsion begins when the hematite mobility changes from positive to negative and increases as hematite mobility becomes more negative. In Figure 6.2, electrostatic repulsion is shielded at high $[KCl]$ and increases as $[KCl]$ decreases. According to theory, once electrostatic repulsion is present between particles and collectors the particles would become very stable with respect to deposition (i.e., collision efficiency drops sharply). The observations of this research and earlier deposition studies (Gregory and Wishart, 1980; Kallay et al., 1983; Elimelech and O'Melia, 1990; Litton and Olson, 1993) show a gradual decrease (relative to theory) in the collision efficiency as electrostatic repulsion increases (Figures 6.1 and 6.2).

The discrepancy between predicted and observed collision efficiencies has been attributed to surface heterogeneity, both physical (surface roughness) and chemical (non-

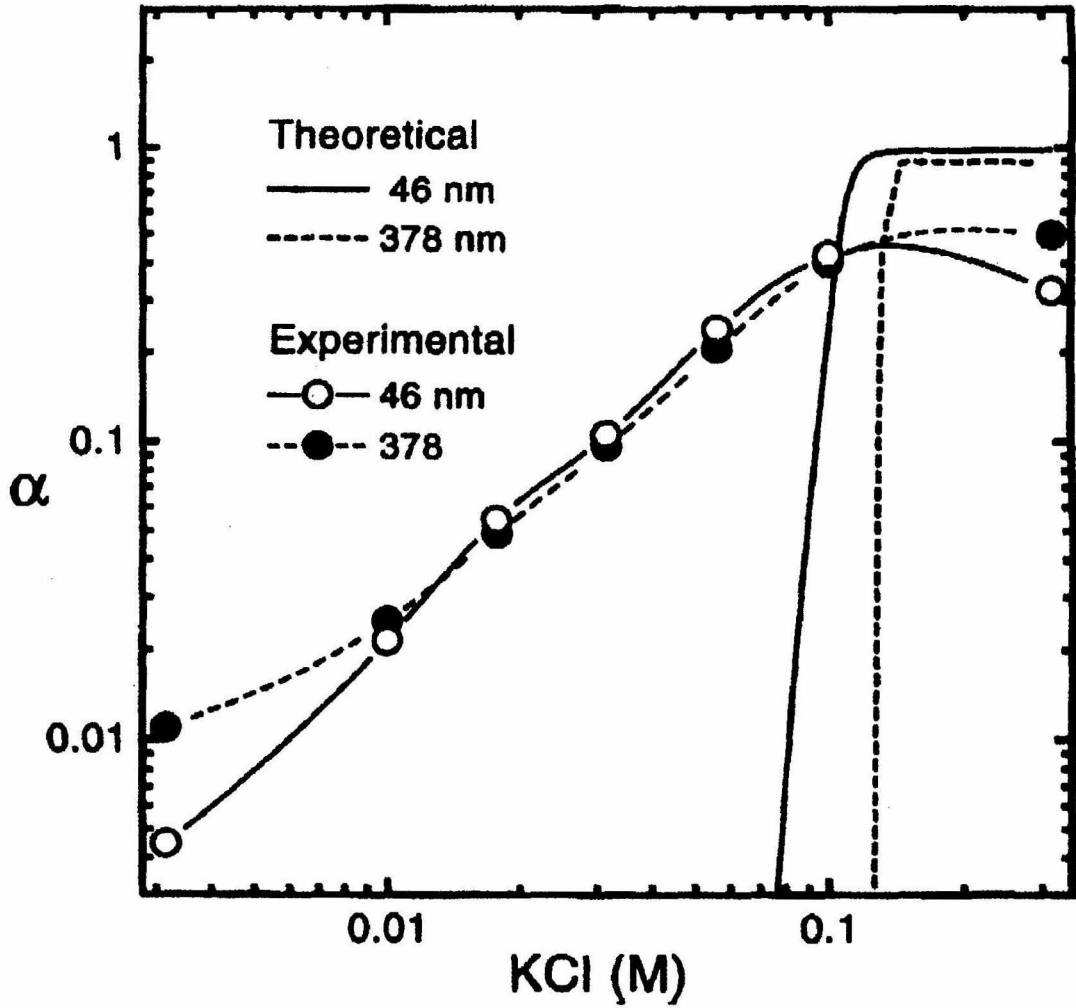


Figure 6.2: Comparison of theoretical and experimental collision efficiencies of two different suspensions of latex particles as a function of [KCl]. The particle diameter is indicated (from Elimelech and O'Melia, 1990).

uniform charge). When the surfaces of particles and collectors are assumed to be perfectly smooth and to have uniform charge distribution, the predicted collision efficiency is of the form shown in Figure 6.2. If the surface potentials are assumed to have normal distributions, then the predicted collision efficiency is shown in Figure 6.3. It is apparent that the collision efficiency is predicted to decrease more gradually when the surface potential is not uniform.

The issue of surface heterogeneity has been addressed experimentally by examining the effects of porous medium cleaning techniques. Litton and Olson (1993) observed a smaller discrepancy between predicted and experimental collision efficiencies when the porous medium (glass beads) was exposed to a more aggressive cleaning technique. These results are shown in Figure 6.4 where the collision efficiency is plotted as a function of pH. Carboxylated latex particles were used, therefore electrostatic repulsion develops at \sim pH 3.8 (the pK_a of the surface groups). The experimental collision efficiencies that are closer to theory correspond to the more aggressive porous medium cleaning technique (HCl plus chromic acid). The smaller discrepancy was attributed to the removal of surface contaminants that formed patches favorable for deposition.

Another experimental study addressing surface heterogeneity was done by Elimelech and co-workers (2000). In this case, a chemically heterogeneous porous medium was artificially produced by combining different amounts of clean and aminosilane-modified quartz sand. The deposition of silica colloids was measured at pH 5.7 in packed beds of varying ratios of aminosilane-modified quartz grains (positively charged at pH 5.7) to clean quartz grains (negatively charged at pH 5.7). The

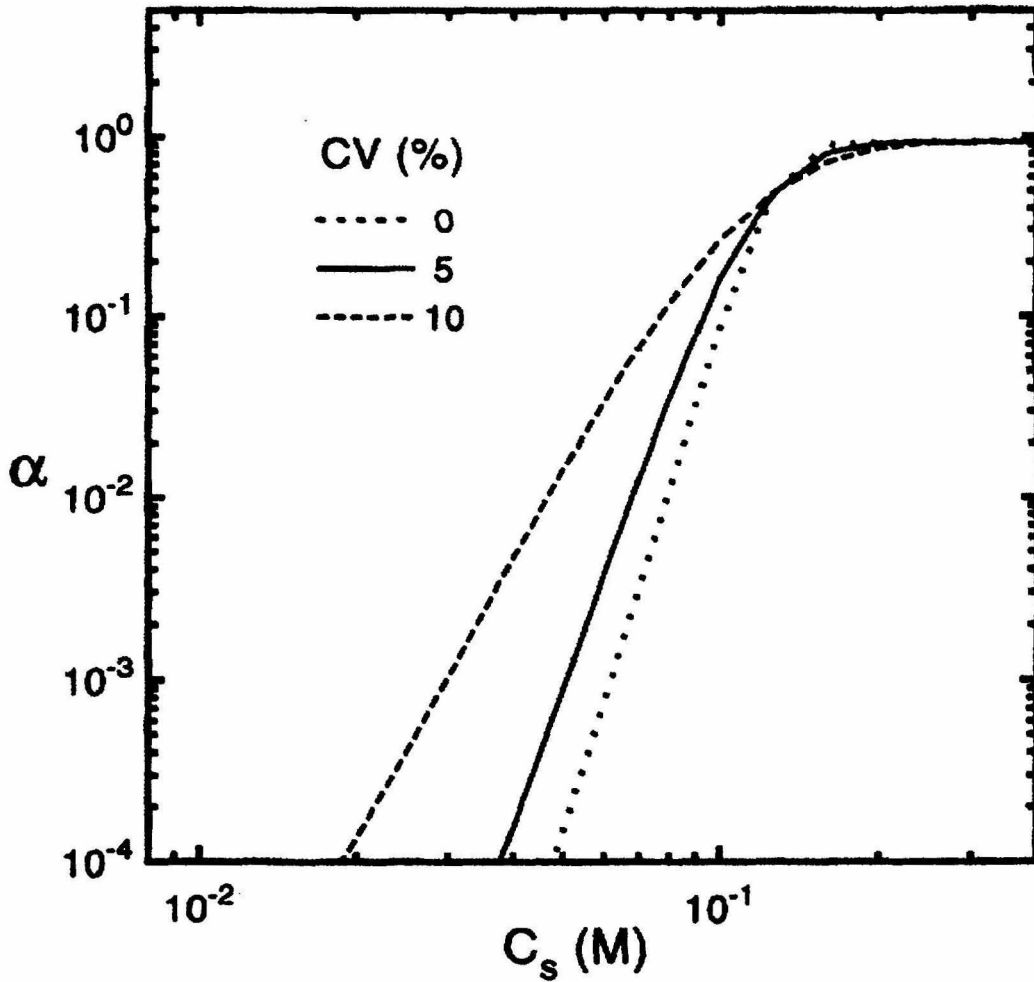


Figure 6.3: Theoretical collision efficiencies as a function of 1-1 electrolyte concentration, C_s , assuming a normal distribution of surface potentials of particles and collectors. The collision efficiencies were calculated for various coefficients of variation (CV) (from Elimelech et al., 1995).

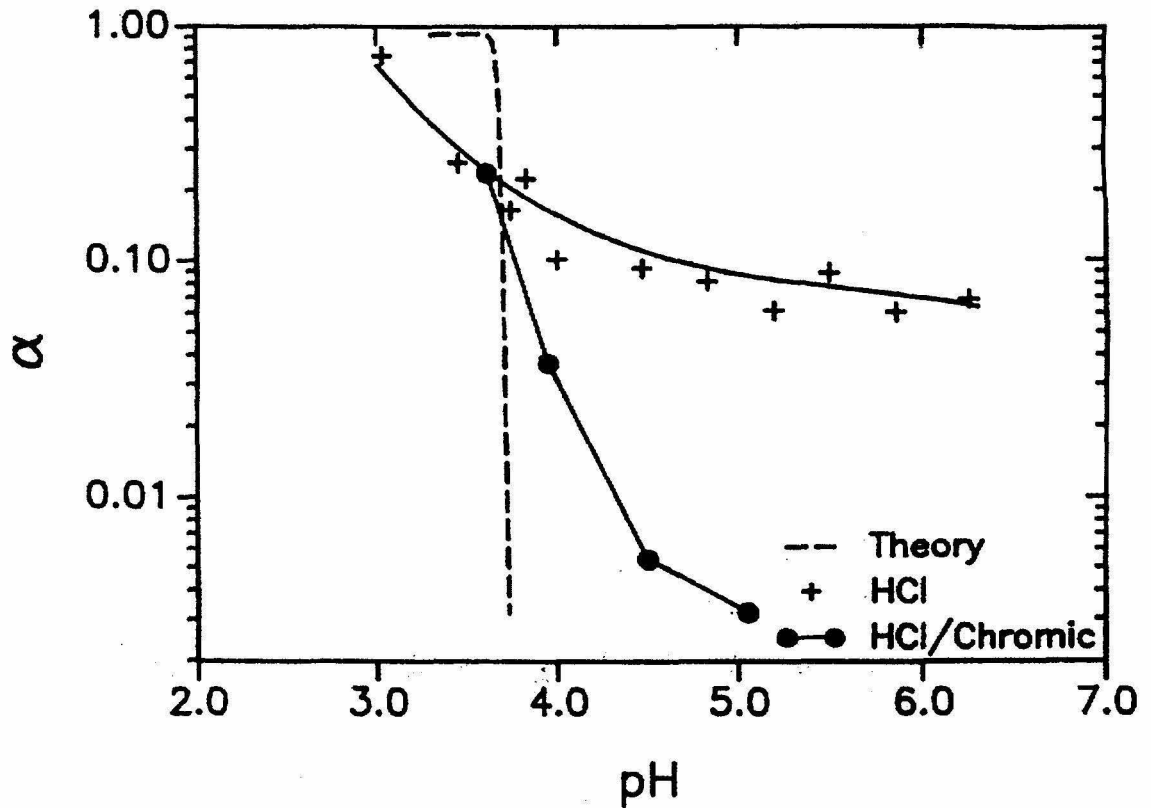


Figure 6.4: Comparison of theoretical and experimental collision efficiencies as a function of pH for carboxylated latex particles. The results for two different porous medium cleaning techniques are shown (from Litton and Olson, 1993).

heterogeneity parameter, λ , was defined as the ratio of the mass of aminosilane-modified quartz grains to the total mass of quartz grains. The modified and clean sand grains were mixed to produce a porous medium with a known degree of macroscopic heterogeneity. The degree of electrostatic repulsion between particles and collectors increases as λ decreases. The experimental collision efficiency is shown as a function of the heterogeneity parameter, λ , in Figure 6.5. A linear relation between collision efficiency (log scale) and λ (log scale) was observed. The decreasing trend in the collision efficiency as the degree of electrostatic repulsion increases resembles the trends in Figures 6.1 and 6.2.

The previously described studies suggest that surface heterogeneity is a critical factor in explaining the gradual decrease (instead of the sharp decrease predicted by theory) in the collision efficiency as the degree of electrostatic repulsion increases. It is expected that collector surface heterogeneity is the reason for the gradual decrease in the collision efficiency as a function of hematite mobility (Figure 6.1) observed in this research. The silica sand (Ottawa 30) used in this research is a natural sand and it is clear from Plate II that the grain surfaces are not smooth. Surface heterogeneity is inevitable in environmental systems, therefore a gradual trend in the decrease in collision efficiency with increasing electrostatic repulsion is expected.

6.1.2 Cases Contrary to Electrostatic Considerations

Electrostatic interaction was the critical parameter in determining the collision efficiency for all but two of the electrolytes investigated. Oxalate and phthalate, although expected to decrease the hematite deposition rate significantly on the basis of electrostatic considerations, cause only slight decreases in the deposition rate (collision efficiency).

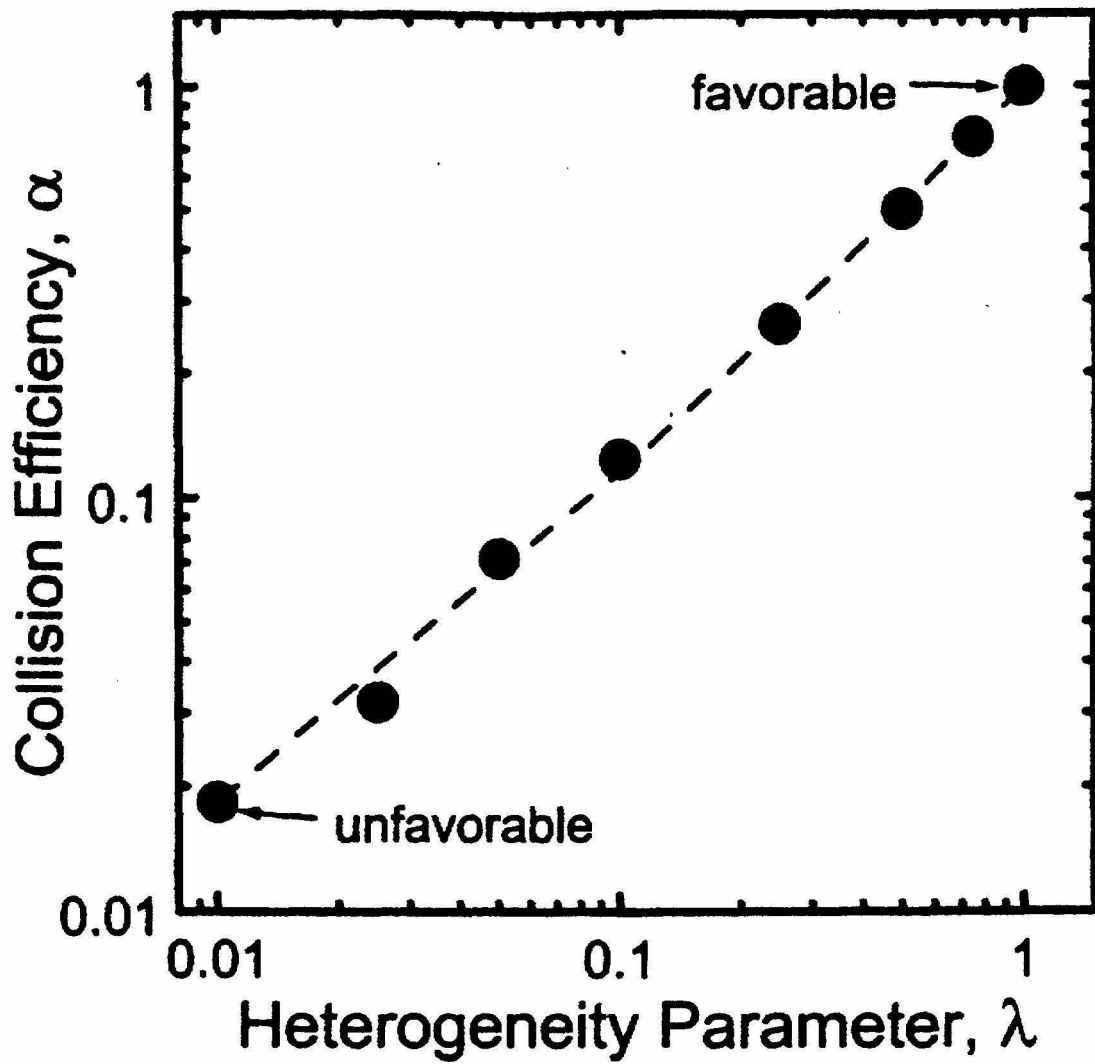


Figure 6.5: Experimental collision efficiencies as a function of the heterogeneity parameter, λ , for aminosilane-modified quartz grains (from Elimelech et al., 2000).

Considered along with oxalate are its related compounds (succinic, adipic, and suberic acid) since they had very similar results. The electrostatic repulsion between a hematite particle and sand grain would have to be overcome by some attractive interaction for deposition to remain relatively favorable. Of the non-DLVO interactions described in the literature (e.g., hydration, hydrophobic, and steric forces), hydrophobic interaction would be the only candidate because hydration forces are repulsive and steric interaction applies when an adsorbed layer of macromolecules is present. However, hydrophobic interaction isn't a plausible explanation for this apparent attraction between particles and collectors because one would expect different collision efficiencies in the presence of oxalic (C_2), succinic (C_4), adipic (C_6), and suberic (C_8) acid.

6.2 Implications for Environmental Systems

The results of this research have implications for water treatment (deep bed filtration) and groundwater quality. A typical scenario in deep bed filtration consists of flowing water through packed beds of silica sand to remove undesirable constituents like colloidal particles. Two common environmental colloids are microbes (bacteria and viruses) and clay particles, which usually have negatively charged surfaces. The silica sand in the bed has surface impurities (e.g., iron oxides) that allow for effective filtration of the negatively charged colloids. If the sand was pure silica, electrostatic repulsion would reduce the effectiveness of the filtration process. The results of this research suggest that specifically adsorbed solutes (e.g., phosphate or humic acids) could alter the surface potential of the iron oxide impurities, thus producing less favorable conditions for filtration.

Groundwater aquifer material is often coated with iron oxides (Ryan and Gschwend, 1990). Negatively charged clay particles experience favorable deposition when the pH is below the pH_{zpc} of the iron oxide. If the surface potential of the iron oxide coatings is altered by the adsorption of humic or fulvic acids, then the clay particle deposition rate would decrease. The clay particles, along with any associated pollutants, would be able to migrate greater distances.

6.3 Summary of Main Conclusions

1. Specifically adsorbed species are able to alter the mobility of hematite particles.
2. Hematite mobility in the presence of polymeric organic compounds is influenced by particle concentration (when related to total solute concentrations). The mobility measurements can be adjusted to match the conditions of corresponding deposition experiments by multiplying the total polyelectrolyte concentration by the proportionality relating the particle concentrations in the mobility measurements to the particle concentration in the deposition experiments.
3. In the absence of specifically adsorbed solutes at pH 6.5 and $[\text{NaCl}] = 1 \text{ mM}$, hematite deposition on silica sand is transport limited. The addition of specifically adsorbed solutes often reduces the hematite deposition rate.
4. Specific adsorption influences hematite deposition rates (collision efficiencies) by altering surface charge and potential, which in turn changes the electrostatic interaction.

5. DLVO theory predicts a drastic decrease in the collision efficiency (see Figure 6.2) at the onset of electrostatic repulsion. The results of this research show a less drastic decrease in the collision efficiency (Figure 6.1) as electrostatic repulsion becomes more significant. This is in agreement with previous studies on particle deposition, and likely a result of surface heterogeneities.
6. The inevitable surface heterogeneity in environmental systems would result in particle deposition behavior similar to the observations of this research (i.e., a gradual decrease in collision efficiency with increasing electrostatic repulsion as opposed to the sharp decrease predicted by theory).

References

- Amirbahman, A. and T. M. Olson (1993). "Transport of humic matter-coated hematite in packed beds." Environmental Science and Technology **27**(13): 2807-2813.
- Amirbahman, A. and T. M. Olson (1995). "The role of surface conformations in the deposition kinetics of humic matter-coated colloids in porous media." Colloid Surface A **95**(2-3): 249-259.
- Au, K. K., A. C. Penisson, S. Yang and C. R. O'Melia (1999). "Natural organic matter at oxide/water interfaces: complexation and conformation." Geochimica et Cosmochimica Acta **63**(19/20): 2903-2917.
- Au, K. K., S. Yang and C. R. O'Melia (1998). "Adsorption of weak polyelectrolytes on metal oxide surfaces: A hybrid SC/SF approach." Environmental Science and Technology **32**(19): 2900-2908.
- Bear, J. (1972). Dynamics of Fluids in Porous Media. New York, Dover Publications.
- Bunn, R. A., R. D. Magelky, J. N. Ryan and M. Elimelech (2000). "Mobilization of natural colloids from and iron oxide coated sand aquifer: Effect of pH and ionic strength." Environmental Science and Technology **36**(3): 314-322.
- Burris, D. R., C. P. Antworth, T. B. Stauffer and W. G. MacIntyre (1991). "Humic Acid-Modified Silica as a Model Aquifer Material." Environmental toxicology and Chemistry **10**: 433-440.
- Cohen Stuart, M. A., G. J. Fleer, J. Lyklema, W. Norde and H. M. H. M. Schedutjens (1991). "Adsorption of ions, polyelectrolytes and proteins." Advanced in Colloid and Interface Science **34**: 477-535.
- Davis, J. A. and R. Bloor (1981). "Adsorption of dissolved organics in lake water by aluminum oxide. Effect of molecular weight." Environmental Science and Technology **15**(10): 1223-1229.
- Dzombak, D. A. and F. M. M. Morel (1990). Surface Complexation Modeling: Hydrous Ferric Oxide. New York, Wiley.
- Elimelech, M. (1990). The effect of particle size on the kinetics of deposition of brownian particles in porous media. Baltimore, The Johns Hopkins University.
- Elimelech, M. (1991). "Kinetics of capture of colloidal particles in packed beds under attractive double layer interactions." Journal of colloid and interface science **146**(2): 337-351.
- Elimelech, M., J. Gregory, X. Jia and R. A. Williams (1995). Particle Deposition and Aggregation: Measurement, Modelling, and Simulation. New York, Butterworth-Heinemann.
- Elimelech, M., M. K. Nagai, C. and J. N. Ryan (2000). "Relative insignificance of mineral grain zeta potential to colloid transport in geochemically heterogeneous porous media." Environmental Science and Technology **34**(11): 2143-2148.
- Elimelech, M. and C. R. O'Melia (1990). "Kinetics of deposition of colloidal particles in porous media." Environmental Science and Technology **24**(10): 1528-1536.
- Elliot, A. H. (1990). Transfer of solutes into and out of streambeds. Environmental Engineering Science. Pasadena, California Institute of Technology.

- Eylers, H. (1994). Transport of adsorbing metal ions between stream water and sediment bed in a laboratory flume. Environmental Science Engineering. Pasadena, California Institute of Technology.
- Faust, B. C. (1985). Photo-induced reductive dissolution of hematite ($\alpha\text{-Fe}_2\text{O}_3$) by S (IV) oxyanions. Pasadena, California Institute of Technology.
- Fokkink, L. G. J., A. Dekeizer and J. Lyklema (1987). "Specific ion adsorption on oxides - surface-charge adjustment and proton stoichiometry." Journal of Colloid Interf. Sci **118**(2): 454-462.
- Gebhardt, J. E. and D. W. Fuerstenau (1983). "Adsorption of polyacrylic acid at oxide/water interfaces." Colloids and Surfaces **7**: 221-231.
- Grolimund, D., M. Elimelech, M. Borkovec, K. Barmettler, R. Kretzschmar and H. Sticher (1988). "Transport of in-situ mobilized colloidal particles in packed soil columns." Environmental Science and Technology **32**(22): 3562-3569.
- Gu, B., T. L. Mehlhorn, L. Liang and J. F. McCarthy (1996). "Competitive adsorption, displacement and transport of organic matter on iron oxide: I. competitive adsorption." Geochimica et cosmochimica Acta **60**(11): 1943-195.
- Gu, B., J. Schmitt, Z. Chen, L. Liang and J. F. McCarthy (1994). "Adsorption and desorption of natural organic matter on iron oxide: Mechanisms and models." Environmental Science and Technology **28**(1): 38-46.
- Gu, B., J. Schmitt, Z. Chen, L. Liang and J. F. McCarthy (1995). "Adsorption and desorption of different organic matter fraction on iron oxide." Geochemica et cosmochimica Acta **59**(2): 219-229.
- Hamaker, H. C. (1937). "The London-Van der Waals attraction between spherical particles." Physics **4**: 1058.
- Hohnson, P. R., N. Sun and M. Elimelech (1996). "Colloid transport in geochemically heterogeneous porous media: Modeling and measurements." Environmental Science and Technology **30**(11): 3284-3293.
- Hunter, R. J. (1981). Zeta Potential in colloid Science. London, Academic Press.
- Iler, R. K. (1979). "The Chemistry of Silica."
- Israelachvili, J. N. (1992). Intermolecular and Surface Forces. New York, Academic Press.
- Johnson, P. R. (1999). "A comparison of streaming and microelectricophoresis methods for obtaining the Psi potential of granular porous media surfaces." Journal of Colloid and Interface Science **209**: 264-267.
- Johnson, P. R. and M. Elimelech (1995). "Dynamics of Colloid Deposition in Porous Media: blocking based on Random Sequential Adsorption." Langmuir **11**: 801-812.
- Jurinak, J. J. (1966). Surface chemistry of hematite: anion penetration effect on water adsorption. Soil Science So. Amer. Proc.
- Kallay, N. and E. Matijevic (1985). "Adsorption at solid/solution interfaces. 1. Interpretation of surface complexation of oxalic and citric acids with hematite." Langmuir **1**: 195-201.
- Kerker, M. (1969). The Scattering of Light and Other electromagnetic Radiation. New York, Academic Press.
- Kummert, R. and W. Stumm (1980). "The surface complexation of organic acids on hyrous $\gamma\text{-Al}_2\text{O}_3$." Journal of Colloid and Interface Science **75**(2): 373-385.

- Kuo, R. J. and E. Matijevic (1980). "Particle adhesion and removal in model systems. 3. Monodispersed ferric oxide on steel." Journal of Colloid Interface Science **78**(2): 407-421.
- Liang, L. (1988). Effects of surface chemistry on kinetics of coagulation of submicron iron oxide particles (α -Fe₂O₃) in water. Environmental Engineering Science. Pasadena, California Institute of Technology.
- Liang, L. and J. J. Morgan (1990). Coagulation of iron oxide particles in the presence of organic molecules. Chemical Modeling of Aqueous Systems II, American Chemical Society, Washington D.C.
- Litton, G. M. and T. M. Olson (1993). "Colloid deposition rates on silica bed media and artifacts related to collector surface preparation methods." Environmental Science and Technology **27**(1): 185-193.
- Lyklema, J. (1989). "Discrimination between physical and chemical adsorption of ions on oxides." Colloid Surface **37**: 197-204.
- Lyklema, J. and G. J. Fleer (1987). "Electrical contributions to the effect of macromolecules on colloid stability." 1987 **25**(2-4): 357-368.
- Lyklema, J. (1985). "How polymers adsorb and affect colloid stability." Flocculation, Sedimentation and Consolidation: Proceedings of the Engineering Foundation conference (Moudgil, B.M.; Somasundaran, P. editors).
- Mau, R. E. (1992). Particle transport in flow through porous media: Advection, longitudinal dispersion, and filtration. Pasadena, California Institute of Technology.
- McCarthy, J. F., T. M. Williams, L. Liang, P. M. Jardine, L. W. Jolley, D. L. Taylor, A. V. Palumbo and L. W. Cooper (1993). "Mobility of natural organic matter in a sandy aquifer." Environmental Science and Technology **27**(4): 667-676.
- Meadows, J., P. A. Williams, M. J. Garvey, R. A. Harrop and G. O. Phillips (1988). "Enhanced Polyelectrolyte Adsorption." Colloids and Surfaces **32**: 275-288.
- Micale, F. J., D. Kiernan and A. C. Zettlemoyer (1985). "Characterization of the surface properties of iron oxides." Journal of Colloid Interface Science **105**(2): 570.
- Matijevic, E. and P. Scheiner (1978). "Ferric Hydrous Oxide Sols." Journal of Colloid Interface Science **63**(3): 509.
- O'Melia, C. R. and W. Stumm (1967). "Theory of water filtration." Journal AWWA: 1393.
- Parfitt, R. L. ((1978)). "Anion adsorption by soils and soil materials." Advanced Agronomy **30**(1).
- Rajogopalan, R. and R. Q. Chu (1982). "Dynamics of Adsorption of Colloidal Particles in Packed Beds." Journal of Colloid and Interface Science **86**: 299.
- Rihnaarts, H. H. M., W. Norde, E. J. Bouwer, J. Lyklema and A. J. B. Zehnder (1996). ""Bacterial deposition in porous media: Effects of cell-coating, substratum hydrophobicity, and electrolyte concentration." Environmental Science and Technology **30**(10): 2877-2883.
- Ryan, J. N. and M. Elimelech (1996). "Colloid Mobilization and transport in groundwater." Colloids and Surfaces A **107**: 1-56.
- Schindler, P. (1981). Surface complexes at oxide-water interfaces, adsorption of inorganics at the solid/liquid interface. Ann Arbor, Ann Arbor Science.

- Schlautman, M. A. and J. J. Morgan (1994). "Adsorption of aquatic humic substances on colloidal-size aluminum oxide particles: Influence of solution chemistry." Geochim. Cosmochim. Acta **58**: 4293-4303.
- Seaman, J. C. and P. M. Bertsch (2000). "Selective colloid mobilization through surface-charge manipulation." Environmental Science and Technology **34**(17): 3749-3755.
- Sigg, L. and W. Stumm (1981). "The interaction of anions and weak acids with the hydrous goethite (α -FeOOH) surface." Colloids and Surfaces **2**: 101.
- Song, L. and M. Elimelech (1994). "Transient Deposition of colloidal particles in heterogeneous porous media." Journal of Colloid and Interface Science **167**: 301-313.
- Sposito, G. (1984). The Surface Chemistry of Soils. New York, Oxford University Press.
- Stumm, W., C. P. Huang and S. R. Jenkins (1970). "Specific chemical interaction affecting the stability of dispersed systems." Croatica Chemica Acta **42**: 223-245.
- Stumm, W., R. Kummert and L. Sigg (1980). "A ligand exchange model for the adsorption of inorganic and organic ligands at hydrous oxide surfaces." Croatica Chemica Acta **53**: 291-312.
- Stumm, W. and J. J. Morgan (1981). Aquatic Chemistry. New York, Wiley.
- Tien, C. (1989). Granular filtration of aerosols and hydrosols. Stoneham, MA, Butterworths.
- Tiller, C. L. (1993). Colloidal stability in natural waters: Experimental and model studies of the role of natural organic matter. Baltimore, the Johns Hopkins University.
- Tipping, E. (1981). "The adsorption of aquatic humic substances by iron oxides." Geochimica et Cosmochimica Acta **45**: 191-199.
- Tipping, E. and D. C. Higgins (1982). "The effect of adsorbed humic substances on the colloidal stability of haematite particles." Colloids and Surfaces **5**(85-92).
- Van De Weerd, H., W. H. Van Riemsdijk and A. Leijnse (1999). "Modeling the dynamic adsorption/desorption of a NOM mixture: effects physical and chemical heterogeneity." Environmental Science and Technology **33**(10): 1675-1681.
- Wang, L., Y. P. Chin and S. J. Traina (1997). "Adsorption of (poly) maleic acid and aquatic fulvic acid by goethite." Geochimica et Cosmochimica Acta **61**(24): 5313-5324.
- Wiese, G. R. and T. W. Healy (1970). "Effect of particle size on colloid stability." Trans Faraday Society **66**: 490-500.
- Yao, K. H., M. T. Habibian and C. R. O'Melia (1971). "Water and waste water filtration: concepts and applications." Environmental Science and Technology **5**(11): 1105.

Appendix

Table A.1: Summary of deposition experiments: hematite particles (67 nm diameter spheres) in packed beds (5cm bed depth, 0.34 porosity) of silica sand (Ottawa 30, 500 μ M diameter grains) with an approach velocity of 1 cm/min and [NaCl] = 1 mM.

Solute	log [Solute] (M)	(C/C₀)_{5 min}	log α_{exp}
NaCl	no NaCl	0.12	-----
	-4.00	0.15	-----
	-3.00	0.16	0.00
	-2.00	0.16	0.00
Phosphate	no ligand	0.16	0.00
	-5.00	0.21	-0.06
	-4.60	0.29	-0.17
	-4.30	0.50	-0.42
	-4.12	0.84	-1.02
	-4.00	0.93	-1.42
	-3.70	0.95	-1.57
Arsenate	no ligand	0.16	0.00
	-5.00	0.24	-0.11
	-4.60	0.35	-0.24
	-4.43	0.58	-0.52
	-4.30	0.96	-1.60
Fluoride	no ligand	0.16	0.00
	-4.30	0.16	0.00
	-3.70	0.16	0.00
	-2.52	0.18	-0.02
Oxalate	no ligand	0.16	0.00
	-3.00	0.34	-0.23
	-2.70	0.42	-0.32
	-2.30	0.34	-0.22
Succinic acid	no ligand	0.16	0.00
	-4.60	0.16	0.00
	-4.00	0.16	0.00
	-2.70	0.30	-0.19
	-2.40	0.37	-0.26

Solute	log [Solute] (M)	(C/C₀)_{5 min}	log α_{exp}
Adipic acid	no ligand	0.16	0.00
	-4.60	0.17	-0.01
	-4.00	0.21	-0.07
	-2.70	0.27	-0.15
	-2.40	0.30	-0.18
Suberic acid	no ligand	0.16	0.00
	-4.60	0.16	0.00
	-4.00	0.16	0.00
	-2.70	0.26	-0.13
	-2.52	0.24	-0.11
Phthalate	no ligand	0.16	0.00
	-4.30	0.18	-0.03
	-3.70	0.23	-0.10
	-3.40	0.26	-0.13
	-3.00	0.27	-0.14
	-2.70	0.45	-0.36
Benzene-tri	no ligand	0.16	0.00
	-5.30	0.24	-0.11
	-4.82	0.45	-0.36
	-4.60	0.79	-0.88
	-4.30	0.94	-1.50
Benzene-tetra	no ligand	0.16	0.00
	-7.30	0.20	-0.05
	-7.00	0.23	-0.10
	-6.60	0.35	-0.24
	-6.40	0.60	-0.55
	-6.30	0.79	-0.89
	-5.30	0.86	-1.09
	-4.60	0.92	-1.32
Aspartic acid	no ligand	0.16	0.00
	-4.00	0.17	-0.02
	-2.70	0.73	-0.76
	-2.40	0.90	-1.24

Solute	log [Solute] (M)	(C/C_o)_{5 min}	log α_{exp}
Butyric acid	no ligand	0.16	0.00
	-4.30	0.17	-0.02
	-3.70	0.16	0.00
	-2.52	0.24	-0.11
Lauryl Sulfate	no ligand	0.16	0.00
	-5.00	0.17	-0.02
	-4.70	0.18	-0.03
	-4.40	0.28	-0.16
	-4.30	0.29	-0.17
PAA	no ligand	0.16	0.00
	-5.30	0.19	-0.04
	-5.00	0.72	-0.74
	-4.82	0.95	-1.56
	-4.30	0.96	-1.65
	-3.30	0.99	-2.42
Leonardite HA	no ligand	0.16	0.00
	-5.00	0.19	-0.04
	-4.82	0.39	-0.29
	-4.70	0.81	-0.94
	-4.52	0.92	-1.32
	-4.00	0.96	-1.67
S.R. FA	no ligand	0.16	0.00
	-5.00	0.23	-0.10
	-4.82	0.41	-0.31
	-4.70	0.87	-1.12
	-3.60	0.98	-1.92
S.R. HA	no ligand	0.16	0.00
	-5.30	0.19	-0.04
	-5.00	0.43	-0.34
	-4.82	0.90	-1.25
	-4.70	0.97	-1.74